NTNU – Trondheim
Norwegian University of
Science and Technology

Ultrasound radiation force transport of drugs in tumors

Petros Tesfamichael Yemane

Medical Technology
Submission date: June 2013
Supervisor: Catharina de Lange Davies, IFY
Co-supervisor: Bjørn Atle J. Angelsen, ISB

Norwegian University of Science and Technology
Department of Physics

Ultrasound Radiation Force Transport Of Drugs In Tumors

PETROS TESFAMICHAEL YEMANE
`petrosty@stud.ntnu.no; petertesfa@yahoo.com`

June 26, 2013

Masters in Medical Technology

Faculty of Natural Science and Technology

Department of Physics

Norwegian University of Science and Technology (NTNU)

Abstract

Delivery of chemotherapeutic agents administered intravenously to solid tumors tissue in optimal quantities is one of the challenges in the clinic. However, ultrasound improves the delivery of the chemotherapeutic agents various ways depending on the frequency and the acoustic intensity applied though thermal and/or mechanical interactions with the biological tissues. The mechanical interaction arises due to the ultrasound parameters through acoustic radiation force or cavitation. The purpose of this study was hence to investigate the potential of ultrasound radiation force for the enhancement of drug uptake in prostate tumors *invivo* using poly(butylcyanoacrylate)(PBCA) nano particles and doxorubicin(Dox) .

In this work, the performance of the transducer (3D probe: LA 8.0/128/4D -1169) used of this experiment was studied. The safety issues for both the transducer and the patient that can occur due to the mechanical and thermal damage which are the main critical limits were discussed. In addition, a high power acoustic waves that are precisely localized and precisely controlled in amplitude was the second limit which was required, hence studied. The optimal drive voltage and duty cycle for probe was therefore found to be 18V and 1.25% respectively at 8MHz transmitted frequency and 1.25μ sec long pulse with reputation frequency of (PRF) 10KHz.

In addition, form the maximum possible settings of the transducer, the ultrasound radiation force (URF), ultrasound thermal heating of the tissue (UTH), and temperature on the tissue were simulated, and found $9800 N/m^3$, $49\mu J/m$ and $4\mu^o K$ respectively. Lastly, based on these findings, *invivo* animal experiment on mice, in which a prostate cancer cells model implemented, was performed, and the distribution of the administered doxorubicin (Dox) and poly(butylcyanoacrylate) (PBCA) nanoparticles on the target tissue was tested. Hence, although it is a little difficult to give a concrete conclusion on the impact of URF on the distribution and penetration of the Dox and the PBCA nano particle with out analyzing in a quantified way, the confocal laser scanning microscopy reveled no legible significant difference was observed for the distribution of the two drugs when we compared without and with ultrasound exposures.

Preface

This report has been submitted for fulfillment of my Master in Medical Technology at Department of Physics Faculty of Natural Science and Technology (NT) in Norwegian University of Science and Technology (NTNU). It was carried out under supervision of Professor Bjϕrn A. Angelsen at the Department of Circulation and Medical Imaging at faculty of Medicine in NTNU.

Acknowledgments

First, I would like to express gratitude to my supervisor Professor Bjϕrn A. Angelsen for his valuable guidance and encouragements, and for his patience in answering all my questions. Second, i would like thank for my supervisor from Department of Physics Professor Catharina de L. Davies for her assistance and also her valuable discussion about drug delivery during my work. I would also like to thank Tonni F. Johansen for his helpful comments during my work.

Then i would like to thanks for Johannes Kvam for implementing the matlab code for the simulations and therapy soft ware. I would also like to thank for Laurens de Bruijn for his discussions and assistance technical issues during my work. Then i would like to thank for Siv Eggen for helping me in providing from the preparing the mice until making the tumor sections. And also for Stein-Martin Fagerland for his work in the confocal microscope analysis. I would also like to thank for my colleague Xianhua Sun for her contribution and discussion about our work.

At last but not least I would like to express my gratefulness to my family for their help and support during my studies.

Contents

List of Figures

List of Tables

1 Introduction

1.1 Background and motivation

Cancer is one of the worst systematic diseases in human kind that requires a systematic and adequate methods of treatment. It is the uncontrolled growth of cells coupled with malignant behavior through invasion and metastasis which is a leading cause of death worldwide, accounting for 7.6 million deaths (around 13% of all deaths) in 2008 [2]. It can be treated using radiotherapy, chemotherapy, or surgery or a combination of two or more of the treatment methods .

For the case of chemotherapy which is the cancer treatment with chemotherapeutic agents that are administered in to the patient, the therapeutic agent has a long and complex way from the point of entry into the circulation to its target cells since they are administered through the blood . Delivery of these chemotherapeutic agents in vivo is therefore a broader issue in the clinic since they could not be delivered to tumor tissue in optimal quantities.

One of the factors that limit the delivery of the nano particles is abnormalities in vascularization of the solid tumors [3–5]. However, compared to normal tissues, blood vessels in tumors are leaky, possessing large gaps between endothelial cells. The second characteristic of microenvironment of solid tumors that limit the delivery of the large chemotherapeutic molecules is high interstitial pressure at the center of a tumor prevents diffusion of drug molecules through the interstitium-extracellular matrix [6–8]. These hindrances to drug delivery create spatial gradients in drug concentrations such that chemotherapeutic agents fail to reach in sufficient dose in to tumors. A huge amount of resources are going for overcoming these problems [3,5,9–15]. One strategy for overcoming such problem is hence by modulating the tumor microenvironment itself for example chemically using enzymes, and/ or physically by radiation or ultrasound [4, 5, 12] .

There has been recent interest in therapeutic applications of ultrasound, primarily because of the medical and cost benefits that could be realized by the non-invasive nature of the procedure. Ultrasound may improve the delivery of cytostatica and nano-particles in various ways depending on the frequency and the acoustic intensity applied though thermal and/or mechanical interactions with the biological tissues. The mechanical interaction effects through cavitation which is the formation and oscillation of gas bubbles, and acoustic radiation force that evolves the transfer of momentum from the ultrasound wave that causes translation of the particles.

Recent development in high-intensity focused ultrasound (HIFU) transducer design, for instance, demonstrates to increase a variety of drug delivery due to interaction with the biological tissues through hypothermia and acoustic cavitation [10] using a pulse mode with a low acoustic powers and duty cycles. There are also vast amount of studies on the use of cavitaion and acoustic radiation force for guiding the targeted microbbules to the vessel wall, for example, Dayton [16, 17]. Radiation force has also shown a possibility of creating gaps between endothelial cells [18], and widen intracellular space to enhance the interstitial transport [19].

There are also an immense amount of researches that studied about the properties of the tumors itself. Hence, it is shown that tumors angiogenic vasculature exhibits larger junction between the endothelial cells [9, 20]. Moreover, the blood perfusion of tumors are lower than that of normal tissues that can be a possibility for reducing the dissipation of heat from the tumors [21].

Therefore, all of effects of the ultrasound waves such as hyportherma, acastic cavitations, and acoustic radiation force, and unique structural and vascular characteristics of the tumors provide hope in improving the delivery of the chemotherapeutic agents to the target tissues [9] .

1.2 Purpose of this study

Knowledge of the acoustic mechanisms of interaction of ultrasound propagation with tissues and its unique features facilitated the development of diagnostic and therapeutic ultrasound. Ultrasounds have been used for the past half-century for imaging the body by using waves with frequency usually in the range 1MHz-50MHz. Today, ultrasonic imaging has become a standard medical procedure for patient diagnosis and a means of providing non invasive therapy, and the current research suggests promising new therapeutic applications of ultrasound in the delivery of drugs and genetic material [22],thrombolysis [23],opening of the blood brain barrier [18, 24] , and tumor therapy.

One of the unique feature of ultrasound is, hence, the ability to focused irradiation to provide selective therapeutic action on the regions of interest for better targeting of therapy through heating, acoustic radiation force, and/or acoustic cavitation.

The transport of drugs to the target cells through the extracellular transport in the interstitium and across the blood vessels is done by convection and diffusion. However, as mentioned earlier, these transports are heterogeneous in tumors [25]. Due to the imperfect walls of the capillaries and the imperfect lymphatic drainage in the tumor, the tumor interstitial fluid pressure is high pressure compared to the normal tissue, with very low pressure gradient from the tumor capillaries and throughout the tumor interstitial fluid [14]. Thus, the transport of the cytostatica from the capillaries towards the cells is mainly produced by diffusion proportional to the negative concentration gradient of the drug, which is a slow process.

Therefore, ultrasound radiation force has a potential to increase the low pressure gradient from the tumor capillaries and throughout the tumor interstitial fluid, hence the convection.This increases the transport of the administered macromolecules and nanoparticles from the capillaries towards the cells in tumors. The target of the project is to study the use of ultrasound for this purpose.

Therefore, the general objective of the work is to develop a therapy ultrasound radiation force mediated drug delivery experiment and test in vivo experiment on mice. Hence, the first goal of this study is to study the performance of the probe used on the experiment, and find the optimal transmitted frequency, drive voltage for the probe, and duty cycle of the pulses that can give minimum heating of the transducer with maximum surface pressure. The second goal is to find the optimal aperture of the traducer with the already selected frequency, voltage, and duty cycle so as to have maximum radiation force on the focus by controlling the heating of the tissue. The third and last goal of this thesis is to develop *invivo* experiment and test the distribution of the administered doxorubicin (Dox) and poly(butylcyanoacrylate) (PBCA) nanoparticles on the prostate tumors. In the *invivo* experiment, we used twelve mice on which three of the mice are injected a Dox , and another three are with PBCA nano particles , both groups followed with isonification of ularasound radiation force (URF). And the other two groups, of three mice each, where one group are only with Dox, and the other group are with PBCA nano particles for observing the effect of the URF on the distribution of the drugs

1.3 Structure of this report

In this paper, we will first introduces the micro environment of the cancer cells and the non linear ultrasound wave equations which is used for modeling of ultrasound radiation force, then a theoretical discussion of the ultrasound radiation force and transducer heating are discussed.

We then shows the material and methods used starting with the characterization and performance of the transducer used on the experiment. In this last part we analyze and simulate some of the parameters used in our numerical evaluations. We will then describe the equations used to model ultrasound radiation force produced by focused nonlinear ultrasound, and set the parameters used in the computations. At last we will describe the vivo experiment that demonstrate the effect of ultrasound radiation force (URF) for drug delivery.

2 Background

2.1 Tumor anatomy and Biology

Chemotherapeutic agents are administered in to the patient through the blood vessels , and goes long and complex way from the point of entry into the circulation and to extracellular matrix and then to its target tumors cells. Due to the aggressive growth of malignant tumors, the capillaries of the tumor have imperfect walls, hence this abnormal characteristic of the tumor microenvironment leads to deficiencies in transvascular transport. In addition, the abnormality of the extrancellular matrix also causes a lack of interstitial transport. [3–5]. Both affects the efficacy of chemotherapeutic agents.

2.1.1 Structure of Extracellular matrix (ECM)(interstitium)

Extracellular matrix(ECM) is the region that surrounds animal cells. It is a complex structure composed of glycoproteins and fibrous proteins such as collagen ,fibers etc as show in figure 1. It is connected to the cytoplasms via integrin proteins present in the plasma membrane. Integrin can also communicate with the intracellular molecules so that communication can exist between the extracellular matrix and cytoplasm. It is the region where the transport of chemotherapeutic agents and nanoparticles is worst due to its complexity. Moreover, it is believed that the content of the fibrillar collagen on the tumor has an inverse relationship with the interstitial diffusion of macromolecules [26].

2.1.2 Transport mechanisms of drugs from the capillaries to the cells in tumors

The delivery of cancer chemotherapeutic and nanomedicine is done through vascular , transvascular, and interstitial transports [25,27].The vascular transport is done based on the perfusion rate of the blood. The blood flow of therapeutic agents on the capillary (convection transport) is given by:

$$q_1 = \frac{\nabla P}{FR} \tag{2.1}$$

Where q_1 is flow rate vessel due to convection, ∇P is the pressure gradient on the capillary, and FR is the flow resistance which is given by:

$$FR = \eta Z \tag{2.2}$$

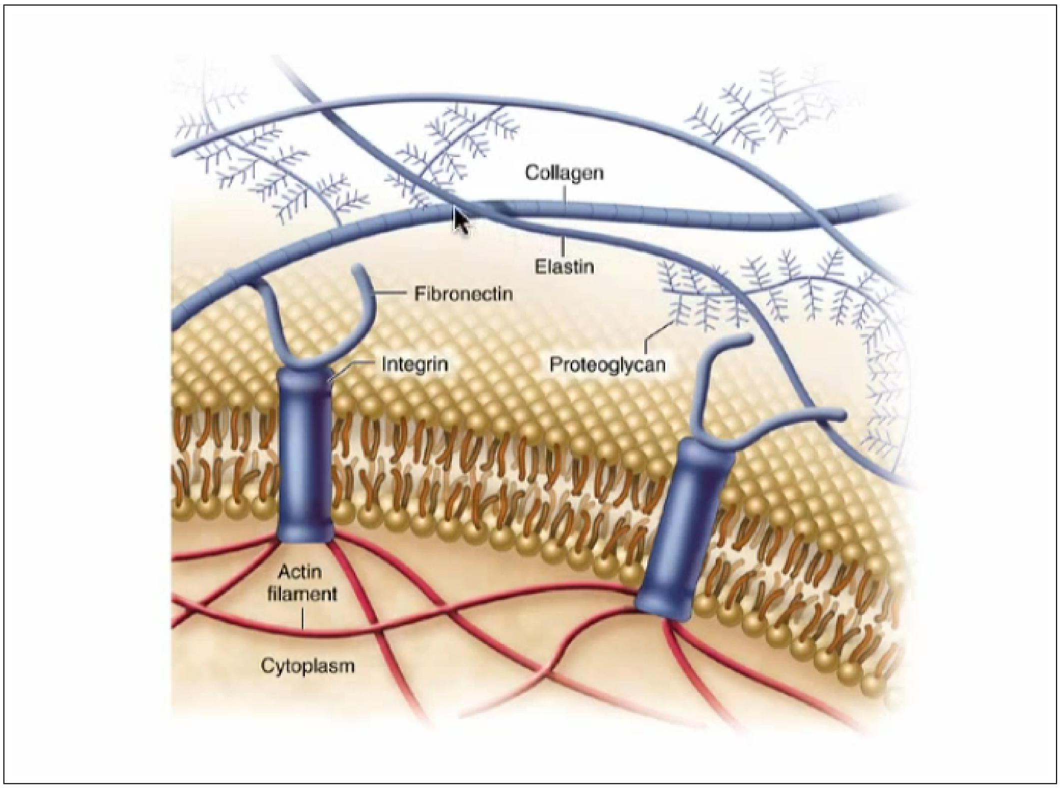

Figure 1: Structure of Extracellular matrix (ECM)

Where η is the apparent viscosity(viscosity resistance) of the medium, and Z is the geometrical resistance.
Therefore;

$$q_1 = \frac{\nabla P}{\eta . Z} \tag{2.3}$$

In tumors, the geometrical resistance and viscosity are higher compared to normal tissue due to their peculiar geometry and branching patterns, and due to hemoconcentration respectively.

Where as, both in the transvascular, and extracellular transport in the interstitium which is the penetration and distribution of the drugs into the extracellular matrix and into the target cells, proceeds by a combination of diffusive and convective transports. Diffusion depends up on the concentration of the gradients, while convention depends on the pressure gradient of the system.This pressure gradient could arise from the extracellular and intracellular fluid pressures in the case of interstitial transport.
In tumors, the tumor interstitial fluid (TIF) which is a watery phase accumulates inside the tumor interstitium is high pressure constitutes which

obstacles to drug delivery [11]. The intestinal fluid pressure (IFP) of human tumor ranging from a minimum of 2.6mm-Hg to a maximum of 40mm-Hg in contrast to the IFP of normal tissue which is typically between -3 and +3mm-Hg [15].

Similarly, the convection for trasvascular transport is driven by the pressure gradient across the microvessel wall which is also minimal at the center of solid tumors because of the elevated interstitial fluid pressure (IFP) that is approximately equal to the microvascular pressure [25, 27].These limits drug penetration across vessel walls into tumors (transvascular) and through tumor tissue (interstitial) to slow diffusion.

However, the gradient of the pressure is minimum at the center of the solid tumor which is approximately equal to the microvascular pressure [28]. This will reduce the transport through the extracellular matrix by convection.

Using Fick's fist law of diffusion, the measure of flux ($mol/m^2.s$) which is the amount of therapeutic agents moved through a cross sectional area in a given time, is given by:

$$\vec{J} = -D.\nabla n \tag{2.4}$$

But $q_2 = A.J$ Hence equation (2.4) becomes

$$q_2 = -D.A.\nabla n \tag{2.5}$$

where q_2 is flow of the therapeutics agents due to diffusion, D is diffusion coefficient, ∇n is concentration gradient, and A is area of the target region (cross-sectional area).

2.1.3 Thermal regulation of blood flow in tumors

Heat is a natural byproduct of metabolism of the tissue and it is regulated through a homeostatic process in which the tissue temperature is controlled by different mechanisms in which it is believed that the dissipation of heat through blood flow is the dominant factor in the thermoregulation of tissues during heating [29].

But for tumors, depending on the age, size and type of the tumors, the distribution of blood perfusion in tumors is quite heterogeneous. Therefore, it is believed that the temperature of tumors rises higher than that in the surrounding normal tissues during heating [21], which could be effective for the treatment through ultrasound thermal heating of the tissue. While for the effect of ultrasound radiation force, the heating could help to increase the blood flow for having constant flow of the targeted particles on the region of interest.

2.2 Prostate cancer

Prostate is a gland in a male reproductive system located in the pelvic, under the urinary bladder and in front of the rectum . Prostate cancer is classified as an adenocarcinoma, or glandular cancer, that begins when prostate gland cells mutate into cancer cells .As other types of cancers, it metastasize to the other parts of the body, particularly to bones and lymph nodes, but most of the prostate cancer grows slowly and at early stages has no symptoms [30]. This cancer type is one of the main leading cause of death in men world wide, and are most likely to occur above the age of 50.

However, it is most successfully treated when found early. Hence, early detections of the protest caner can reduce the mortality rate and the impact on the cured patients health. The presence of prostate cancer may be detected by prostate-specific antigen (PSA), or digital rectal examination (DRE) test. Like other types of cancers, the most common treatments are surgery, radiation, hormone therapy, and chemotherapy.

2.3 Ultrasound basic theory

Ultrasounds (US) waves is the name given to sound waves with frequencies greater than that of human hearing, at approximately greater than 20kHz. The use of ultrasound in medicine is wide ranging and continues to expand.

The purpose of this report is to understand the application of localized radiation force in therapeutics that requires a nonlinear absorption mechanism for local enhancement of radiation force, in contrast to the linear losses that occur along the entire path of the ultrasound wave propagation. Hence, we will therefore restrict ourselves to modeling of the nonlinear propagation of ultrasonic waves in tissues.

The acoustic phenomena analyzed in this work take place in a tissue that can be approximate as fluid medium. It is assumed that the fluid medium is continuous and remains continuous under the action of any external perturbation.

When a sound wave propagates through an isotropic and heterogeneous materials, the variation of displacement along the propagation direction will cause a compression of the material, which generates a pressure. For small volume change, the relative volume compression is given by

$$-\frac{\delta v}{\Delta V} = \nabla\vec{\psi}(\vec{r},t) \tag{2.6}$$

where $\vec{\psi}(\vec{r},t)$ is the particle displacement vector from an equilibrium position $\vec{r}$.

As a compressional wave propagates, the relative displacement of different parts of the medium leads to localized changes of density. These are described by mass density condensation ρ_1/ρ_o, Here, ρ_o is the density in the unstrained material while$\rho_1 = (\rho - \rho_o)/\rho_o$.

Localized changes of density cause localized changes of pressure, p, (referred to as acoustic pressure) through the equation of state($p = p(\rho, S)$) for the medium at isentrope $S = S_o$ using Taylor series is given by:

$$p = P - P_o = A\rho_1/\rho_o + B(\rho_1/\rho_o)^2)/2 + ... \tag{2.7}$$

Where P is the absolute pressure, Po is the ambient pressure ,and A, B are constants which are given by:

$A = \rho_o(\frac{\partial p}{\partial \rho}) \mid_{0,S}$ and $B = \rho_o^2(\frac{\partial^2 p}{\partial \rho^2}) \mid_{0,S}$

where the subscripts in the partial derivatives indicate that they are evaluated at the unstrained state for an isentropic process.

If only the first term is taken we obtain the linear wave equation which the acoustic pressure, p, also satisfies .But for diagnostic devices it is necessary to consider nonlinear waves in which in two order are considered.Hence, we will use the two order of the equation.

Therefore, following the tissue elasticity equation, the acoustic pressure to the second order of $\nabla\vec{\psi}(\vec{r},t)$ is given by

$$p = -A\nabla\vec{\psi}(\vec{r},t) + A\beta_n(\nabla\vec{\psi}(\vec{r},t))^2 \tag{2.8}$$

Where $\beta_n = 1 + \frac{B}{2A}$ which is called the nonlinear parameter of the material. And the net force on the volume element is given by the localized changes of pressure (the negative pressure gradient) and is proportional to its volume. Using Newton's second law for a plane wave, the relation between the force and acceleration is given by [31]:

$$\rho(\vec{r},t)\frac{\partial\vec{u}(\vec{r},t)}{\partial t} = -\nabla p(\vec{r},t) \tag{2.9}$$

and also the compressibility for a plane wave is given:

$$\frac{\partial p(\vec{r},t)}{\partial t} = -\kappa^{-1}\nabla\vec{u}(\vec{r},t) \tag{2.10}$$

where $\rho(\vec{r},t)$ is the mass density as a functions of spatial and time coordinates, and $\vec{u}(\vec{r},t)$ is the particle velocity. This equation is generally valid for beams with a smooth phase around the main propagation direction [32].

Using equation (2.8) , equation (2.6) can be rewrite as the constitutive equation for the nonlinear tissue elasticity

$$\frac{\delta v}{\Delta V} = -\nabla.\vec{\psi}(\vec{r},t) = (1 - \beta_p(\vec{r})p(\vec{r},t))\kappa(\vec{r})p(\vec{r},t) + h_{ab} \otimes_t \kappa(\vec{r})p(\vec{r},t) \quad (2.11)$$

Where $\kappa(\vec{r})$ is the linear bulk compressibility of the material, and $\beta_p(\vec{r}) = \beta_n(\vec{r})\kappa(\vec{r})$, and and $h_{ab}(\vec{r},t)$ is a convolution kernel that represents absorption of wave energy to heat.This equation describes the relation between the relative volume compression of a small volume of tissue with an applied acoustic pressure p.

Combining equations (2.4) and (2.6), the wave equation for a homogeneous nonlinear tissue becomes :

$$\nabla(\frac{1}{\rho(\vec{r},t)}(\nabla p(\vec{r},t))) - (1 - \beta_p(\vec{r})p(\vec{r},t))\kappa(\vec{r})p(\vec{r},t) - h_{ab} \otimes_t \kappa(\vec{r})p(\vec{r},t) = 0 \quad (2.12)$$

But soft tissues are composed of different material types such as fat, muscle, connective tissue, ..etc which gives spatial variations of the mass density and elasticity. Hence we need to introduce spatial heterogeneity. We will model this heterogeneous material by separating the material parameters into a slowly varying (scale $\sim \lambda$) component (denoted with the subscript a for average) and a rapidly varying component (denoted with the subscript f for fluctuations), i.e.

$$\rho(\vec{r},t) = \rho_a(\vec{r}) + \rho_f(\vec{r}) \quad (2.13)$$

$$\beta_n(\vec{r}) = \beta_{na}(\vec{r}) + \beta_{nf}(\vec{r}) \quad (2.14)$$

$$(2.15)$$

And we note that the second term of equation (2.12) has also a slow and fast variation of the compressibility and density.

Let us introduce $\gamma = \frac{\rho_f}{\rho}$ we get that

$$\frac{1}{\rho} = \frac{\rho_a}{\rho\rho_a} = \frac{\rho - \rho_f}{\rho\rho_a} = \frac{1}{\rho_a} - \frac{\gamma}{\rho_a} \quad (2.16)$$

and inserting this into (2.13) and approximating $\nabla \rho_a \approx 0$, we get:

$$\begin{aligned} &\underbrace{\nabla^2 p(\vec{r},t) - \frac{1}{c_o(\vec{r})^2}\frac{\partial^2 p(\vec{r},t)}{\partial t^2}}_{\text{linear propagation}} + \underbrace{\frac{\beta_p(\vec{r})}{c_o(\vec{r})^2}\frac{\partial^2 p(\vec{r},t))^2}{\partial t^2}}_{\text{nonlinear propagation}} - \underbrace{h_{ab}(\vec{r},t)\otimes_t \frac{1}{c_o(\vec{r})^2}\frac{\partial^2 p(\vec{r},t)}{\partial t^2}}_{\text{absorption}} \\ &= \underbrace{\frac{\sigma_l(\vec{r})}{c_o(\vec{r})^2}\frac{\partial^2 p(\vec{r},t)}{\partial t^2} + \nabla(\gamma(\vec{r})\nabla p(\vec{r},t)}_{\text{Linear scattering source terms}} - \underbrace{\frac{\sigma_n(\vec{r})}{c_o(\vec{r})^2}\frac{\partial^2 p(\vec{r},t)^2}{\partial t^2}}_{\text{Nonlinear scattering source term}} \end{aligned} \tag{2.17}$$

where $c_o(\vec{r})$ is the linear wave propagation velocity for low field amplitudes which is given by:

$$c_o(\vec{r}) = \frac{1}{\sqrt{\rho_a(\vec{r})\kappa_a(\vec{r})}} \tag{2.18}$$

and the nonlinear wave propagation velocity $(c(\vec{r}))$ is given as

$$c(\vec{r}) = \frac{1}{\sqrt{\rho_a(\vec{r})\kappa_a(\vec{r})(1-\beta_n\kappa_a(\vec{r})p(\vec{r},t))}} \tag{2.19}$$

$$\approx c_o(1+\beta_n\kappa_a p) \tag{2.20}$$

And $\sigma_l(\vec{r})$ and$\gamma(\vec{r})$ are linear scattering parameters given by the relative spatial variation of the material compressibility and mass density, and $\sigma_n(\vec{r})$ is a nonlinear scattering parameter.

$$\sigma_l(\vec{r}) = \frac{\kappa_f(\vec{r})}{\kappa_a(\vec{r})} \tag{2.21}$$

$$\sigma_n(\vec{r}) = (2\beta_{na}(2+\sigma_l)\sigma_l + \beta_{nf}(1+\sigma_l)^2)\kappa_a p \tag{2.22}$$

$$\approx 4\beta_{na}\sigma_l\kappa_a p \tag{2.23}$$

From the nonlinear wave equation (2.17) we observe that, the wave is propagating with a propagating velocity that depends on the volume compression that the relative variation of the wave velocity is less than 0.05 [31, 32], and the squared pressure term on the left hand side of the nonlinear wave equation models the generation of nonlinear forward propagation effects. The squaring of the pressure generates harmonics of the center frequency of the forward propagating pulse.In addition , the linear and nonlinear scattering sources are generated due to the linear and nonlinear parameters of the material.Thus, increases in absorption of the wave in the medium, means also increase in radiation force for diagnostic devices as we will see the relation in section 3. Example of the linear non-distorted pulse ,and the nonlinear distorted pulse are shown in fig 2.

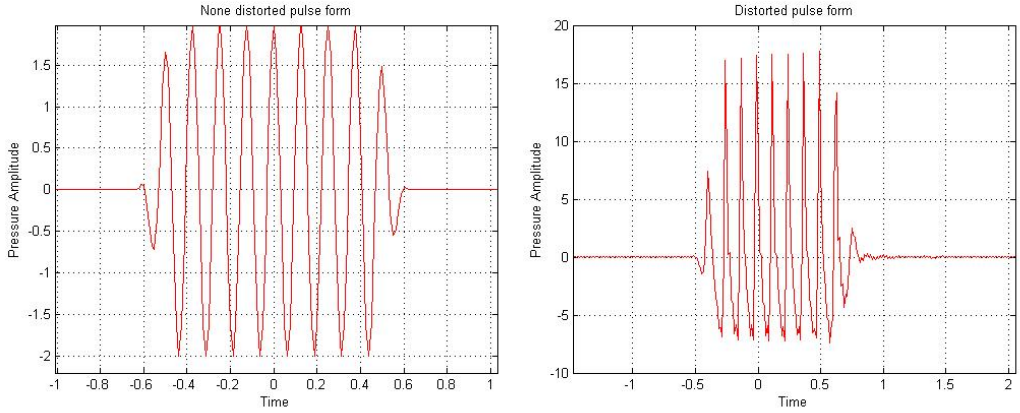

(a) Non distorted pulse

(b) Distorted pulse

Figure 2: Non distorted pulse, and the distorted pulse due to non linearity

The nonlinear heterogeneous wave propagation equation(2.17) is complex and must be solved by numerical simulations, as we will see later when using ABERSIM [33] which is a soft were developed by Department of Circulation and Medical Imaging[1].

---

[1] Norwegian University of Science and Technology, Trondheim, Norway

3 Ultrasound radiation force

3.1 Introduction

To apply acoustic radiation force for drug delivery, we need to understand how the ultrasound (acoustic) radiation force is generated on the target object.

Since sound waves carry momentum, when this sound wave in a medium hits an object, part of its momentum becomes a force on the object. As discussed in section 2.3, nonlinear properties of wave motion in the propagating medium increases the absorption, hence to the radiation force on the object. Since the physical processes leading to acoustic radiation force are quite complex, we will simplify to viscous fluid medium and a small volume object as reference to [31]. But before we described the radiation force, first we will see the relation between radiation intensity and the pressure, then the acoustic radiation pattern of the wave in a medium, and then the frequency dependent attenuation coefficient of the ultrasound wave in tissues.

We will then describe the performance of transducer, and at last we will show the theoretical simulation method used for simulation of the URF, ultrasound thermal heating(UTH) on the tissues, and Temperature on the tissues.

3.2 Radiation intensity

Ultrasonic waves propagated through medium through exchange of energy between potential and kinetic energy. Hence, part of the exchange energy on the small volume element ΔV is used to built up acoustic wave energy, while the other is lost due to acoustic energy absorption as heat. For analysis of the energy transfer in acoustic wave motion in detail refer to reference [31]. For a pressure wave propagating in a medium, the acoustic radiation intensity ($\vec{I}$) which is a measure of the flow of the acoustic energy per unit time unit are carried by the sound wave radiated by a source, is defined as the product of the sound pressure $p(\vec{r},t)$ and the particle velocity $u(\vec{r},t)$ in the medium through which the sound wave is traveling :

$$I(z,t) = p(\vec{r},t)u(\vec{r},t) \tag{3.1}$$

The average radiation intensity over a cycle is given by :

$$< I(z,t) >= Re[\frac{p(\vec{r},t)u(\vec{r},t)^*}{2}] \tag{3.2}$$

where <> indicates average , $*$ indicates the complex conjugate ,and Re indicates taking the real part of the product. For a plane wave, and using accelaration relation Eq (2.9), the average intensity becomes:

$$< I(\vec{r}, t) >= \frac{p_o^2}{2Z_o} \tag{3.3}$$

where p_o^2 is the input pressure amplitude, and Z_o is the acoustic characteristic impedance of the medium.

3.3 Acoustic radiation pattern

3.3.1 Basic theory

The radiation field of an ultrasonic transducer is evaluated as the principle of Huygens principle, which states that every point of a wave front generated from finite aperture may be considered the source of secondary wavelets that spread out in all directions with a speed equal to the speed of propagation of the waves.To calculate the beam profile of an ultrasonic transducer, the transducer surface is modeled as an infinite number of point sources, each emitting a spherical wave. The field at a particular location consists of the summation of the spherical wavelets generated by all the point sources on the transducer [31].

3.3.2 Radiation Pattern

The acoustic wave produced due to the vibration of the transducer surface will propagate to the load which is biological material in medical ultrasound transducers. Hence, the radiation pattern depends upon the vibration of the transducer surface, and geometrical structure of the element of the transducer. For one elements transducer of a plane vibrating surface in a rigid baffle assumption, the radiated acoustic energy in the frequency domain is given by [31]

$$H(\vec{r}, w) = \int_{s_t} d^2 r_o \frac{e^{-ik|\vec{r}-\vec{r}_o|}}{2\pi \mid \vec{r} - \vec{r}_o \mid} L(\vec{r}, \vec{r}_o) M_n(\vec{r}_o) \tag{3.4}$$

Where $M_n(\vec{r_o}) = \rho U_n(\vec{r_o})$ is represents the surface momentum distribution, and $L(\vec{r}, \vec{r}_o)$ is absorption .
Hence, the pressure field is given by

$$P(\vec{r}, w) = iwH(\vec{r}, w) = iw \int_{s_t} d^2 r_o \frac{e^{-ik|\vec{r}-\vec{r}_o|}}{2\pi \mid \vec{r} - \vec{r}_o \mid} L(\vec{r}, \vec{r}_o) M_n(\vec{r}_o) \tag{3.5}$$

To get a simplified relation between the pressure wave propagated on the radiated medium and the aperture of the element, let us simplify the Eq. (3.5) assuming that the wave is radiated from a rectangular aperture element with incident pressure of P_o, and propagating in a linear medium.

$$P(\vec{r}, w) = iw \int_{s_t} d^2 r_o \frac{e^{-ik|\vec{r}-\vec{r}_o|}}{2\pi \mid \vec{r} - \vec{r}_o \mid} L(\vec{r}, \vec{r}_o) P_o \tag{3.6}$$

The pressure at the focus (F), which is the distance of the beam axis from the radiating surface to the point where the acoustic response is maximum, will become

$$P_F(\vec{r}, w) = iw \int_{s_t} d^2 r_o \frac{e^{-ikF}}{2\pi F} P_o \tag{3.7}$$

where $k = k_r - ik_d$, where k_r is the propagation wave number and k_d is the absorption. Hence, integrating Eq. (3.7)

$$P_F(\vec{r}, w) = iw \frac{e^{-ik_rF - k_dF}}{2\pi F} P_o A_t \tag{3.8}$$

Where A_t is area of the transmitting aperture.
Therefore, we see from Eq (3.3) that the average intensity is proportional to the pressure square, hence to the area of the transmitted aperture squared. The intensity on the focus would be, hence, increased by increasing the transmitting aperture of the transducer, but we are also limited by heating of the tissue, and also on the 3dB or 6dB opening angle of the beam depending on the depth of the focus and center frequency as we see in the next paragraph.

For an array with M number of elements , the radiated acoustic energy is given by [31]:

$$H(\vec{r}, w) = \sum_m w_m e^{-iw\tau_m} \frac{1}{2\pi} \mid \vec{r} - \vec{r_m} \mid) e^{-ik|\vec{r}-\vec{r_m}|} L(\mid \vec{r} - \vec{r_m} \mid, w) H_{el}(\vec{e}_{\vec{r}-\vec{r}_m}) \tag{3.9}$$

Where $H_{el}(\vec{e}_{\vec{r}-\vec{r}_m})$ is represents the element directivity function,τ_m focusing delay for element number m, w_m is the apodization and L is absorption .

Using Franuhofer approximation for array field, we can separate the array factor $(A(\vec{r}, w))$ and element factor$(H_{el}(\vec{r}, w))$ [31]. Hence, at far field of the medium, for a rectangular-aperture transducer with length of 2a in the azimuth direction(x1) and 2b in the elevation direction (x2) , the radiated acoustic energy is [31]:

$$H(\vec{r}, w) = \frac{sin(Mkp/2(sin(\theta - sin\theta_o)))}{(sin(kp/2(sin(\theta - sin\theta_o))))} H_{el}(\vec{r}, w) = A(\vec{r}, w) H_{el}(\vec{r}, w) \tag{3.10}$$

where θ is the angle of the beam form axial axis (z), and θ_o is the steering angle ,p is the center to center distance between array elements, $A(\vec{r}, w)$ is called array factor or diffraction factor.

And the directivity function of the beam$H_{el}(\vec{r}, w)$, for a piston equivalent radiation surface hypothesis that is the velocity profile at the acoustic port of the transducer is uniform, and the element as a rigid baffle means that a rigid reflection in which the gradient of the pressure on the surface on interface of medium is zero, is given by:

$$H_{el}(\phi, \psi) = \frac{1}{r} sinc(2a/\lambda sin(\phi)) sinc(2b/\lambda sin(\psi)) \tag{3.11}$$

where $H_{el}(\phi, \psi)$ is the spacial frequency response of the single element and is obtained by taking the Fourier transform of the uniform distribution of the excitation across the aperture size of the element, and $sin(\phi) = x1/$r and $sin(\psi) = x2/r$, $\vec{r}$ is the direction of the beam. And *sinc* denotes the *sinc* function $sin(\pi x)/\pi x$.

From equation (3.11), the beam width in the azimuth and elevation directions is given by the period of the corresponding sinc functions. For a given depth r, the period in the azimuth direction is proportional to the $(\lambda/2a)$ from the property of the sin function, hence the beam width. Similarly, the period in the elevation direction is proportional to the $(\lambda/2b)$.

Hence, base on the -3dB beam profile of equation (3.11), we can select the number of elements that can get contribution from the elements for a given focal length and center frequency.

3.3.3 Focal area of the beam

Focal area of the beam is the area in which the acoustic response is maximum, and is given by the beam width multiplied by the depth of the focus. The beam width($D_F(XdB)$ is defined by the lateral/elevation beam width at the focus with XdB amplitude of the beam loss with respect the maximum value. And the beam depth is the focal zone around the focus where the beam amplitude is within XdB of the maximum value. It is the region where the traducer performs best.

The theoretical evaluation of the beam width on equation (3.11) at focus depth of Z_F is:

$$D_F(-XdB) = 2.Z_F sin(\phi_{(-XdB)}) \tag{3.12}$$

Where $sin(\phi_{(-XdB)})$ is the angle from the focus to the end point of the aperture at -XdB of the beam.

3.4 Attenuation in tissue

Acoustic attenuation is a measure of the energy loss of sound propagation in media. We know that the soft tissue are composed of complex molecules with dimensions approximately 10-100nm [31].Hence, when ultrasound beam propagate in medium, it is attenuated in three ways depending on the dimensions of the interacting medium. When the dimension of the interacting medium is larger than to the wave length of the wave, the ultrasound beam can be attenuated through reflection and scattering at interface , where as when the dimension of the medium is equal to the wave length, the wave actuates through scattering. While, when dimension of the medium is smaller than that of the wave length of the propagating wave, the beam can be attenuated through absorption. The acoustic absorption can occurs by heat conduction between the particles and the fluid, or/ and by viscous friction between the particles and the fluid due to the difference in compressibility and mass density.

Ultrasound wave propagating in soft biological tissue is connected with dispersion ,hence the acoustic attenuation typically exhibits a frequency dependence which can be described by a power law given by [33, 34]:

$$\sigma(f) = af^b \tag{3.13}$$

Where $\sigma(f)$ is the attenuation coefficient, f is the frequency, a is the attenuation constant, and b is the frequency- power exponent.

Acoustic attenuation in water is a frequency-squared dependent (b=2) while for most soft tissues b is from 1 to 2 [35], hence, besides the medium length and attenuation constant(a), attenuation coefficient in soft tissue is also non-linearly dependent on the frequency of the incident ultrasound beam. Increasing the frequency will increase the resolution but also attenuation. Therefore, there is a tradeoff between resolution and attenuation when we select the operating frequency of a transducer. For imaging, we need to have a higher signal to noise ratio for having good resolution where as for therapeutic applications it is the attenuation which is more important for having higher transfer of energy to the medium.

3.5 Ultrasound Radiation force

As illustrated in section 3.4 when ultrasonic sound waves propagates to a tissue, it interacts with the medium through absorption and scattering mechanisms. These interactions results a transfer of momentum from the propagating ultrasonic wave to the tissue which is called ultrasound radiation force (URF). URF is a time averaged force exerted by an acoustic field on an object or boundary surface. Modeling tissue as a viscous fluid in response to ultrasonic wave propagation, under plane wave assumptions, acoustic radiation force (F) can be related to the acoustic extinction cross section (σ_e) and ultrasound propagation velocity (c) of the tissue, and the temporal average intensity of the acoustic beam (I) by:

$$\Delta F = \frac{\sigma_e < I > \Delta V}{c} \tag{3.14}$$

This force is in the form of a body force in the direction of the wave propagation. And the ultrasound intensity (I) is proportional to the square of the pressure as equation (3.1), and $\sigma_e = \sigma_a + \sigma_s$is the extinction cross section of acoustic intensity, as the sum of the the absorption cross section σ_a and the scattering cross section σ_s. It is good to note the contributions of scattering in the computation of the momentum transfer is very few, which seems reasonable in soft tissues where the majority of the attenuation of ultrasound arises from absorption.

As equation (3.14) we see that radiation force, is connected with intensity, hence, energy densities, which is a quadratic terms containing squares of velocities and displacements. Therefore, any theory dealing with acoustic radiation force must retain at least all second order terms to valid even at small amplitudes.

It is also important to note that the intensity depends on focusing and absorption, which both depends on frequency, and similarly do the extinction cross section depend on frequency. Therefore, it is necessary to model the frequency dependent extinction cross section of the wave on the medium.

The maximum radiation force that can be achieved in the focal region hence depend the aperture and focal length of the transducer, and the amplitude and frequency of the irradiated acoustic wave. Moreover, the increase on radiation force at focal region depends on non linear absorption of the medium resulted from the non linear propagation of wave form distortion which causes higher order harmonics.These dependencies open for optimization of radiation aperture, focusing, and frequency of the ultrasound radiation force beam, depending on the depth and dimensions of the irradiated medium that is tumor in our case.

Depending on the above parameters, the ultrasound radiation force can be used for streaming purposes, increasing the pressure gradient on the ECM, and changing the permeability of the blood vessels. This streaming occurs in direction of the beam away from the transducer [36]. All the parameters are adjusted depending on the performance of the transducer.

3.6 Transducer heating

A medical ultrasound transducers are driven by an electrical power in which a significant percentage of this power is lost as thermal power on the transducer itself. This causes an increase in temperature through out the probe, specially at the front face [37]. This can cause a damage to the transducer itself, and/or biological effect by generating heat on tissues. The other mechanisms that can cause biological effect is due to the absorption of ultrasound when it propagates through the tissue. These two effects can make the medical use of ultrasound hazardous if precautions are not taken. In this section we will see only to first case.

As reference [38], the amount of heat dissipated on the transducer due to the thermal effect is given by:

$$Q = mc\Delta T \tag{3.15}$$

Where m is mass of the transducer, c is specific heat capacity of the transducer, ΔT is change in temperature.This can be written as

$$Q/\Delta t = mc\Delta T/\Delta t \Rightarrow \Delta T/\Delta t = W_t/mc \tag{3.16}$$

Where W_t is the power dissipated on the transducer. Note that, we denoted power with W not to create confusion with pressure.

$$\Delta T/\Delta t = W_t/\rho LAc \tag{3.17}$$

where ρ, L , and A are the density, thickness and area of the transducer respectively.

Here we will assumed that the transducer is as a single thermal unit, and is driven by the electric power of the piezoelectric material.Therefore, $W_t = W_e - Wa$, Where W_e and W_a are the electric input power and the acoustic out power of the transducer respectively.

Thus, $W_t = W_e(1 - \eta)$, where η is efficiency of the transducer.

For a transducer operating in to a load, then the rate of change in temperature will be:

$$\Delta T/\Delta t = \frac{W_e(1-\eta)}{\rho L A c} \tag{3.18}$$

The heat is generated only from the piezoelectric material, and the thickness (L) of the piezoelectric material is $\lambda/2$, so,$L = c_o/2f$ where c_o and f are the velocity of sound and center frequency of the piezoelectric material.

$$\Delta T/\Delta t = \frac{W_e 2f(1-\eta)}{\rho c_o A c} \tag{3.19}$$

This can be written as:

$$\Delta T/\Delta t = \frac{I.2f.(1-\eta)}{\rho c_o c} \tag{3.20}$$

Where $I = W_e/A$ which is the intensity of the transducer.
Knowing the properties of the piezoelectric material, equation (3.19) or (3.20) can be used for simulation of the heat dissipated on the the probe.

3.7 Simulation of power and heat lost on the transducer based on measurements

We note that both the ultrasound radiation force (URF) and the tissue heating (UTH) are $\sim P^2$. Hence, to get high values of URF and UTH it is important to have as high transmit pressure as possible. However, maximal transmit pressure is limited by heating of the transducer array, and can also give unwanted tissue heating when running the ultrasound radiation force scanning. We therefore run pulsed scanning sequences, where we define:
T_{on} time period of pulse on
T_{off} time period of pulse off
$T_r = T_{on} + T_{off}$ reputation period of pulses

Note that, the URF and UTH have different purposes which depend on the center frequency of the probe, hence we select the center frequency based on the purpose. For this work ,for instance, we focus on the URF.

Driving the transmit transducer with the voltage amplitude V_{tt} at the angular frequency w_o, the power delivered to the transducer array is

$$W_{in}(w_o) = N_{el}\frac{\mid V_{tt}\mid^2}{2\mid Z_{el}(w_o)\mid} cos\theta_{el}(w_o) \tag{3.21}$$

whereN_{el} is the number of elements in the transmit aperture, and Z_{el} is the electric input impedance to the array element with phase θ_{el}. A transmission line model assumption for the cable is used to estimate the electrical impedance of the element transducer. A simplified circuit diagram of the one transducer element impedance with the transmission model assumption of the cable is shown in figure 3. More over, it is assumed that the transmission is lossless.

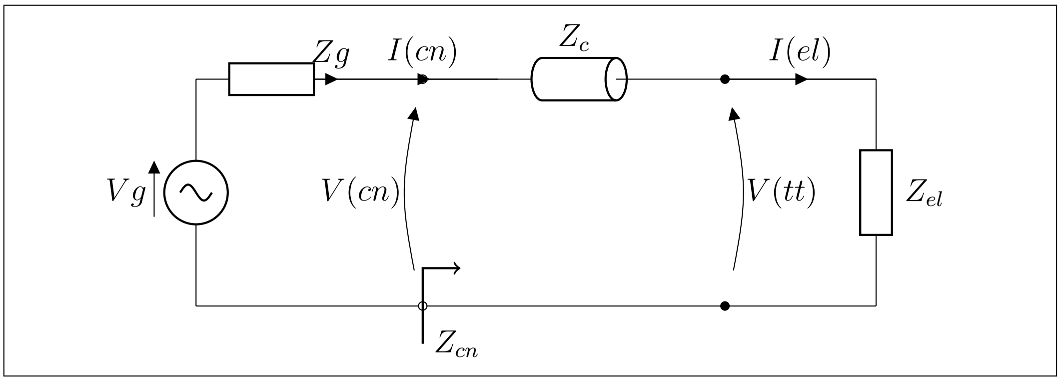

Figure 3: Equivalent circuit Schematics used in the estimation to model the cable, with the transducer impedance.

Where Vg and Zg are the voltage source and internal impedance of the generator respectively, and the input impedance Z_{cn} is given by

$$Z_{cn} = Z_c \frac{Z_{el} + jZ_c tan(kl)}{Z_c + jZ_{el} tan(kl)} \tag{3.22}$$

Where $Z_c = \sqrt{(}L/C)$,$c_{cable} = \sqrt{(}1/(LC))$ which is the speed of the signal on the cable.
and $kl = \frac{2\pi}{\lambda_{cable}} l_{cable}$ and l_{cable} is length of the cable.

For estimation of the voltage applied on the transducer element(V_{tt}), we represented the transmission line as lumped circuit shown in figure 4.
Where
$Za = iZ_c tan(\gamma/2)$, $Zb = \frac{iZ_c}{sin(\gamma)}$, and $\gamma = kL$ where, Z_c is characteristic impedance of the cable, k is the wave number. Hence,the applied voltage on the element can be estimated using :

$$V_{tt} = H_{it} V_{cn} \tag{3.23}$$

where H_{it} is the electrical transfer function from the connector to the element that can be evaluated from the impedance.

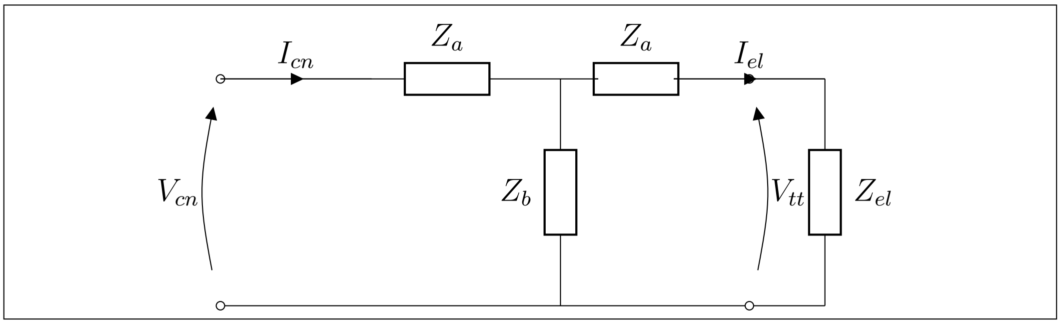

Figure 4: Lumped equivalent circuit of the transmission line with the transducer load

The output acoustic power is

$$W_{ac}(w_o) = N_{el}A_{el}\frac{\mid P_t \mid^2}{2Z_o} = N_{el}A_{el}\frac{Z_o^2 \mid H_{tt}(w_o) \mid^2 \mid V_{tt} \mid^2}{2Z_o}$$
$$= N_{el}A_{el}\frac{Z_o^2 \mid H_{tt}(w_o) \mid^2 \mid V_{tt} \mid^2}{2} \quad (3.24)$$

$P_t(w_o) = Z_oH_{tt}(w_o)V_{tt}$ and $A_t = N_{el}A_{el}$
whereH_{tt} is the transfer function from element voltage to surface vibration velocity of the transducer array element. A_{el} is the radiation area of the transducer element, A_t is the whole transmit aperture area. The efficiency of the transducer is hence

$$\eta(w_o) = \frac{W_{ac}(w_o)}{W_{in}(w_o)} = A_{el}\frac{Z_o \mid H_{tt} \mid^2 \mid Z_{el}(w_o) \mid}{cos\theta_{el}(w_o)}$$
$$= A_{el}\frac{\mid P_t(w_o) \mid^2 \mid Z_{el}(w_o) \mid}{cos\theta_{el}(w_o) \mid V_{tt}(w_o) \mid^2 Z_o} \quad (3.25)$$

and the loss fraction is the transducer loss in relation to the transmitted acoustic power

$$\gamma_{tt}(w_o) = \frac{W_{trl}(w_o)}{W_{ac}(w_o)} = \frac{W_{in}(w_o) - W_{ac}(w_o)}{W_{ac}(w_o)} = \frac{1}{\eta(w_o)} - 1 \quad (3.26)$$

The heat loss in the transducer per pulse is

$$Q_{trl}(w_o) = W_{trl}(w_o)T_{on} = \gamma_{tt}(w_o)\eta_{tt}(w_o)W_{in}(w_o)T_{on}$$
$$= (1 - \eta_{tt}(w_o))N_{el}\frac{cos\theta_{el}(w_o) \mid V_{tt}(w_o) \mid^2}{2 \mid Z_{el}(w_o) \mid}T_{on} \quad (3.27)$$

which gives an average heat power delivered to the transducer assembly

$$W_{trav}(w_o) = \frac{Q_{trl}(w_o)}{T_r} = (1 - \eta_{tt}(w_o))N_{el}\frac{cos\theta_{el}(w_o) \mid V_{tt}(w_o) \mid^2}{2 \mid Z_{el}(w_o) \mid}\frac{T_{on}}{T_r} \quad (3.28)$$

where we note that$\frac{T_{on}}{T_r}$ is the duty cycle of the pulsing scheme.The maximum average heat power W_{trm} that can be delivered to the transducer assembly is determined from experiments by the varying the driven voltage and duty cycle. This gives the maximal driving voltage ($V_{ttm}(w_o)$) at angular center frequency w_o and duty cycle. This gives us the maximum transmitted pressure as

$$| P_{tm}(w_o) |= Z_o H_{tt}(w_o) \mid V_{ttm}(w_o) \mid \tag{3.29}$$

We use ABERSIM to simulate the maximal transmitted wave $P_m(r, w; w_o)$ with P_{tm} as the transmit pressure amplitude of the transmit burst at angular frequency w_o. This allows us to calculate the maximal radiation force from Eqs. (3.45) and (3.47), and tissue heat delivery from Eqs. (3.51) and (3.52), limited by probe transfer function, probe heating and maximal transmitter voltage, as a function of the transmitted center angular frequency w_o.

3.8 Simulation of beams

3.8.1 Introduction of ABERSIM for simulation of the wave equation

As mentioned in section 2.3 the solution to the wave equation of equation (2.17) can be evaluated only numerically. Hence, an ABERSIM [33] which is a soft were developed by Department of Circulation and Medical Imaging[2], is used to simulate the wave equation numerically.

Abersim is an open-source toolkit for simulating 3D nonlinear acoustic forward wave propagation through heterogeneous and absorbing medium like soft tissue [40]. The software has an interface for MATLAB, which allows an easy access to the processing of treated data, and graphic displays, as well as a pure C implementation for computational speed purpose and has also advantage of MPI parallel computing resources.For more detail refer to the ABERSIM manual.

For the simulation of the wave equation we neglect the left hand side of the scattering terms in equation (2.17) that gives [41]

$$\nabla^2 p(\vec{r}, t) - \frac{1}{c_o(\vec{r})^2}\frac{\partial^2 p(\vec{r}, t)}{\partial t^2} + \frac{\beta_p(\vec{r})}{c_o(\vec{r})^2}\frac{\partial^2 p(\vec{r}, t))^2}{\partial t^2} - h_{ab}(\vec{r}, t) \otimes_t \frac{1}{c_o(\vec{r})^2}\frac{\partial^2 p(\vec{r}, t)}{\partial t^2} = 0 \tag{3.30}$$

---

[2] Norwegian University of Science and Technology, Trondheim, Norway

The wave equation has two solutions propagating in opposite directions. Hence. ABERSIM selects the solution only propagating into the body, i.e. the positive z-direction, and solves it at a user-defined range of depth steps. Introducing a retarded time τ which is given by

$$\tau = (t - z/c_o), p(z,t) \to \hat{p}(z,\tau) \tag{3.31}$$

Eq.(3.30) in terms of the retarded time becomes

$$\frac{\partial^2 \hat{p}}{\partial z^2} - \frac{2}{c_o(\vec{r})}\frac{\partial^2 \hat{p}}{\partial z \partial \tau} + \nabla_\perp^2 \hat{p} + \frac{\beta_p(\vec{r})}{c_o(\vec{r})^2}\frac{\partial^2 \hat{p}^2}{\partial \tau^2} - h_{ab} \otimes_t \frac{1}{c_o(\vec{r})^2}\frac{\partial^2 \hat{p}}{\partial \tau^2} = 0 \tag{3.32}$$

Assuming the beam as a collimated we can use the paraxial approximation which means that we can neglect $\frac{\partial^2 \hat{p}}{\partial z^2}$, hence, equation (3.32) will left only

$$\frac{\partial^2 \hat{p}}{\partial z \partial \tau} = \underbrace{\frac{c_o(\vec{r})}{2}\nabla_\perp^2 \hat{p}}_{\text{diffraction}} - \underbrace{h_{ab} \otimes_t \frac{1}{2c_o(\vec{r})}\frac{\partial^2 \hat{p}}{\partial \tau^2}}_{\text{absorption}} + \underbrace{\frac{\beta_p(\vec{r})}{2c_o(\vec{r})}\frac{\partial^2 \hat{p}^2}{\partial \tau^2}}_{\text{nonlinear distortion}} \tag{3.33}$$

The temporal Fourier transform of equation. (3.33) hence becomes

$$\begin{aligned}\frac{d\hat{p}(z,\vec{r}_\perp,w)}{dz} =& - i\frac{c_o(\vec{r})}{2w}\nabla_\perp^2 \hat{p}(z,\vec{r}_\perp,w) - \frac{iw}{2c_o(\vec{r})}H_{ab}\hat{p}(z,\vec{r}_\perp,w) \\ &+ \frac{iw\beta_p(z,\vec{r}_\perp)}{2c_o(\vec{r})}\hat{p}(z,\vec{r}_\perp,w) \otimes_w \hat{p}(z,\vec{r}_\perp,w)\end{aligned} \tag{3.34}$$

3.8.2 Numerical estimation of extinction cross section

To simulate the intensity as a function of depth, and especially in the focal region, we use ABERSIM. We then need an assessment of the extinction cross section, which is defined through

$$dI = -\sigma_e(w) I ds \tag{3.35}$$

where I is the intensity averaged across one oscillation. Using the relationship between the pressure amplitude and the average intensity $I = P^2/2Z0$ we get:

$$dI = \frac{PdP}{Z0} = -\frac{\sigma_e(w)P^2}{2Z0}ds \Rightarrow dP = \frac{\sigma_e(w)}{2}Pds \tag{3.36}$$

for constant extinction cross section we hence get for plane waves

$$I(w,z) = I_o \exp(\sigma_e(w)z) P(w,z) = P_o \exp(\frac{\sigma_e(w)}{2}z) \tag{3.37}$$

We write the frequency variation of the extinction cross section as

$$\sigma_e(w) = \sigma_a(w) + \sigma_s(w) = \sigma_{ao}((\frac{w}{w_o})^b + \sigma_{ro}(\frac{w}{w_o})^a) \tag{3.38}$$

where $\sigma_{ro} = \frac{\sigma_{so}}{\sigma_{ao}} \approx 0.15 - 0.2$ and $a \sim 2 - 4$ and $b \sim 1 - 1.5$

To get numerical values of the extinction cross section we relate this to the wave attenuation that is measured as

$$\sigma_e(w) = \frac{2log(P_o/P)}{zloge} \tag{3.39}$$

$2log(P_o/P) \sim \alpha dB/cmMHz \sim 10^2 dB/mMHz$ where α is typically 0.5. This gives
$2log(P_o/P) = (20loge)\frac{\sigma_e(w)z}{2} = 10^2\alpha z f_o$

$$\sigma_e(w_o) = \sigma_{ao}(1 + \sigma_{ro}) = \frac{10\alpha w_o}{loge2\pi}m^{-1} \tag{3.40}$$

Selecting a value for σ_{ro}, we get the extinction cross section as a function of angular frequency w for a burst of pressure oscillations transmitted with center angular frequency w_o

$$\sigma_e(w_o; w) = \sigma_{ao}(w_o)((\frac{w}{w_o})^b + \sigma_{ro}(\frac{w}{w_o})^a)m^{-1} \tag{3.41}$$

$\sigma_{ao}(w_o) = \frac{10\alpha}{(1+\sigma_{ro})loge}\frac{w_o}{2\pi}m^{-1}$
For $f_o = 8MHz$, and $\alpha = 0.5$, we get at w_o

$$\sigma_e(w_o; w) = \sigma_{ao}(1+\sigma_{ro}) = \frac{10\alpha w_o}{loge2\pi}m^{-1} = \frac{10 * 0.5 * 2\pi * 8}{loge * 2\pi}m^{-1} = \frac{92}{1 + \sigma_{ro}}m^{-1} \tag{3.42}$$

3.8.3 Simulation of the wave equation including the extinction cross section

Since ABERSIM has a potential to solve the diffraction, absorption, and the nonlinear distortion terms separately using the splitting approach [33], it simulates the wave equation with the extinction cross section . From Eq.(3.34) , we get for plane waves

$$\frac{dP(z,w)}{dz} = \frac{w}{2c_o}H_{abi}(w)P = \frac{\sigma_e(w)P}{2} \tag{3.43}$$

where the last relation is obtained comparing to Eq.3.36. We hence see that

$$H_{abi}(w; w_o) = \frac{-c_o}{w}\sigma_e(w_o; w) = \frac{-c_o\sigma_{ao}(w_o)}{w}((\frac{w}{w_o})^b + \sigma_{ro}(\frac{w}{w_o})^a)m^{-1} \tag{3.44}$$

This expression is inserted into the ABERSIM for simulation of the wave field.

3.8.4 Ultrasound radiation force (URF) simulation

We assume that we transmit a burst of pressure oscillations at center angular frequency w_o and duration Tp. From simulations of the pressure wave field with ABERSIM, we calculate the radiation force from equation (3.14) as

$$\bar{F}(0,z,w_o) = \frac{\Delta F(z,w_o)}{\Delta V} = \frac{1}{2\pi c Z_o Tp}\int dw \sigma_e(w_o;w) \mid P(z,0,w_o,w) \mid^2 (N/m^3) \tag{3.45}$$

where Tp is the pulse length and P(w,0,z) is the Fourier transform of the whole ultrasound pulse. We note that

$$cZ_o = \rho c^2 = \frac{1}{\kappa} \tag{3.46}$$

Inserting the expressions for the extinction cross section, we get

$$\bar{F}(0,z,w_o) = \frac{\sigma_{ao}(w_o)}{2\pi c Z_o Tp}\int dw((\frac{w}{w_o})^b + \sigma_{ro}(\frac{w}{w_o})^a) \mid P(z,0,w_o,w) \mid^2 (N/m^3) \tag{3.47}$$

We have made use of Perceval theorem

$$\bar{g}(\vec{r}) = \frac{1}{Tp}\int dt g(t;\vec{r})^2 = \frac{1}{2\pi Tp}\int dw \mid g(w;\vec{r}) \mid^2 \tag{3.48}$$

3.8.5 Comparison of URF to pressure gradient

A pressure $p(\vec{r},t)$acting on a surface S of a (fluid) volume V produces the following net force on the volume

$$\vec{F}(\vec{r},t) = \int d^2 r \vec{n} p(\vec{r},t)^2 = -\int d^3 r \nabla p(\vec{r},t) \tag{3.49}$$

where $\vec{n}$ is the outward unit normal to the surface S. For a small volume ΔV we approximate the volume integral as

$$\Delta\vec{F}(\vec{r},t) = -\nabla p(\vec{r},t)\Delta V \tag{3.50}$$

Comparing to Eq.(3.14) we see that the pressure gradient produces a similar volume force as the radiation force. This $\frac{\Delta F}{\Delta v}$ has the form of a pressure gradient with the unit Pa/m. Pressures in the body are usually measured in mmHg, which has the following relation to Pa/m
$1mmHg \sim \rho_{Hg} gh = 13546 * 10^3 Kg/m^3 * 9.81 m/s^2 * 10^-3m = 132.9 N/m^2 (Pa)$

3.8.6 Ultrasound thermal heating(UTH) on the tissue simulation

Energy delivered to the tissue is the amount of energy absorbed on the tissue from the propagation of the ultrasound wave. Hence it related to the intensity and the abortion cross section.Therefore, energy delivered to the tissue per pulse and unit length of the beam is

$$\frac{\Delta Q_h(z,w_o)}{\Delta z} = \frac{1}{2\pi Z_o}\int dw\sigma_a(w) \mid P(z,\vec{r}_\perp,w_o;w) \mid^2 Joule/m \tag{3.51}$$

Dividing this expression with the pulse length, Tp, we get power delivered, i.e. I Watt/m. This also holds for the rest of the expressions below. Inserting the expression for σ_a from equation (3.38), we get

$$\frac{\Delta Q_h(z,w_o)}{\Delta z} = \frac{\sigma_{ao}(w_o)}{2\pi Z_o}\int dw(w/w_o)^b \int d^2r_\perp \mid P(z,\vec{r}_\perp,w_o;w) \mid^2 Joule/m \tag{3.52}$$

We define the area of the beam as

$$A_b(z,w,w_o) = \frac{\int d^2r_\perp \mid P(z,\vec{r}_\perp,w_o;w) \mid^2}{\mid P(z,0,w_o;w) \mid^2} Joule/m \tag{3.53}$$

$\int d^2r_\perp \mid P(z,\vec{r}_\perp,w_o;w) \mid^2 = A_b(z,w,w_o) \mid P(z,0,w_o;w) \mid^2$
This allows us to write Eq.(3.49) as

$$\frac{\Delta Q_h(z,w_o)}{\Delta z} = \frac{1}{2\pi Z_o}\int dw\sigma_a(w)A_b(z,w,w_o) \mid P(z,0,w_o;w) \mid^2 \tag{3.54}$$

Energy per m^3 delivered to the tissue, averaged across the beam

$$\frac{\Delta Q_h(z,w_o)}{\Delta V} = \frac{\Delta Q_h(z,w_o)}{\Delta z A_b(z,w_o)}$$
$$= \frac{1}{2\pi Z_o A_b(z,w_o)}\int dw\sigma_a(w,w_o)\int d^2r_\perp \mid P(z,\vec{r}_\perp,w_o;w) \mid^2 Joule/m^3 \tag{3.55}$$

Applying the definition of A_b in Eq.(23,24) we get

$$\frac{\Delta Q_h(z,w_o)}{\Delta V} = \frac{1}{2\pi Z_o A_b(z,w_o)}\int dw\sigma_a(w)A_b(z,w,w_o) \mid P(z,0,w_o;w) \mid^2 \tag{3.56}$$

SI-units:$Nm/s = Watt, Nm = Joule = Watts$ To find the heating given by a pulse, the volumetric heat capacity for constant pressure of the tissue is approximately [42]

$$C_p = 4.2106 Joule/m^3 oK \tag{3.57}$$

3.8.7 Acoustic temperature on tissue simulation

A large challenge in calculation of the increase in temperature of the tissue, is that blood flow and thermal diffusion provides a strong transport of delivered heat to neighboring tissue, i.e.cooling. Neglecting the cooling of blood flow and diffusion, we can calculate the temperature increase from one ultrasound pulse as

$$\Delta T = \frac{\Delta Q_h(z, w_o)}{\Delta V C_p}$$

$$= \frac{1}{2\pi Z_o A_b(z, w_o) C_p} \int dw \sigma_a(w) A_b(z, w, w_o) \mid P(z, 0, w_o; w) \mid^2 oK \qquad (3.58)$$

To include the effect of cooling from blood flow and diffusion, we consider a fairly large region of the tumor. The scanning pattern and number of ultrasound pulses per unit time, will then give the heat energy delivered to the region, while blood flow (volume/sec) through the region presents heat energy removed from the region. We can assume that the heat capacity of blood and tissue is close to the same, but knowing the heat transfer coefficient from tissue to blood is essential.

4 Material and Methods

4.1 Introduction

In this section we will introduce the transducer used for the experiment and shows the measurment methods for describing the performance of transducer. Then we will describe the simulation set up method used for simulation of the URF, ultrasound thermal heating(UTH) on the tissues, and Temperature on the tissues. At last we will describe the methods and materials used in vivo experiment on mice.

4.2 Transducer performance

4.2.1 Presentation of the transducer

The transducer used on the experiment is called a 3D probe ans shown in figure 5b. It is used for imaging and therapy with ultrasound radiation force implementing on Ultrasonix SonixRP (Ultrasonix Medical Corp., Vancouver, Canada) scanner presented in figure 5a in a convectional imaging modality and a new therapy scanning modality software which is implemented by Department of Circulation and Medical Imaging[3]. It is designed and manufactured by Vermon (Tours, France, [39]) with a product name of LA 8.0/128/4D -1169, and has 128 elements in a linear array organized in a stack as show in figure 6. The general specification of the transducer is shown in the table 1. The transducer has also a lens for elevation focusing which is desired to transmit the highest energy to the focus. The probe has a capacity to scan mechanically in the elevation with a selected speed , and to the azimuth directions with in a chosen foci's depending the region of interest.

---

[3] Norwegian University of Science and Technology, Trondheim, Norway

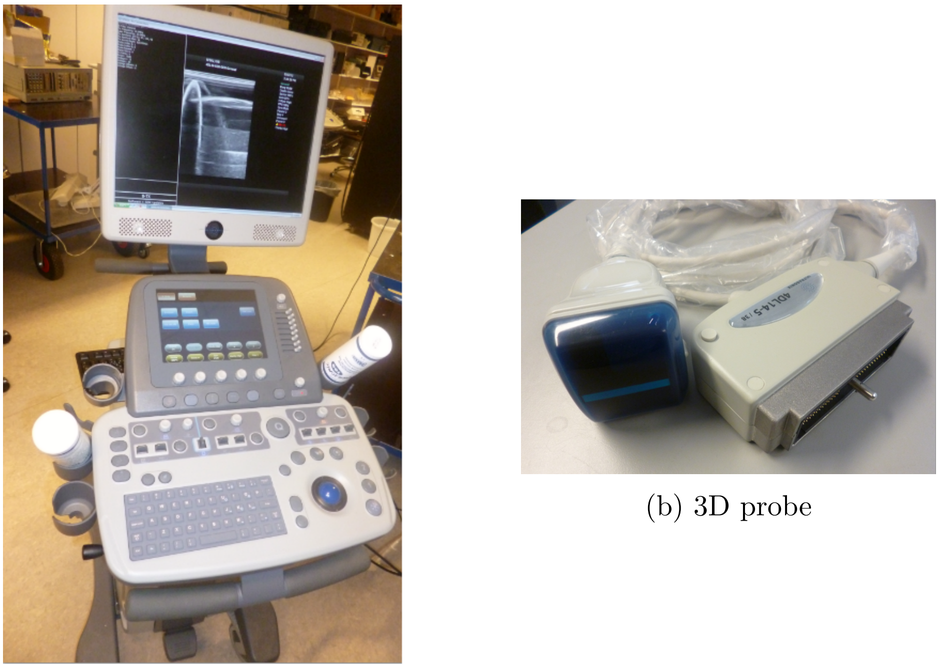

(a) Ultrasonic scanner

(b) 3D probe

Figure 5: The Ultrrasonic sonixRP scanner and the 3D probe

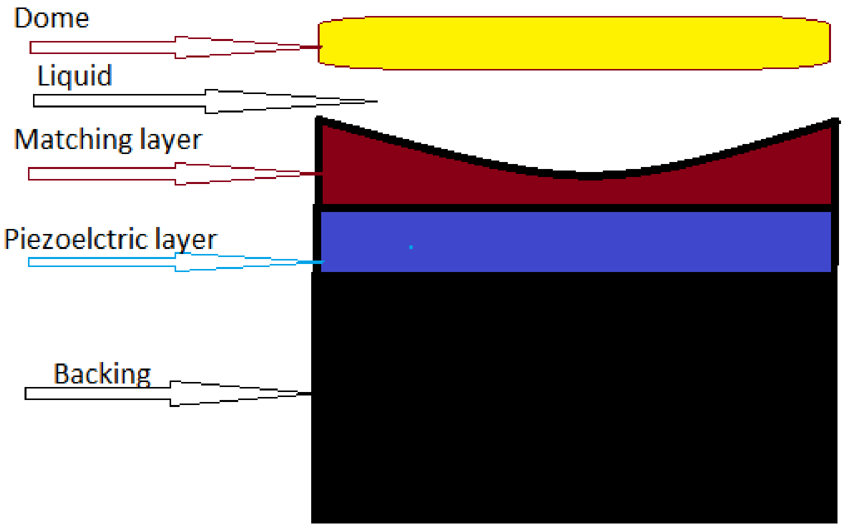

Figure 6: 3D transducer Linear array element stack [1]

Table 1: The characteristic specification of the transducer

center frequency	8 MHz
Band width	5.6MHz, > 70%
Number of elements	128 active
pitch	0.3mm
Elevation element width	5mm
Elevation focus	28mm

This is characteristic specification of the transducer from the manufacturer

4.2.2 Electrical impedance and Acoustic pressure measurements

The electrical impedance of the transducer element and the acoustic power propagating out of one transducer element when loaded in water were measured. The magnitude and phase of electrical impedance of the transducer, 128 elements, is measured using an impedance analyzer. The impedance analyzer that we used is Agilent 4294A Precision Impedance Analyzer (Hewlett-Packard, Palo Alto, CA). Before used, the instrument was calibrated when both in open and short states with load to compensate the impedance of the cables that used to connect with transducer's connector and the analyzer. A computer is used to analyze the data which was collected using a matlab software of the instrument.

The acoustic field generated by one elements were characterized by performing an acoustic measurement in degassed, deionized water with a 3 axis scanning system designed for use in the characterization and measurement of ultrasonic beams as shown in the set up figure 7. Since the transducer is loaded on the water, we can assume that the medium is homogeneous and linear medium which means that we neglect the absorption . A ten cycles pulse from a pulse generator ((Wave generator WW2571, from Tabor Electronics Ltd) was used to generate a $16V$ electric pulse centered at $8MHz$. Pressure wave form were collected using a calibrated 200μm diameter hydrophone (HGL-1426, Onda Corporation) and displayed on a LeCroy Xs44s digital storage oscilloscope. The measured pressure waveforms was in axial direction.

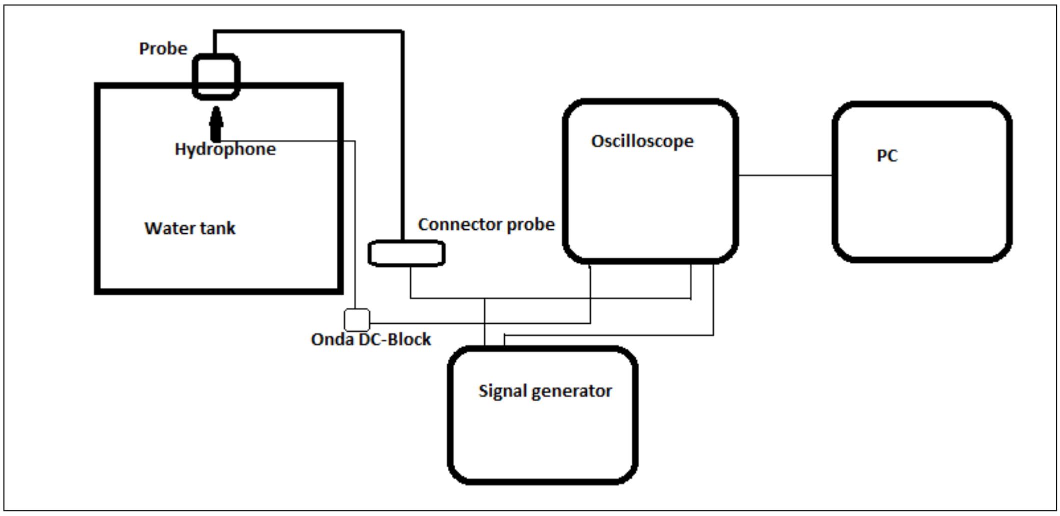

Figure 7: Acoustic pressure measurement set up in water tank using hydrophone.

4.2.3 Temperature measurement on the transducer

To experience the heating of the transducer, a temperature measurement was done when the probe is loaded to air, and to a glove of water similar to the set up for our real experiment. The measurement of temperature on the transducer surface was done using temperature Sensor: Omega HH147, RS232 Data Logger Thermometer, with K probes, affixed to front of probe (on the dome) avoiding any contact from the acoustic out put wave, and on the side of the probe , by doing some gel and tape to improve contact .The transducer was driven by the Ultrasonix SonixMDP ultrasound scanner. The set up of the experiment is shown in figure 8. Moreover, we measured the surface temperature with a Fluke Ti10 IR-thermographic camera of range 8-14μm to get some information on the heating exactly inside the elements in addition to the after mentioned measurements. We measured the temperature by varying the input power, duty cycle, and the aperture using the scanner.

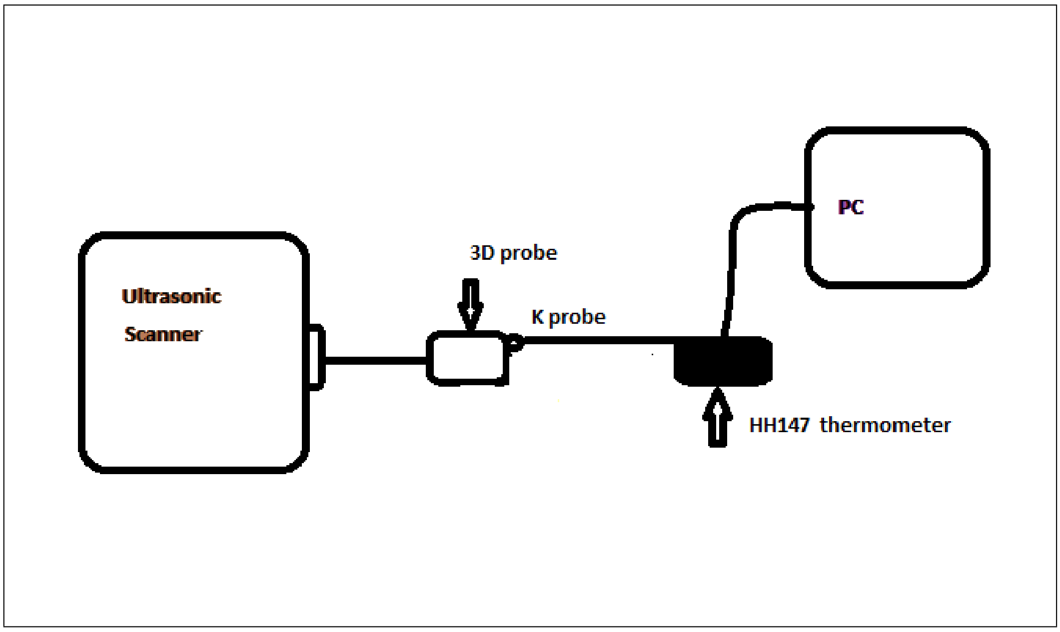

Figure 8: Temperature measurement set up on the transducer using temperature Sensor: Omega HH147, RS232 Data Logger Thermometer with K probes affixed to front of probe

4.3 Simulation of beams

4.3.1 Set up and Procedures of the simulation of URF, UTH, and Temperature on the tissue in ABERSIM

The full 3D non-linear wave propagation of the pulses were simulated with ABERSIM based on the procedures of reference [33]. The matlab code version of R2010a used for the simulation is shown in appendix C. The simulation is done based the pulse characteristic of the transducer and the tissue characteristics shown in table 2 and 3 respectively.

Moreover, the frequency dependent absorption coefficient used in this simulation are also in table 4. Although we implemented a prostate cancerous cells on the leg of the mice in our experiment, the tissue parameters as shown in table 3 are selected based on the average properties of the soft tissues. Because, most of the propagation distance takes place in water but only approximately 3mm focal depth on the tissue. And the simulation method has also a lack of capacity to simulate the propagation according to specific boundary properties of the medium . Therefore, it is reasonable to use the average properties of the tissue than the specified tissue parameter for the whole propagation distance.And the attenuation constant of the health prostate tissue is found to be $0.78 \pm 0.24 dB/MHz.cm$ [43] which could affect the result of our simulation with small magnitudes. Hence, our simulations are an approximation values. The parameters such as acoustic pressure output, pulsed duration, pulse repetition frequency, and duty cycle were chosen based the performance of the transducer.

In addition, the acoustic pressure beams at focus (25mm) was characterized using hydrophone in water tank following the previous procedures except that the probe is connected with the scanner, for half aperture with single pulse, and for 14.4mm (48 elements) aperture with 48cycles where both were driven with 22volt amplitude at 8MHz. The measurements were done both in azimuth and elevation directions. The set up is the same to figure 7, except that the transducer was connected to the scanner.

Table 2: The pulse characteristic of the transducer

center frequency fc(MHz)	5-11
Number of periods Np	10
Number of elements	32 - 128
Azimuth Aperture (Da (mm))	9.6-38.4
Focal length in azimuth (Fa(mm))	25
Focal length in elevation (Fe(mm))	25
Acoustic pressure output (Po(MPa))	0.15
Pulse duration($T_{on}(\mu s)$)	1.25
Simulation resolution in elevation (mm)	3.10^{-4}
Simulation resolution in azimuth (mm)	3.10^{-4}
Simulation resolution in axial (mm)	1.10^{-3}

The pulse characteristic of the transducer used ABERSIM simulation. The frequencies and the focus are selected based on the band width of the transducer and elevation focusing respectively. While the other parameters are depending on the performance of the transducer.

Table 3: Average acoustic parameters values for soft tissues

	$c_o(m/s)$	$\rho(kg/m^3)$	$\kappa(10^{-12}Pa^{-1})$	β_n	$Cp(10^6 JoK^{-1}m^{-3})$
	1561	1060	420	3.9	4.2
Reference	[44], [43]	[44]		[32]	[42]

Since most of the propagation distance takes place in water but only approximately 3mm focal depth on the prostate tissue, we used average tissue acoustic characteristic in ABERSIM simulation.

Table 4: The frequency dependent attenuation coefficient

$\alpha dB/cm.MHz$	α_{ro}	a	b
0.5 [44]	0.15	2.5	1.1

The frequency dependent attenuation coefficient used in ABERSIM simulation, where, $\alpha_{ro} = \alpha_{so}/\alpha_{ao}$ is ratio of the scattering attenuation constant to absorption attenuation constant, a is the frequency- power exponent for scattering, b is the frequency- power exponent for absorption. The values of the α_{ro},a, and b are chosen for having maximum URF

4.4 Animal experiment

4.4.1 Mice and Tumors

The experiment is done on Female Balb/c nude mice (C.Cg/AnNTac-Foxn1nu NE9, Taconic, Denmark) based on the apparatus below and PC-3 prostate adenocarcinoma cells (American Type Culture Collection, Manassas, VA, USA) which were cultured in Dulbeccos Modified Eagle Medium (Life Technologies Corporation, Carlsbad, CA, USA) with 10 % FBS at $37C$ and $5\%CO_2$ were injected on the one hind leg between the hip and the knee. All the procedures were done based on reference [45], hence, a more detailed procedure of the preparation of the cells and injection to the mice can be found at that reference. The size of the tumor on the each mice exposed to the ultrasound were measured and shown in table 5.All the tumors have an elliptical shape as shown in figure 9 with an average dimension of their volume of 15mm in axial, 22mm in azimuth and 7mm in elevation.

Table 5: Size of the tumor measured, and set up for the therapy scanning.

Parameters	Mouse192	M. 193	M. 194	M. 197	M. 198	M. 201
Drug	Dox	Dox	Dox	NP	NP	NP
Depth (mm)	25	22	24	24	25	25
Axial size of tumor(mm)	16	14	16	16	14	12
Azimuth size tumor(mm)	24	20	19	26	24	20
Elevation size tumor(mm)	6	8	9	8	5	6
Number of foci)	5	5	5	5	5	4
Length of focus F1(mm))	19	19	19	19	19	22
Length of focus F2(mm))	22	22	22	22	22	25
Length of focus F3(mm))	25	25	25	25	25	28
Length of focus F4(mm))	28	28	28	28	28	31
Length of focus F5(mm))	31	31	31	31	31	

The table shows the sizes of the tumor measured using 3D-mode imaging, and set up for the therapy scanning.The number of focus are found from the axial beam width, and their positions are chosen depending on the elevation focus. Note: Dox is doxorubicin, NP is PBCA nanoparticles , and M is mouse. Depth is the distance from the surface of the probe to the center of the tumor.

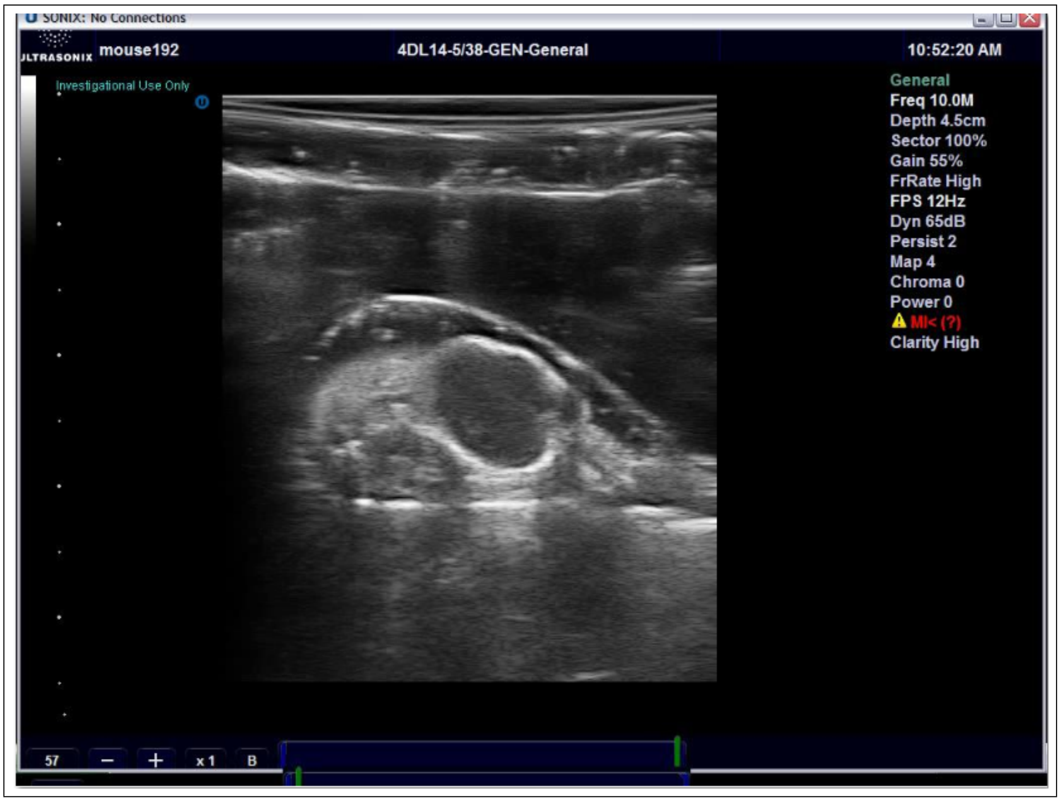

General
Freq 10.0M
Depth 4.5cm
Sector 100%
Gain 55%
FrRate High
FPS 12Hz
Dyn 65dB
Persist 2
Map 4
Chroma 0
Power 0
⚠ MI< (?)
Clarity High

Figure 9: B-mode Image of one of the tumors exposed to radiation force. The figure shows the size and positioning of the tumor during the experiment.The elliptical shape of the tumor describes the azimuth and axial dimensions of the tumor center at 25mm from the surface of the probe.

4.4.2 Drugs

Doxorubicin is a cytotoxic drug used in chemotherapy, and has also fluorescent substance which is useful to observe the distribution and penetration of the drug on the target region during confocal microscopy analysis. The halve-life of dox is from 12 to 18.5 hours when released from libosomes [46]. It was administered at a dosage of 10 mg/kg, and at a concentration of 1 mg/kg. Since the mice had a body weight of 20 g, they were given 200 ul intravenously.

Poly(butylcyanoacrylate) (PBCA) nanoparticles which is a drug used for treatment of tumors in the brain, was obtained from SINTEF [4]PBCA nanoparticles. Its size is around 100nm, and do not contain any cytotoxic drug, hence they are labeled with the fluorescent dye Rhodamine 6G to

---

[4] Company for Scientific and Industrial Research, NTNU

observe the distribution and penetration of the drug on the target region using confocal microscope. The concentration of the drug administered intravenously on the mice was 6,2 mg/ml and 200 ul.

4.4.3 Ultrasound Exposure Set-Up and Treatment

The traducer presented in section 4.2.1 was used for insonfication of the tumor. The transmit frequency of the transducer is 8MHz, and have acoustic intensity at the focus of 20.94 W/cm^2 with a peak negative pressure of 0.5MPa as described in table 8. It was connected to the ultrasonics RP scanner and in contact with a water bag in which the water was deionized and degassed by boiling and was at room temperature at the time of ultrasound exposure. The bag has an acoustic characteristic impedance of water so as to reduce the reflection, hence absorption, of the sound wave from and in the water bag. And a gel was placed between both the tumor and the water bag, and the water bag and the transducer to have good acoustic contact.

The ultrasonic RP scan was used for 3D imaging using the sonix soft ware for imaging using that transducer for positioning and measuring of the tumor size both in azimuth and elevation directions,and for therapy scanning. The therapy software which is developed by Department of Circulation and Medical Imaging[5] has a capacity to scan in multi foci's depending on the axial tumor size at one azimuth to have a constant intensity over the whole irradiated tumor area, and we used one element steps which is 0.3mm in azimuth scan plane to avoid any untreated regions and have a concentrated beams due to the small magnitude of the heating resulted from the simulation which hardly cause cavitaton on the tissue, and also to run the probe mechanically in the elevation direction (normal to the azimuth plane) (with a beam width of 1.5mm) from -20^o to 20^o depending the size of the tumor in the elevation direction with a constant speed.This means that with one scan, it will cover an area of $0.45mm^2$ of the tumor. And the number of foci's are selected based on the -6dB axial beam width of the URF which is 3mm, as shown in table 5.

The mice were administered with Dox and PBCA nanoparticles drugs intravenously via the vein during the treatment as described in terms of groups and group sizes in table 6. Half of the mice were exposed to ultrasound radiation force prior to injection, while the other half were unexposed controls. The URF is done immediately after the administration of the drug since the circulation time for the drug to be on the target region with high concentra-

---

[5] Norwegian University of Science and Technology (NTNU), Trondheim, Norway

tion will not take longer time.

The duration of the ultrasound exposure was 10 minutes means that with a duty cycle of 1.25%,hence,with the effective exposure of 7.5 seconds . And for the mice that did not get URF, the drugs were also allowed to circulate for 10 minutes. After completion of the ultrasound exposure a bolus of 100 ul at a concentration of 1 mg/ml of fluorescent (FITC-lectin) which is a photosensitive material, were given intravenously to label the blood vessels [45] for visualizing blood vessels in the microscope, followed by preparation of frozen tumor sections for analyzing using confocal microscopy.

The mice were given surgical anesthesia by a subcutaneous injection of Hypnorm and Dormicum and placed in a flat table into the insonfication area where the center of the tumor was aligned by guiding through imaging so that the tumor was located in the area of maximum intensity of the sound waves, as illustrated in figure 10. Each mouse then received an intravenous injection of their respective drugs via the vein and thereafter was exposed to URF.

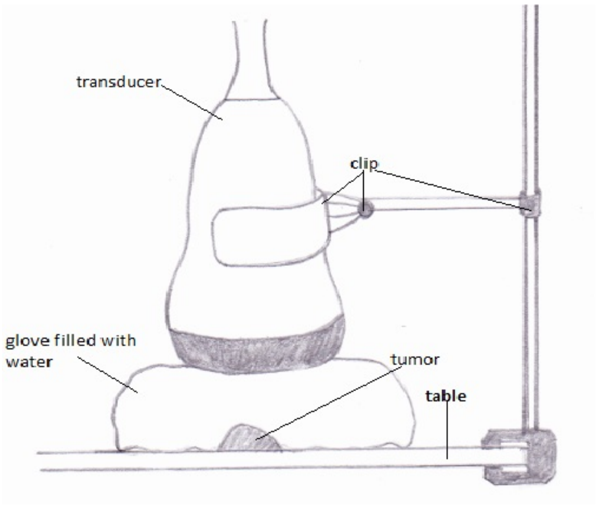

Figure 10: The figure demonstrates an overview of the set up of the experiment (the scales are not correct). The anesthetized mice are situated on the flat table and a water bag with gel in both its upper and lower side of the water bag for acoustic coupling with the ultrasound transducer. The transducer is in contact over the upper part of the water bag and generates a focused pulses to the mice.

In addition, the temperature of the tumor were measured both before and around 20 seconds after isonfication to determine the increase in temperature on the tumor tissue due to ultrasound radiation force exposure.

Table 6: The experimental description of the groups and group sizes of the mouse studied in the experiment

Group 1	3 mice	Doxorubicin	URF
Group 2	3 mice	Doxorubicin	-
Group 3	3 mice	PBCA nanoparticles	URF
Group 4	3 mice	PBCA nanoparticles	-

4.4.4 Confocal laser scanning microscope

For studying the effect of the ultrasound radiation force on the distribution of the released doxorubcin , PBCA nano-particles and blood vessels using confocal laser scanning microscope CLSM (Leica SP8, Jena, Germany), the frozen tumor were made in tumor sections after insonfication and embedded in OTC Tissue Tek and frozen in liquid nitrogen. Tumor sections were made at five depth levels, with 25 μm between each level. Then, the tissues were placed in microscopic slides and imaged with confocal laser scanning microscopy using an objective of 20x/0.7 using a tile scan function.The image were taken along a radial track from the periphery through the center to the other periphery with a resolution of 512 X 512 pixels. The image size of each section are 581.25x581.25 μm, hence, pixels sizes of 1.14 x 1.14 μm.

Doxorubicin and FITC-bound lectin was excited using 540nm helium/-neon and 488 argon laser lines respectively, and detected in the range of 560-650 nm and 500-550nm respectively. While the nano paricles was exited using 510nm helium/neon laser line and detected in the range of 510-570nm. During the image acquisition all the necessary settings such as laser current, transmission, detector gain, and amplitude gain and amplitude offset were chosen to minimize noise and to use most of the gray scale.

5 Results

5.1 Result about 3D probe performance

5.1.1 Electrical impedance

For computing the input power and efficiency of the transducer, knowing the electrical impedance of the element is very essential as equation (3.21) shows. Therefore, the electrical impedance of each element of the transducer at the connector is first measured using the impedance analyzer are shown in figure 11a. At 8MHz, the magnitude of their impedance are distributed from 32 to 50 Ω and phase of -55 to -32°. For the 64th element for example, has a magnitude of 32 Ω and phase -50 ° as shown in figure 11b. To estimate the impedance of the transducer at the electrodes, three different models for the the 2.15m coaxial cable of capacitance 60pF/m and characteristic impedance of 80Ω are used. The electrical impedance of one element estimated on the electrode is hence shown in figure 11b. It is found that the transmission and the π models gave us approximately the same values while the capacitance model is off from the two models. However, since we driven with the high frequency which is 8MHz in the experiment, it is reasonable to approximate the 2.15m coaxial cable to a transmission model than the other two models used on the computation. Hence, the magnitude and phase of the electrical impedance of the element at 8MHz is found 86 Ω and -64°. These numerical value was used in all our computations.

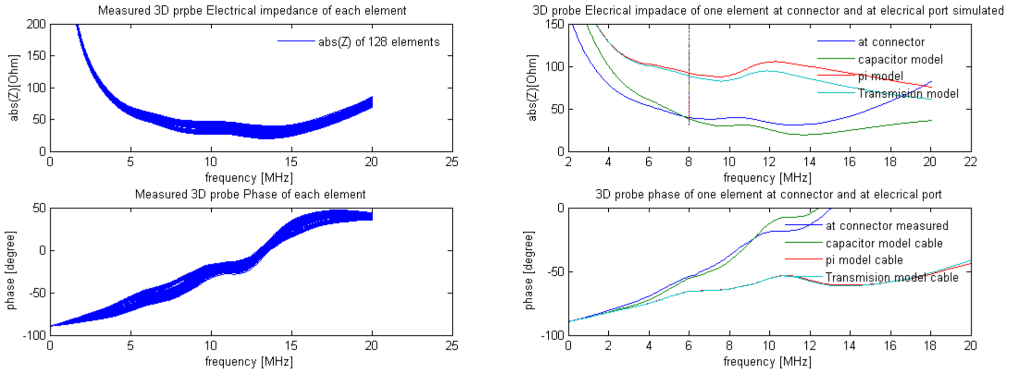

(a) Electrical impedance measured for all elements

(b) Estimated electrical impedance of one element

Figure 11: Electrical impedance of each element of the transducer measured on connector, and estimated for one element on the electrode using three models assumption for the cable: 1) the cable as a capacitor, 2) the cable as a π-model ,and 3) the cable as a transmission model.

5.1.2 Power dissipated on the transducer

In order to compute the power dissipated on the transducer, we computed the driven voltage on the element as shown in figure 12b, hence the power input on the transducer based equation (3.21). The driven voltage on the electrode is estimated from the electrical transfer function as show in figure 13 using eq.(3.23) and found to be approximately twice of the input voltage at the connector. In addition, as shown in figure 14a, we measured the acoustic pressure at 1.5mm from the surface of the transducer from the axial beam measured, and found 94 kPa at 8MHz center frequency, and the axial beam profile which is the root mean square value of the pressure from 10 elements of the transducer is shown for further information in figure 14b.

The acoustic pressure measured from the 10 center elements is used for estimation of the surface acoustic pressure of the probe from one element. Since the elements are excited from a signal generator, the beams are unfocused , hence, on the far-field region of the beam the amplitude of the beam falls off gradually from the main lobe of the beam due to diffraction. The far-field region from the 10 elements with 0.3mm in azimuth and 5mm in elevation direction each as shown in table **??** of the transducer will be around ($r_f = D_a^2/(2\lambda)$) is 23mm , whereλ is the wave length of the wave, and D_a is the azimuth of the transducer.

Hence, at around 1.5mm from the surface of the probe, we will be on the extreme near-field region of the beam ,i.e$r_f/4 = 5.75mm$, in which the beam will have less diffraction and will be more less constant for a homogeneous medium, so that the surface pressure of the transducer element is approximated to that pressure, and hence computed the output acoustic power using the estimated surface acoustic pressure. From these computations we estimated the power and heat dissipated on the transducer as show in figure 15 .

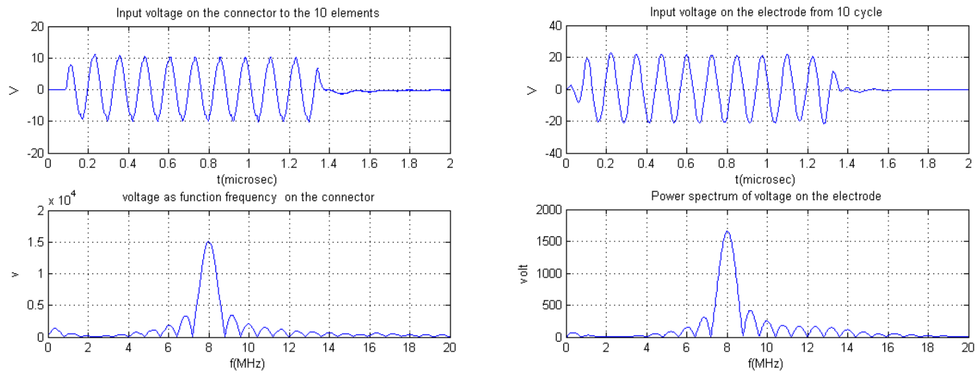

(a) Voltage on the connector

(b) Voltage on the electrode

Figure 12: Voltage input on connector and on electrode respectively . The input voltage is measure while the voltage on the electrode is simulated using the electrical transfer function from the connector to the electrode

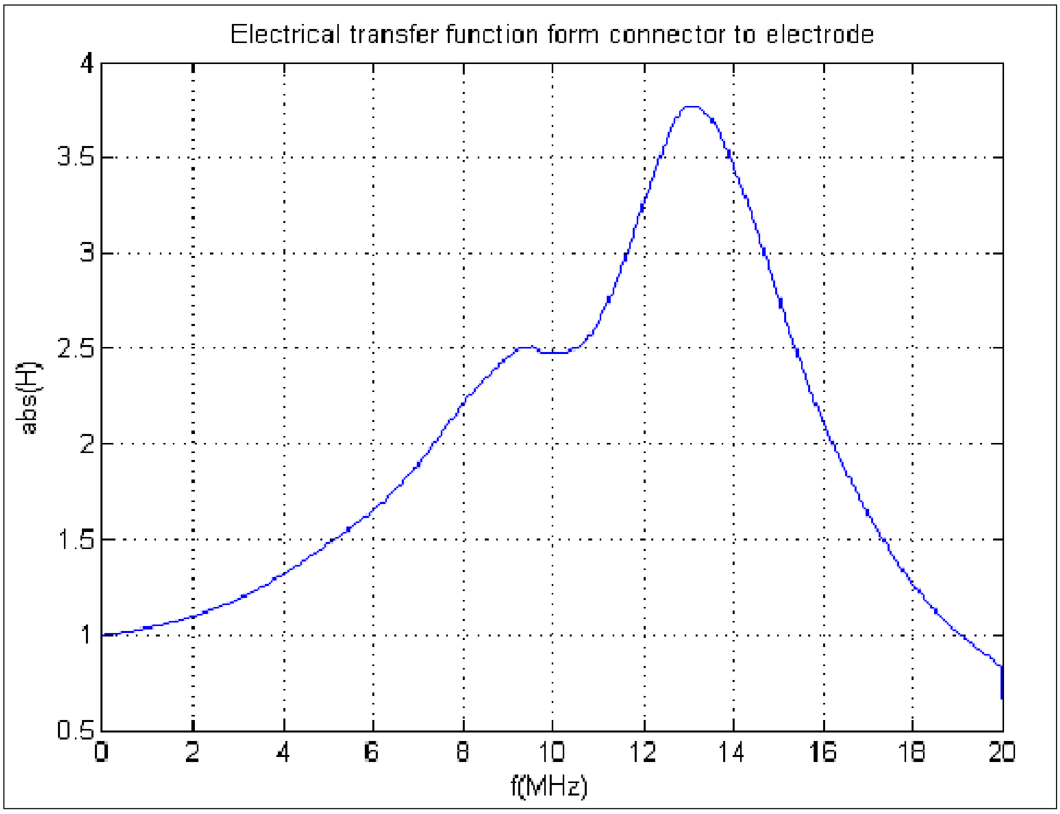

Figure 13: The electrical transfer function from the connector to the electrode simulated using the impedances

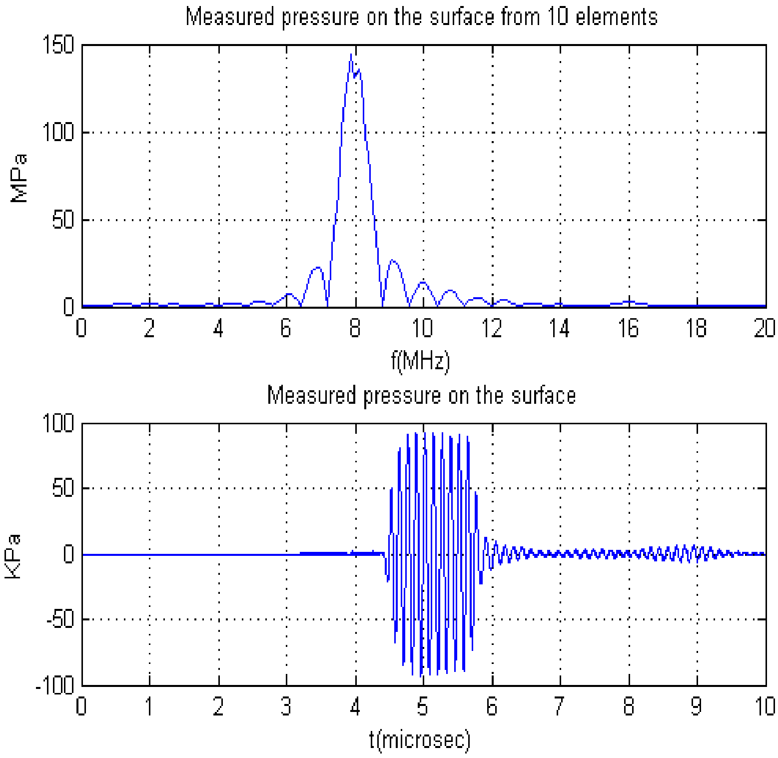

(a) Pressure on the surface of the transducer

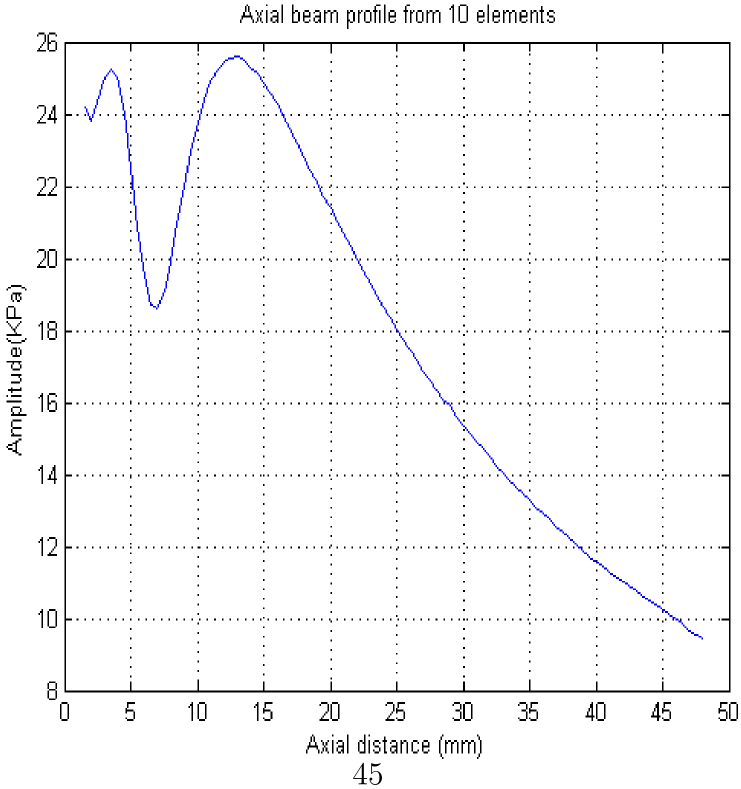

(b) The axial beam profile of the pressure measured from the 10 elements

Figure 14: Pressure on the surface of the transducer estimated and the axial beam profile of the pressure measured from the 10 elements by exciting with 10.9V on the connector (22V on the electrode) of 8MHz center frequency. The surface pressure found is 94kPa.

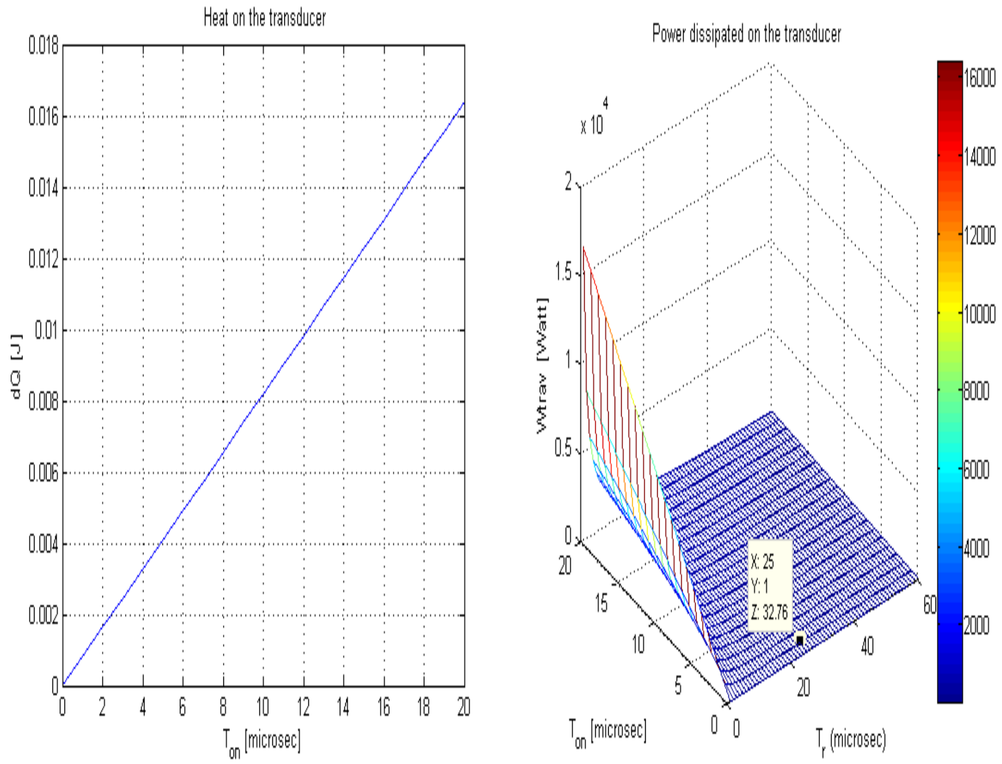

(a) Heat delivered on the transducer from 48 elements

(b) Power delivered from 48 elements

Figure 15: Heat and Power delivered on the transducer from 48 elements at 8MHz of 22V amplitude on the electrodes (or 10.9 V on the connectors). The power delivered is as function of on time (Ton) and repetition time(Tr)

An estimation of the power and heat dissipated on the transducer as shown in figure 15 has been obtained from the measured total acoustic power output when loaded into water combined with an estimate of the transducer's efficiency and the input electrical power to the transducer.The input electrical power of the transducer can vary depending on the driven voltage and frequency. Similarly, the efficiency of the transducer really dependent on the design and material property of the transducer, and also on the bandwidth of the transducer. Therefore, when the transducer element is excited with 10 cycles pulse of 10V amplitude on the connector (22V on the electrode calculated from the electrical transfer function show in figure 13) at 8MHz frequency, we got an electrical input power of 17.1Watt per element, and an acoustic power of 53.4mWatt per element. Hence, we have got an efficiency of 0.31% as shown in figure 16. These estimations were obtained from measurements of electrical power delivered to the transducer, and measured total acoustic power [38] .

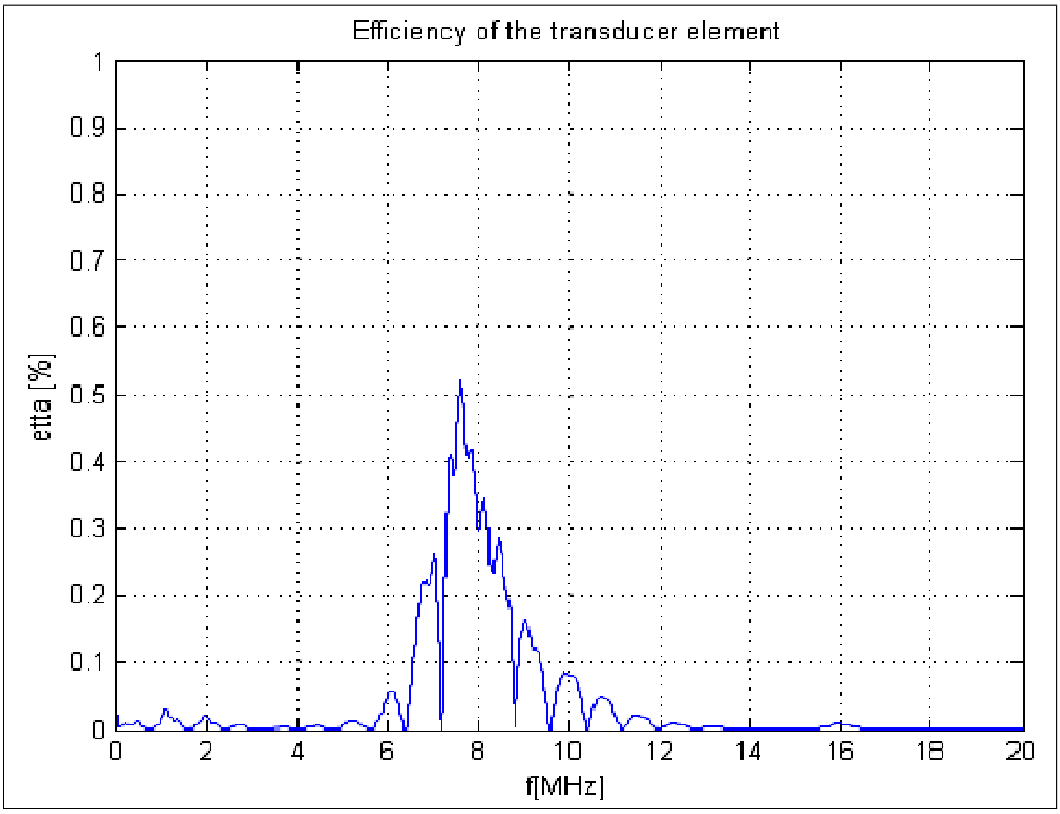

Figure 16: Efficiency of one element of the transducer estimated at 8MHz. This evaluated from the input electrical input power and the acoustic out put power at 8MHz transmit frequency of the transducer, and is found 0.31%

The power dissipated on the transducer as function of driving voltage on the electrode and duty cycle is show in figure 17. These were evaluated based on equation (3.28) except that the driven voltage is a peak voltage but not frequency dependent voltage. From this measurement, we see for instance at 35V with duty cycle of 5% that, 7 Watt of power will be dissipated. However, it is not easy to determine the effect of this amount of power on the transducer with out having a clear picture about the material properties of the probe. Hence, to understand and answer the above question we did temperature measurements .

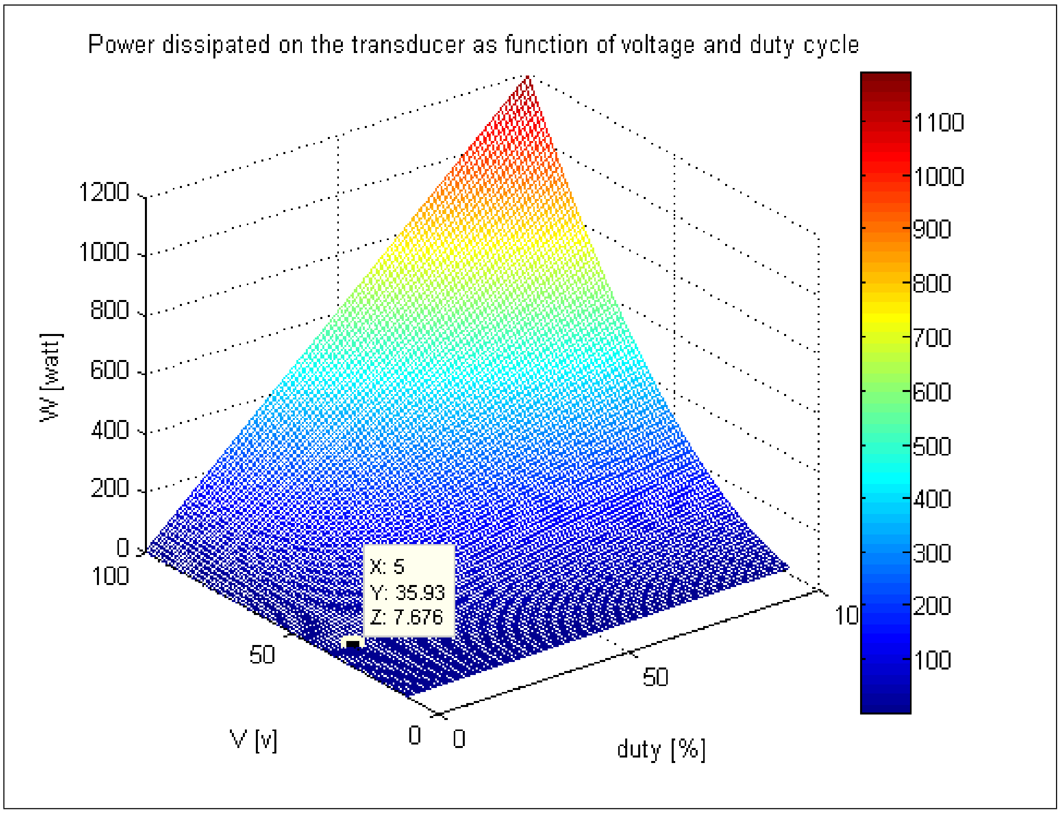

Figure 17: The power dissipated on the transducer of 48elements with respect applied voltage on the electrode

The surface pressure estimated per element on the transducer as a function of amplitude voltage on the connector is shown in figure 18. Transducer is a linear time invariant system, hence, the surface pressures has a linear dependence on the driven voltage, and was calculated for varies driven voltages from the surface pressure measured at 10V as shown in figure 14a.

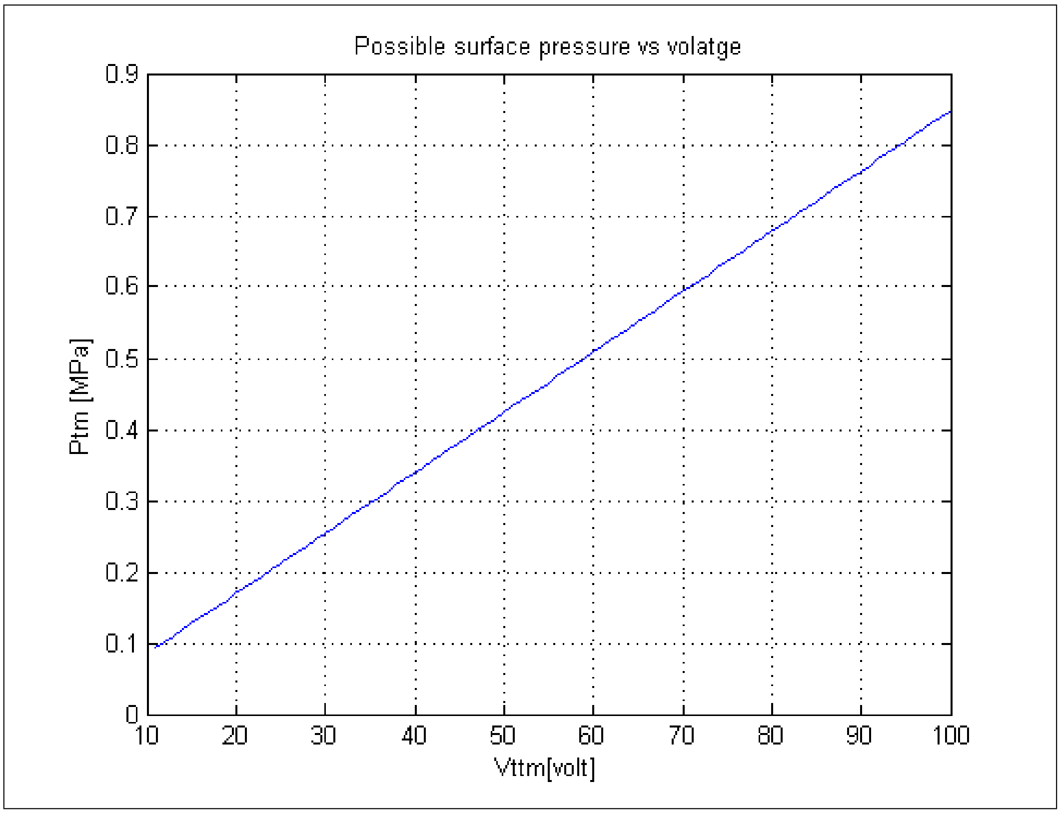

Figure 18: surface pressure estimated per element on the transducer as a function of amplitude voltage on the connector. This is estimated from the measured acoustic pressure driven by 10V. Hence, we found the surface pressure of 0.15MPa for 18V .

5.1.3 Temperature measurements for the 3D probe

The temperature of the transducer is one of the key element for characterizing the performance of a transducer. If the heat capacity of the transducer materials are known, we can easily convert the estimated dissipated power to the temperature to see the change in temperature on the surface. Hence, we experienced the increase in temperature of the traducer surface with time by varying the input power and the aperture of the transducer with different duty cycles.

The increase in temperature of the 3D probe surface with respect the driving voltage and duty cycle for a certain duration measured for the full and half aperture size of the probe when loaded in air are shown in the figure 19 and 20 respectively. And we have got maximum increase in temperature of 22^oC and 20^oC from 2μsec pules length and 3.3% duty cycle driven by

45V (41.5Watt $\sim 21.8 Watt/cm^2$) , and 6μsec pules length and 6.5% duty cycle driven by 45V(41.3Watt $\sim 43 Watt/cm^2$) from the full and half apertures respectively. In addition, we see that when the driven voltage is 25V with 10% duty cycle (39.2 $\sim 20.4 Watt/cm^2$) for the full aperture, and to 30V with 10% duty cycle (28.2Watt $\sim 29.4 Watt/cm^2$) for the half aperture , the maximum temperature is around 50^oC. The voltages were read directly converting from the power level index of the wikisonix document [47].

Moreover, as shown in figure 21, the temperature increase experienced from the 48 elements when loaded in water bag was 5^oC when we increased the driven voltage to 36V (voltage were monitored using a $1 MOhm 10$: 1probe and a LeCroy Xs44s digital storage oscilloscope), which seems reasonable due to the cooling.

However, the inside surface temperature on the elements measured with IR-thermographic camera using a scheme of 20 volt and 18 volt amplitudes with 10cycles pulses of 1.25% duty cycle for an aperture size of 14.4mm (48 elements) settings also resulted to a raise of the temperature to 57^oC in 5min , and 53^oC in 10min and remained constant. One example of such measurement is shown in figure 22. The image shows the distribution of the heat on the active elements of the array.

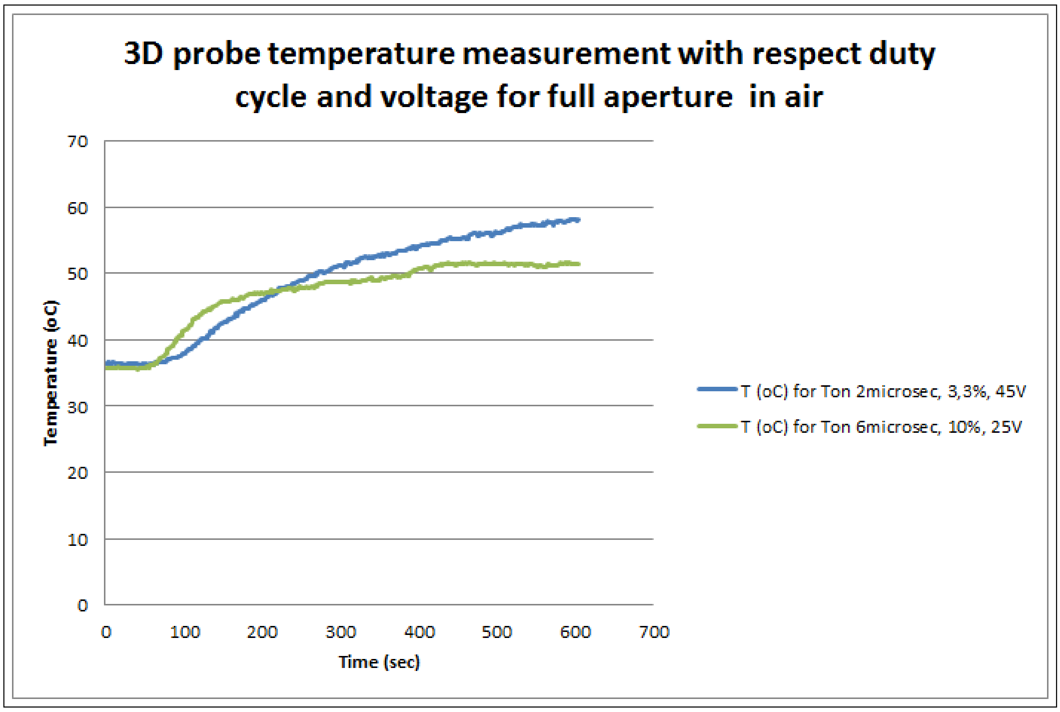

Figure 19: Temperature measured on the probe when loaded in air for full aperture.Note: Ton is the time at which the pulse is on

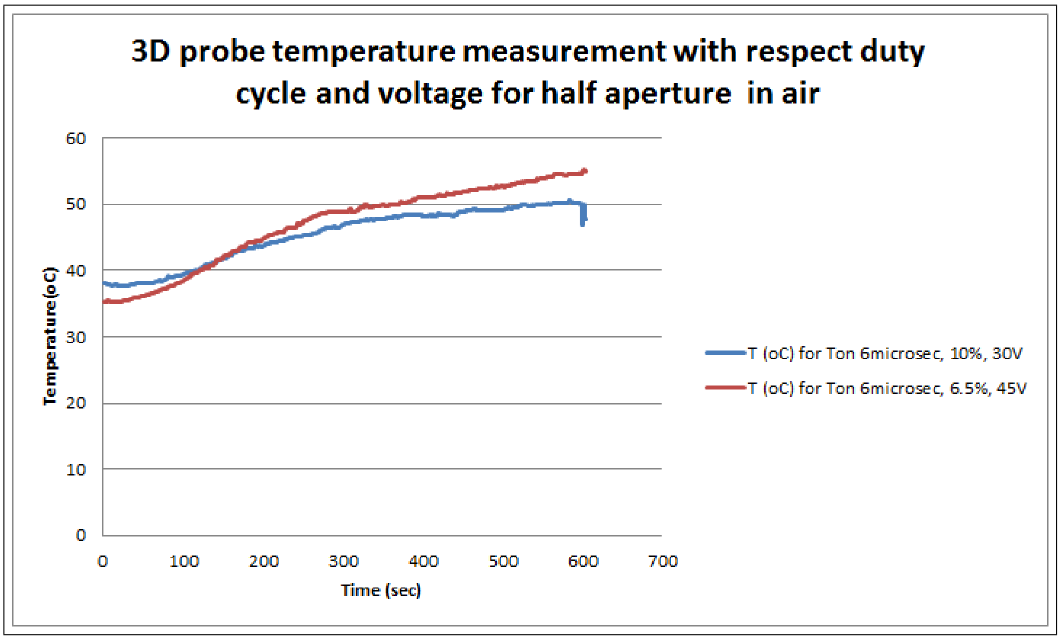

Figure 20: Temperature measured on the probe when loaded in air for half aperture.Note: Ton is the time at which the pulse is on

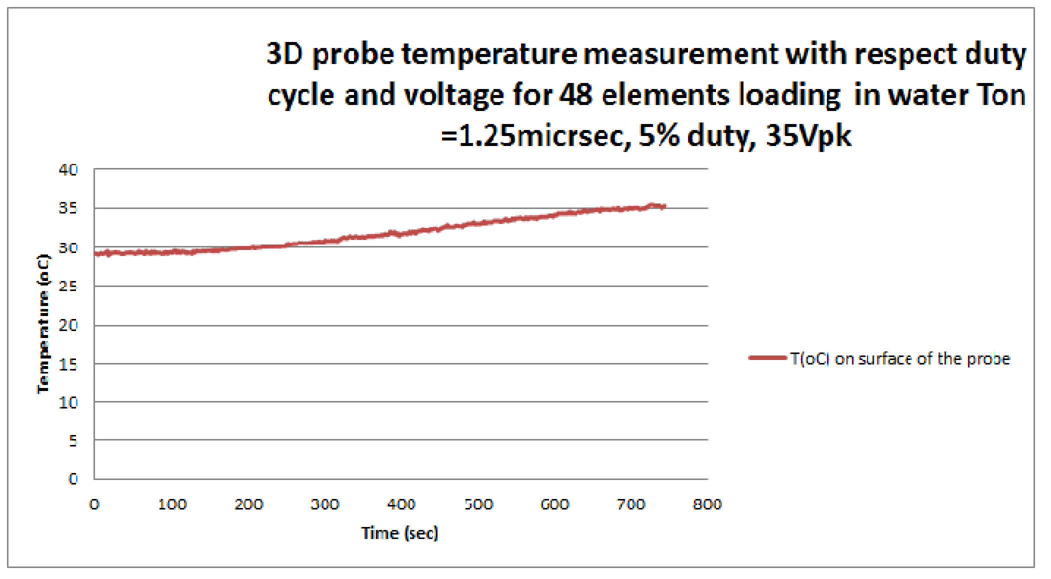

Figure 21: Temperature measured on the probe when loaded in water for 14.4mm aperture (48 elements) :Note that, Ton is the time at which the pulse is on, the voltage is a peak voltage and was monitored using a $1MOhm10:$ 1probe and a LeCroy Xs44s digital storage oscilloscope.

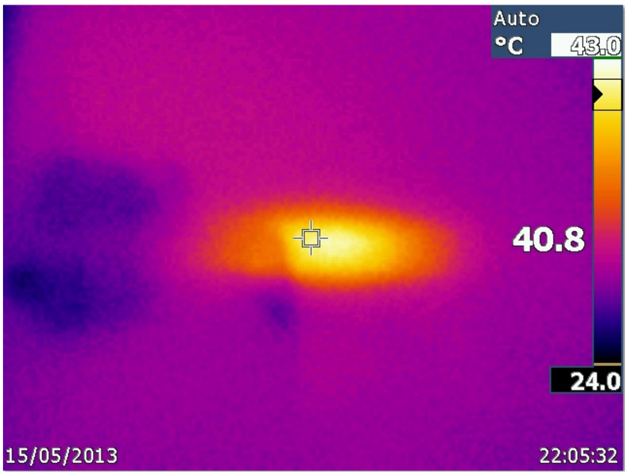

Figure 22: Thermal image of 4DL probe, showing heating of active elements of array. Dark area to left shows the thermocouple sensor affixed to the probe.

5.2 Results from beam simulations

5.2.1 Beam Profile simulated and measured using water tank

The measurement in water tank, and simulation for the beam profiles in the azimuth and elevation planes allows for understanding of the azimuth and elevation beam widths induced on the focal plane.The measurements were done for 19.4mm aperture(64 elements) and 14.4mm aperture of (48 elements) driven by an amplitude voltage of 22V at 8MHz center frequency as shown in figure 23 and 25 respectively. An ABERSIM simulation was done for the azimuth and elevation directions with water acoustic properties for 14.4mm aperture of (48 elements) as shown in figure 25 and table 7, but for both directions, we found a large difference between the measured and simualted results. In the elevation direction, the deviation is occurred due to the elevation focus with lens which was focused at 28mm depth.

While for the azimuth direction, the deviation from the measurement could possible also be affected by the size of the active elements of the array which could be smaller than the pitch (the distance between two center elements) of the element 0.3mm, since we don't know how much kerf (the spacing between two neighboring elements) are used. In addition, the elevation focus due to lens has also impact on the result of the azimuth width of the measurement. From the two results, we have got the -6dB beam widths measured of 1.5mm azimuth and 2mm in elevation on the focus for both apertures while 0.4mm and 1mm in azimuth and elevation from the simulation respectively as shown in tabel 7.

From the rf pressures shown in figure 24 for the 19.4mm aperture and 26 14.4mm aperture, we found at the focus a +1.6MPa and -0.5 MPa pressure, and +1.3MPa and -0.6 MPa pressure respectively and found until 6th harmonics which possible can increase the extinction cross section, hence the ultrasound radiation force. Similarly, as we see on the pulse form on the focus from the ABERSIM simulation in figure 27b, we only observed until 1st harmonics (even until 2nd) with almost negligible distortion of the beam, but this was due to the low initial surface pressure (figure27a) as it is proven in figure 28b with large surface pressure (28a) but with the same setting of the other parameters. As equation (3.8), the pressure in focus is proportional to the area of the transmuting aperture, the pressure from the 14.4mm aperture is hence decreased by a factor of 0.7 which is the ratio of their azimuth diameters. The mechanical index (MI) becomes 0.2 which is a measure of the potential that can induce cavitatin in tissues. Figure 31 also shows the propagation of the beam from the ABERSIM simulation, hence describes the shape of the beam profile over the whole medium.

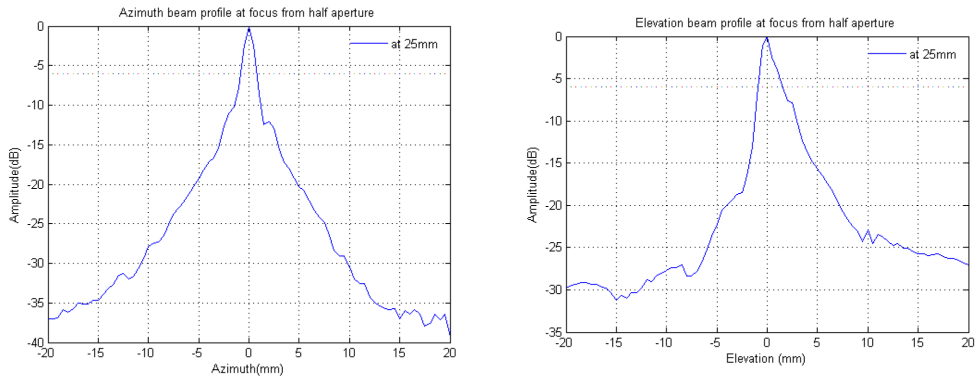

(a) Azimuth beam profile

(b) Elevation beam profile

Figure 23: Azimuth and elevation beam profile at focus of 25mm for half aperture measured in water driven with 22V amplitude from a cycle pulse

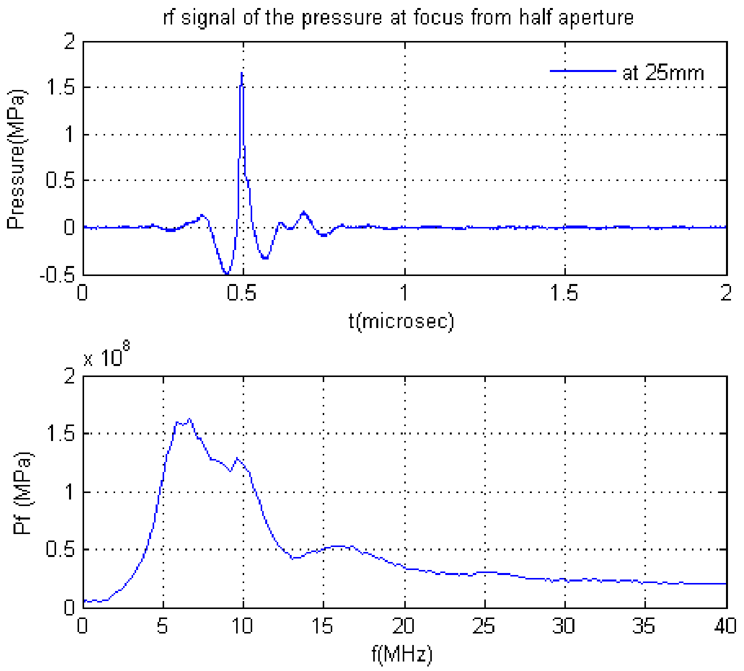

Figure 24: rf signal and frequency spectrum of pressure on focus of 25mm measured in water driven with 22V amplitude

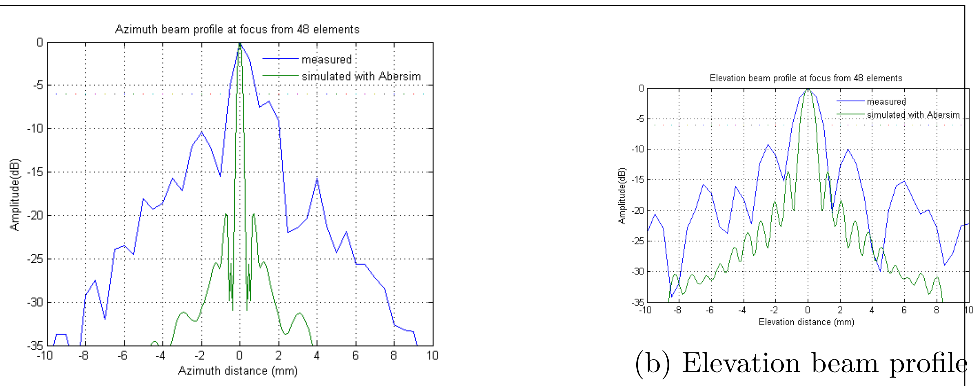

(a) Azimuth beam profile

(b) Elevation beam profile

Figure 25: a)Azimuth and elevation beam profile measured and simulated using ABERSIM at focus of 25mm for 14.4mm aperture measured in water driven with 22V amplitude from 48 pulses

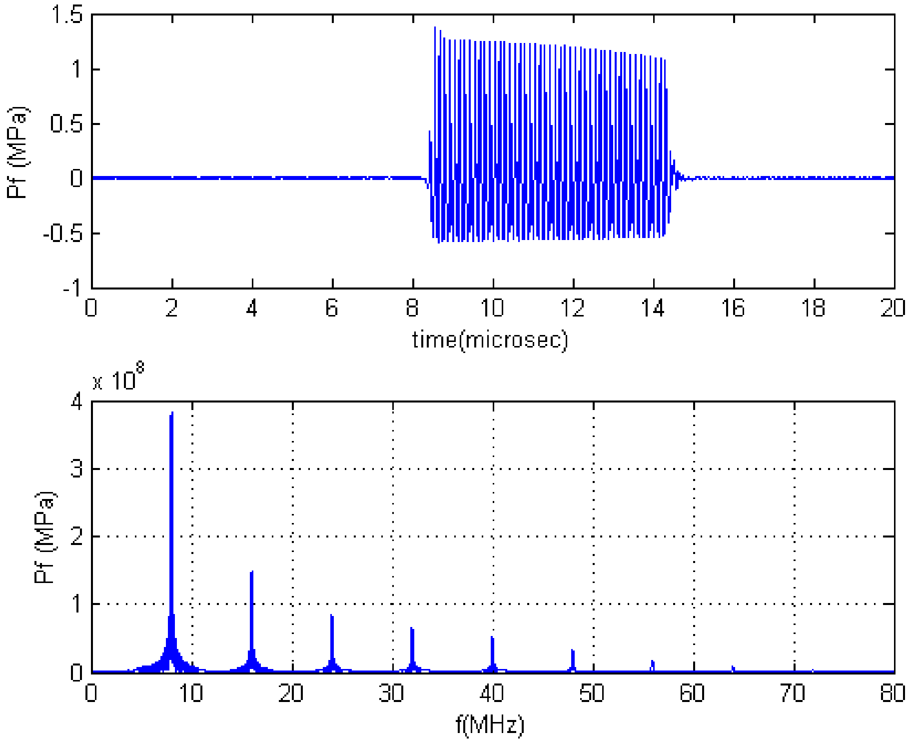

Figure 26: rf signal and frequency spectrum of the pressure on focus of 25mm measured in water driven with 22V amplitude

Table 7: The beam width from 14.4mm aperture

	Measured		Simulated	
	-3dB	-6dB	-3dB	-6dB
Azimuth beam width(mm)	0.9	1.5	0.268	0.354
Elevation beam width(mm)	1.2	2	0.71	0.98

The beam width measured and simulated using ABERSIM from 14.4mm aperture from figure 25

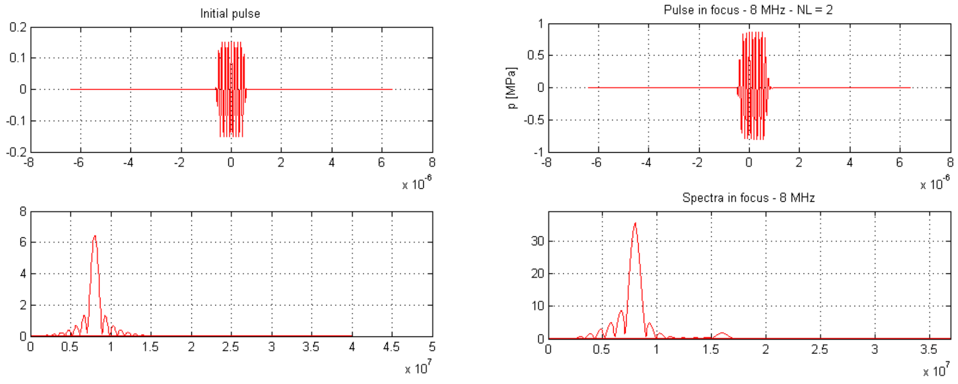

(a) Initial pulse

(b) Pulse form at the focus

Figure 27: Initial and at focus pulse forms used and simulated on the ABERSIM simulation for simulation of URF, UTH, and temperature on the tissue respectively from 0.15MPa surface pressure

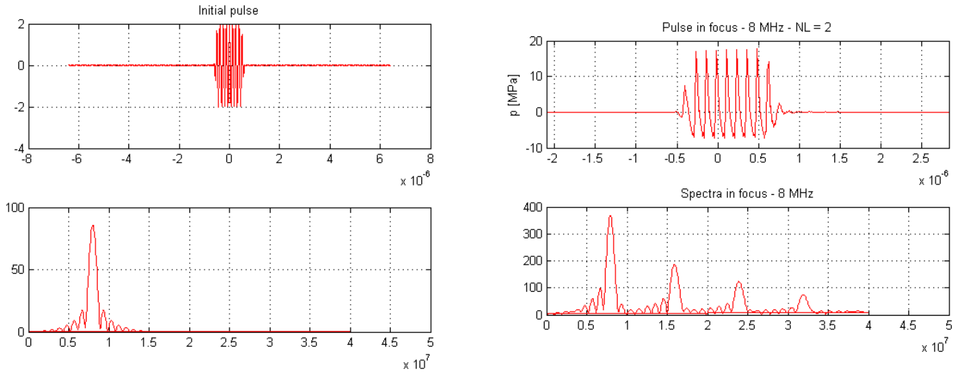

(a) Initial pulse (b) Pulse form at the focus

Figure 28: Initial and at focus pulse forms used and simulated on the ABERSIM simulation respectively from 2MPa surface pressure. This is only to show distortion of the field at focus

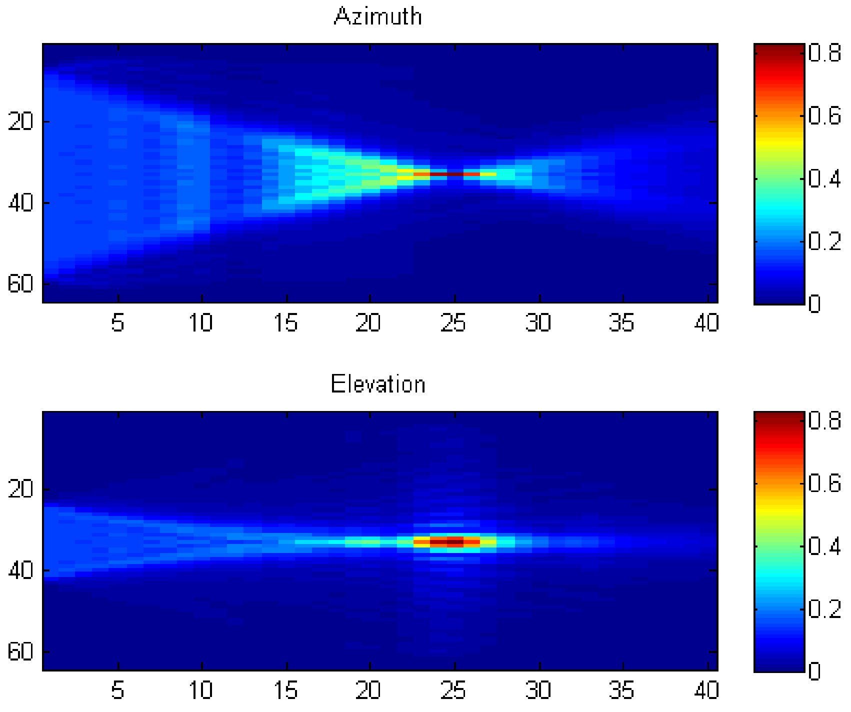

Figure 29: Azimuth and elevation beam profile simulated at $8MHz$ center frequency of 14.4mm aperture. The color bar indicates pressure in MPa

5.2.2 Radiation force

Figure 30a shows the magnitude of the ultrasound radiation force(URF) as functions of transmitted frequency and depth from 14.4mm (48 elements) aperture size. It is found that the magnitude really dependent on the transmitted frequency of the probe. Therefore, as we observed in figure 30b, it reveled that the magnitude of the URF is maximum which is $9.8KN/m^3$ at 8MHz center frequency at the focus (25mm depth), and a pressure of 0.9MPa at the focus as shown in figure 31. The decrement of the pressure from the measured pressure on the water tank is due to loss on the medium in the simulation.

Moreover, the figures in figure 32 shows that the magnitude of the URF increase with increase in aperture size at the focus with 8MHz center frequency and peaked at half aperture size(19.2mm) but it is constant after an aperture size of 20.1mm. Because the contribution form the elements far from the center elements of the array would be small due to small opening angle at 25mm focus. However, the ultrasound thermal heating and temperature of the tissue are also increasing as it is shown in figure 34and 36 respectively.

In addition, the -6dB axial beam width of the URF at the focus was evaluated based figure 31 and found to be 3mm .

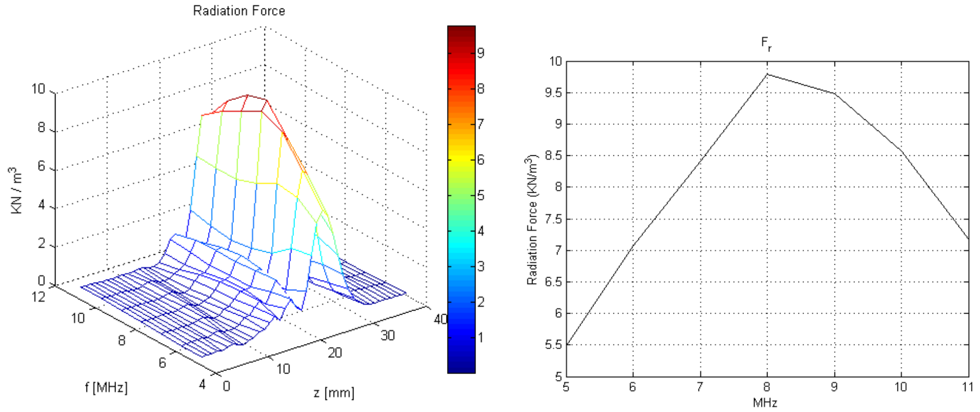

(a) Radiation force at different center frequencies with respect depth

(b) Radiation force at focus of 25mm

Figure 30: Radiation force from a single 10 cycle pulse a) at different frequencies with respect depth, b) at focus of 25mm with respect frequencies , both from 14.4mm (48 elements) aperture size, and found a maximum of $9.8KN/m^3$ at 8MHz

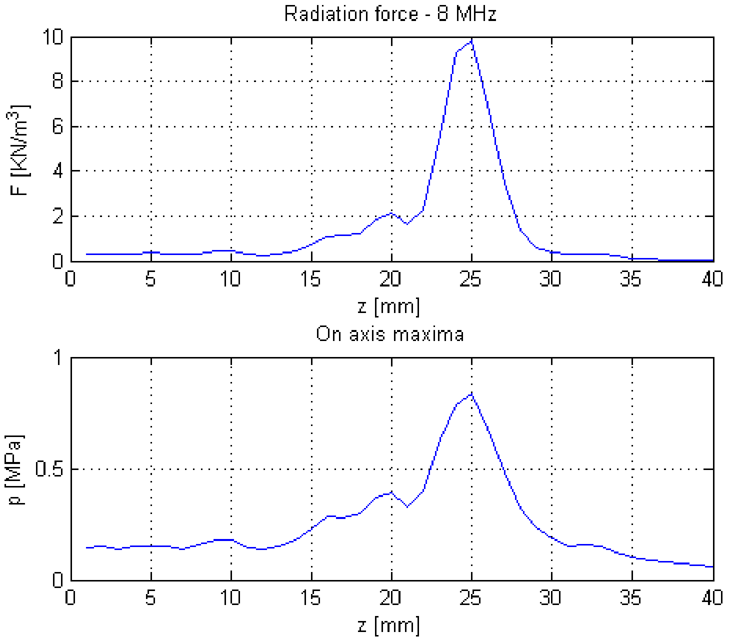

Figure 31: Radiation force axial profile at focus of 25mm simulated at $8MHz$ center frequency of 14.4mm aperture

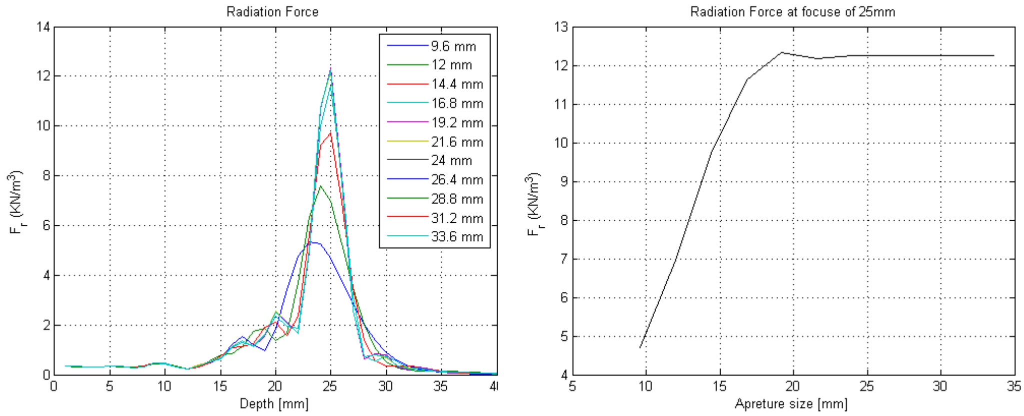

(a) Radiation force at 8Mhz with respect depth

(b) Radiation force at focus of 25mm with respect to aperture size

Figure 32: Radiation force from a single 10 cycle pulse a) at 8MHz frequency with different aperture size and depth, b) at 8MHz center frequency and focus of 25mm with respect aperture size

5.2.3 Heat delivered on the tissue

Figure 33a shows the magnitude of the ultrasound thermal heating (UTH) of the tissues as functions of transmitted frequency and depth from 14.4mm (48 elements) aperture size. And it is found that the heat delivered dependent on the transmitted frequency of the probe and has a monotone attenuation with depth for each transmitted frequency since it is the total absorbed power that does the tissue heating, as shown in figure 33b . Therefore, as we observed in figure 33b, it reveled that the magnitude of the UTH at 8MHz center frequency at the focus (25mm depth) is approximately $49\mu J/m$.

However, the figures in figure 34 shows that the magnitude of the UTH increased with increasing in aperture size at the focus at 8MHz center frequency. When the aperture size increased to 25mm, the magnitude of the UTH will be approximately doubled.

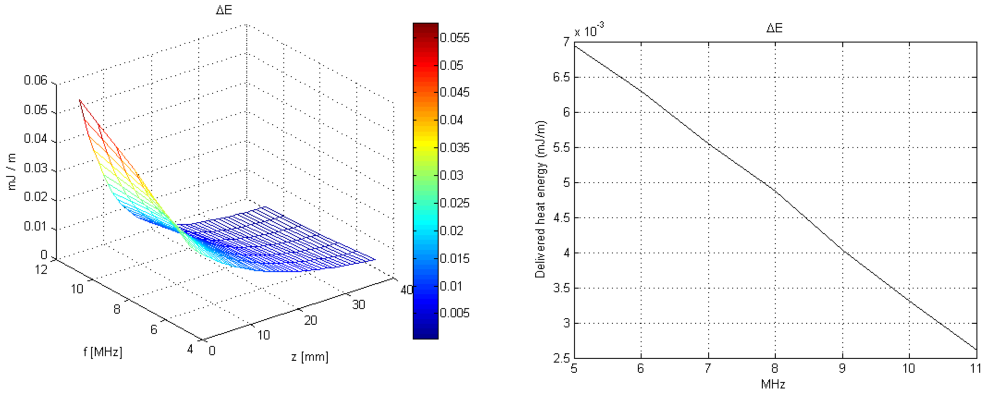

(a) Heat delivered at different center frequencies with respect depth

(b) Heat delivered at focus of 25mm

Figure 33: Heat delivered to the tissue from a single 10 cycle pulse a) at different frequencies with respect depth, b) at focus of 25mm with respect frequencies, both from 14.4mm (48 elements) aperture size

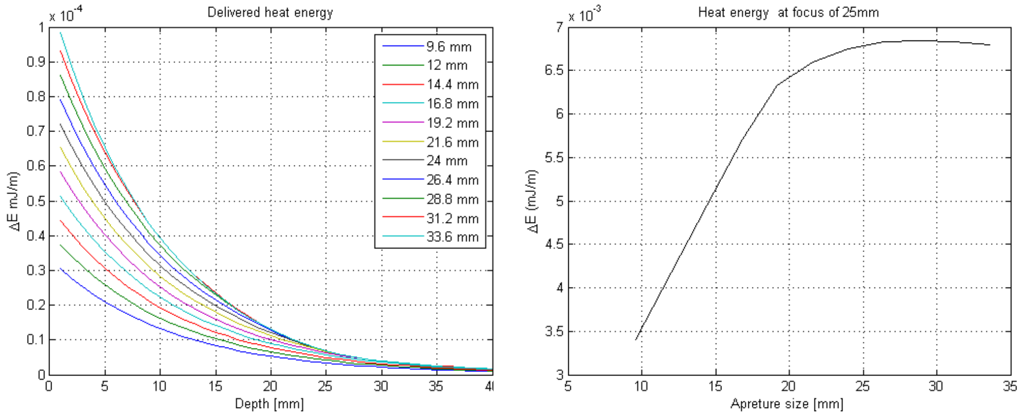

(a) Heat delivered at 8Mhz with respect depth

(b) Heat delivered at focus of 25mm with respect to aperture size

Figure 34: Heat delivered to the tissue from a single 10 cycle pulse a) at 8MHz frequency with different aperture size and depth, b) at 8MHz center frequency and focus of 25mm with respect aperture size

5.2.4 Temperature delivered on the tissue

From figure 35 , we found the temperature on the tissue exposed due to the pressure wave is in the range of $\mu^o K$ and is maximum at 8MHz transmit frequency for 14.4mm aperture size at focus (25mm). In addition, figure

36 reveled that, the temperature increase with increasing aperture size until 20mm but remain constant if the aperture is increased farther more. The reason is due to small in f-number (FN).

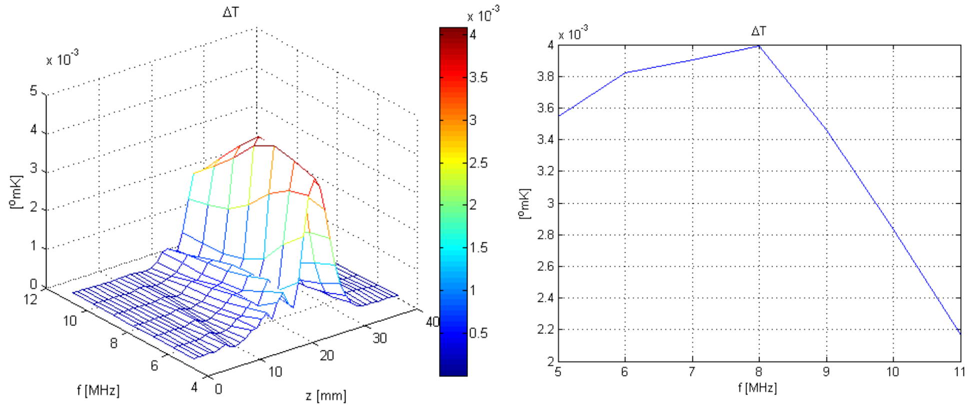

(a) Temperature delivered at different center frequencies with respect depth

(b) Temperature delivered at focus of 25mm

Figure 35: Temperature delivered to the tissue from a single 10 cycle pulse a) at different frequencies with respect depth, b)at focus of 25mm with respect frequencies, both from 14.4mm (48 elements) aperture size

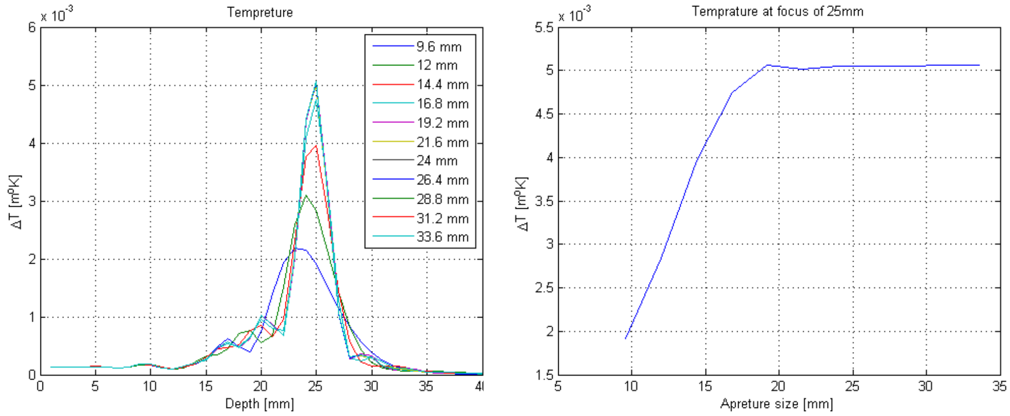

(a) Temperature delivered at 8Mhz with respect depth

(b) Temperature delivered at focus of 25mm with respect to aperture size

Figure 36: Temperature delivered to the tissue from a single 10 cycle pulse a) at 8MHz frequency with different aperture size and depth, b) at 8MHz center frequency and focus of 25mm with respect aperture size

5.3 Result from animal experiment

5.3.1 Thermal effect

The temperature measured on the mice before and after exposure to URF shows a $0.1^{o}C$ decrement in temperature on the tissue. The temperature measured before the exposure was $28.2^{o}C$ while after the exposure become $28.1^{o}C$.

5.3.2 Distribution of Dox

Comparison of the dox distributions in prostate tumors between mice treated without ultrasound (Dox alone) and with ultrasound (Ultrasound and Dox together) obtained form the confocal laser microscopy are shown in figures 37. The result shows a higher dox fluorescence at the periphery of the tumor sections than at center for both of the exposure and non-exposure groups. However, since the dox are small in size, diffusion will play a great role in transporting them from the vessels to ECM. However, it is found also much florescence in side the cells. In the insonation groups, there were hardly to see the blood vessels through out the tumor sections, and the fluorescent signals of dox are very week, and not accurately distinguished but there is good distributions of florescence . However, it is very difficult to conclude with out comparing the quantified values of the florescences from the two treatment methods. Hence, an intensive further analysis is required. Since it takes much time for such analysis, we didn't get time to do it.

5.3.3 Distribution of PBCA nanoprticles

The distribution of the PBCA nano particles in prostate tumors between mice treated without ultrasound (nano particles alone) and with ultrasound (Ultrasound and nano particles together) obtained form the confocal laser microscopy are also shown in figure 38. However, distinguishing the nanoparticles from the background signal level in both of the treatments is difficult and also no significant difference between the two treatments. However, in the ultrasound exposed groups we found very few blood vessels compare to the unexposed control. We gave enough concentration of nano particles but they could be diluted or trapped on the vessels. However, we see some dotes but are difficult to differentiate whether they are art facts or nano particles. So, other method of analysis has to be done.

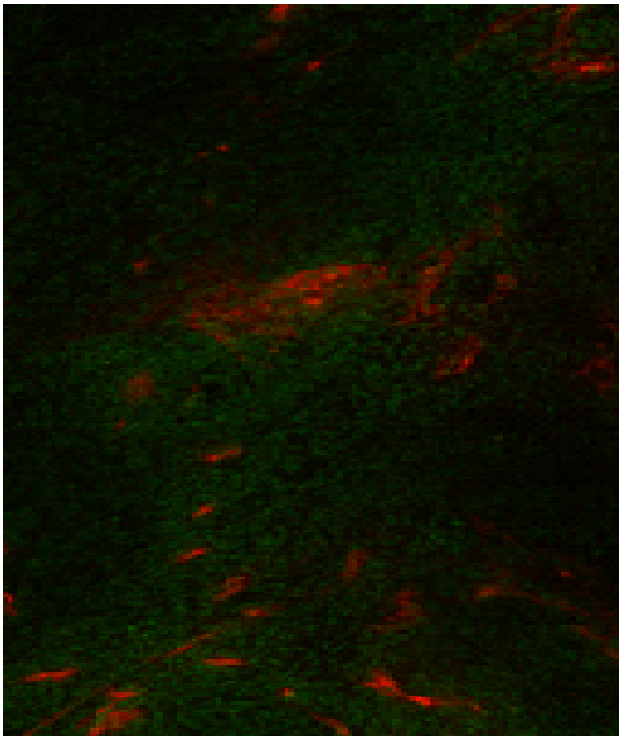

(a) Dox with out ultrasound

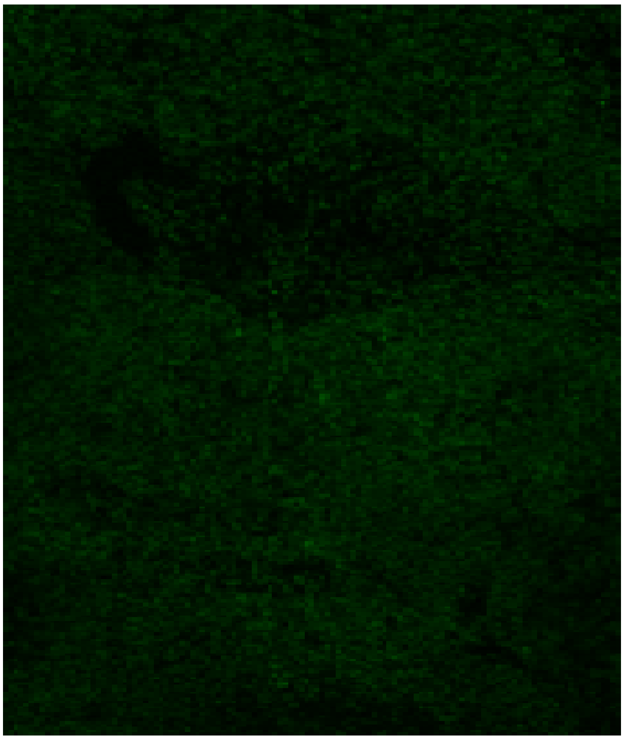

(b) Dox with ultrasound

Figure 37: Confocal laser scanning microscopy images doxorubicin from sections of tumors not exposed to ultrasound (a), and exposed to 8MHz transmit frequency ultrasound. The image shows distribution of doxorubicin (green) and FITC labeled capillaries(red). In ultrasound-exposed tumors, it is hardly to see the blood vessels.

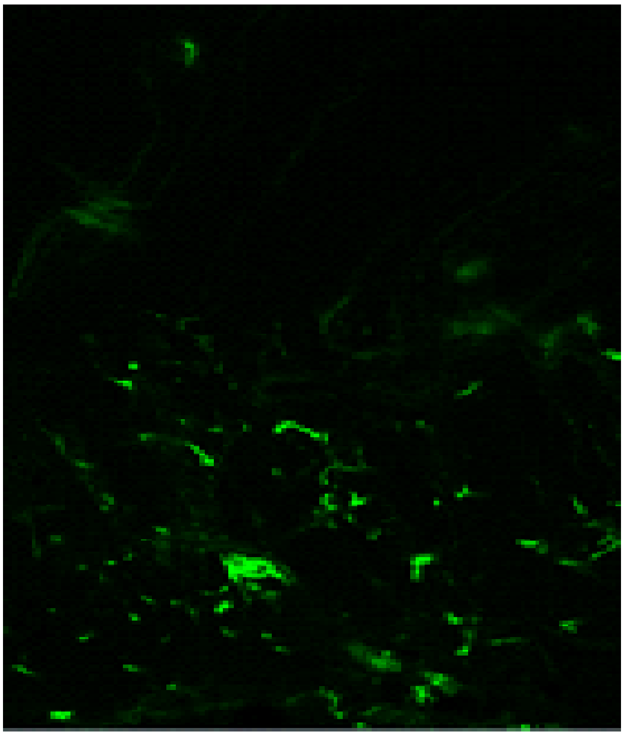

(a) Nano particle with out ultrasound

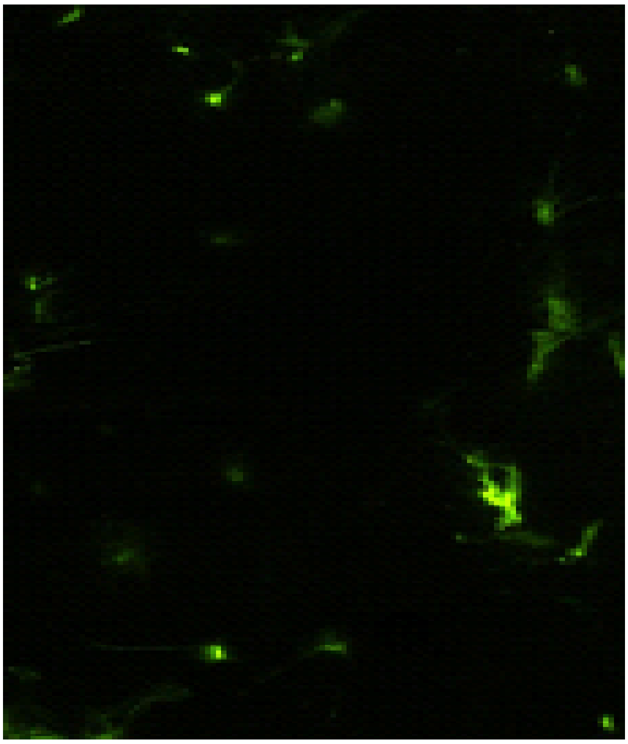

(b) Nano particle with ultrasound

Figure 38: Confocal laser scanning microscopy images of nano particle from sections of tumors not exposed to ultrasound (a), and exposed to 8MHz transmit frequency ultrasound. The image shows distribution of rhodamine(red) and FITC labeled capillaries(green). In ultrasound-exposed tumors, there are very few blood vessels compared to the unexposed treated tumor.

6 Discussions

6.1 Power and heat losses

Designing a transducer for maximum URF and also UTH is limited by the heating of the transducer assembly due to electrical or mechanical and radiation losses , and the maximum available voltage from the transmitters (scanner). Both the mechanical as well as radiation losses are produced due to the thickness vibrations while the electrical loss is due to the material itself and resistance of the electrodes. Therefore, the performance of the transducer is determined by properties of the material elements, and its design. However, the heating of the transducer can be hence controlled mainly using the maximum possible voltage driven for the elements but also through the length and reputation of the pulses. These parameters are selected base on the dissipated power on it as equation (3.28).

From the result in figure 16, it is found that the transducer is inefficient for high power applications. One reason could be due to its operation for a broad-band pulse [38] so that some parts of the electrical power could be contained on the spectral components. The second reason is the design and property of the materials of the probe [48]. In addition, since the transducer is designed for imaging, the dome (plastic material on the outer surface of the probe, $c = 2220ms^{-1}$ [1]) and the liquid material in between($c = 1370ms^{-1}$ [1]) could have higher acoustic impedance so that some acoustic waves were attenuated hence lower the heat on the surface of the transducer's dome, and also seems to have lower thermal conductivity as we did in temperature measurements. The result indicates that, there is more power loss on the transducer which limits the supply voltage, in other words to the out pressure and ultrasound radiation force.

Using equation(3.29), we estimated the maximum transmitted pressure from the transducer. From that equation, we can see that the only variable that we need to estimate is the maximum voltage from the transmitters which is linear dependent to the pressure, but also to the power dissipated on the transducer.

Therefore, when we see the result of figure 15b, the power dissipated on the transducer could be adjusted by selecting appropriate voltage and duty cycle. For example, at lower voltage and duty cycle, the power loss is not much that can damage the transducer or create heat on the surface that can burn the tissue in contact to the transducer surface, although the dissipated power could be lost mostly on the lens [37] which is located on the surface of the transducer than other materials around the transducer. However, if it is loaded to cooling system like water, part of the heat lost on the transducer could dissipated to the medium if the transducer will be used for such system like to our experiment.

From the temperature measurement results which we were used to understand the loss of the power, we observed that, the increase in temperature is more pronounced with the driving voltage, but other factors such as duty cycle, aperture size, frequency and efficiency are also important parameters as we see in equation (3.28) [38]. According to International Standards temperature limits, the maximum temperature of the probe in contact with the patient to $43^{o}C$, either internally or externally, or to $50^{o}C$ when running in air [49].These limits could be for the transducers which have a direct contact with patient. But in our system we used a water bag for having a homogeneous medium and lower attenuation of the wave from the surface of the probe to our focusing (target).

In addition, clinical use for external ultrasound probes limits temperature rise above ambient to $27^{o}C$ when operating in air and $10^{o}C$ when operating into a tissue mimicking phantom [1], but here the time limitations are not detailed. Hence, as our temperature measurements show in figures 19, 20 and 21 reveled that, the maximum increase in temperature is $22^{o}C$, $20^{o}C$ and $5^{o}C$ respectively which are on the limits.

From K probe thermometer measurements, it seems that the transducer array has a large thermal conductivity and would therefore spread out the heating. However, the inside surface temperature on the elements measured with IR-thermographic camera using a scheme of 20 volt and 18 volt amplitudes with 10cycles pulses of 1.125% duty cycle for an aperture size of 14.4mm (48 elements) settings resulted to raise the inside surface temperature of the array to $57^{o}C$ in 5min , and $53^{o}C$ in 10min and remained constant, respectively. However, the maximum inside temperature of piezocomposite materials limited by low thermal glass transition temperature (Tg) usually around $60^{o}C$ ($140^{o}F$) for low power application transducers, while, a high glass transition temperature (Tg) above $120^{o}C$ polymer matrices for high power application transducers [48].But, here there is no any clear information for which of the two application it is.

Hence, from these temperature measurements, we conclude that:
1) The transducer is for a low power application so that the maximum inside temperature of the array should be less than $60^{o}C$ [48]. In addition,

since the probe is designed for imaging and was hence designed to have a direct contact with patient, the International Standards temperature limits, the maximum temperature of the probe in contact with the patient to 43^oC, either internally or externally, or to 50^oC when running in air [49] must also fulfilled.
2) The dome and the liquid materials could have low thermal conductivity .
3) Since the efficiency of the transducer found is too low, the out put acoustic power is attenuated on the dome and the liquid materials so that it becomes difficult detect the heat by the K probe thermometer as comparable to what is lost on the elements.

6.2 Selection of the voltage and duty cycle

The safety issues for both the transducer and the patient that can occur due to the mechanical and thermal damage are the main critical limits when we are thinking on the choosing the voltage and duty cycle. In addition, a high power acoustic waves that are precisely localized and precisely controlled in amplitude are also required. Therefore, the driven voltage and the duty cycle was selected based on these two important requirements.

The main determinant elements for selection of the voltage and duty cycle hence are the loss of power, and the surface pressure on the transducer, and has an inverse effect in relation to the voltage means that an increase in voltage will increase the surface pressure which is required, but also increases the power loss which has a negative impact on the transducer. Hence, there is a tradeoff between the power loss and surface pressure on selecting the driven voltage. While, the duty cycle has effects on the power loss and exposure time during the scan which has also an inverse relationship.

Therefore, from all the results, found from the power losses and temperature, measurements, the transducer will be safe if it is driven at 8MHz with a maximum voltage of 18V on the connector and duty cycle of 1.25% means that a pulse length of 1.125μ sec and pulse repetition frequency of 10KHz.

Therefore, from the result in figure 18 at 18V (voltage on the connector), we estimated the maximum possible transmitted pressure from the transducer is 0.15MPa ($0.68 W.cm^{-2} \sim 10.2 mW/element$). This surface pressure, with the duty cycle and the pulse length chosen were set on the ABERSIM simulation for estimation of the URF, UTH, and temperature on the tissue.

6.3 Ultrasound radiation force (URF)

One of the main mechanical effect of interaction of the high focused ultrasound intensity with biological tissues is through radiation force. It is the transfer of momentum from the ultrasound waves to the particles that induced a translation in the direction of the propagation of the waves. If the size of the particles are comparable to the size of the water molecules, we can treat the system as a fluid in which the momentum transfered to the particles from the local URF will cause streaming on the medium which is called acoustic streaming [50]. While if the system has less liquid, such as solid tissue, the URF which is transfered momentum from the ultrasound to the tissue will induce a small displacement and strain on the tissue, hence translation of particles. However, the translation of the particles depends on sizes and structure of the therapeutic particles, magnitude of the local URF, and the medium itself.

We known that it is the local ultrasound radiation force that produces transport of drugs, and hence is the local radiation force maximum on beam axis in the focal region which is important due less coupling on the medium. However, the maximum radiation force that can be achieved in the focal region depend on the aperture and focal length of the transducer, and the amplitude and frequency (in relation to extinction cross section dependency) of the irradiated acoustic wave in addition to the nonlinearity of the medium which increase the extinction cross section, and focusing for increasing the local average intensity [51]. As stated in previous section, the amplitude of the pulse and center frequency were selected based on the performance and design of the transducer, and extinction cross section depends on the properties of the medium. While, the number of elements used are selected based on the following three reasons:
1) the azimuth focal length.
2) amount of radiation force, heat and temperature on the focus.
3) power dissipated to the transducer.

The azimuth focal length which is 25mm chosen was restricted by the elevation focus of the transducer due to lens at 28mm [1], although we have a possibility to use a multiple foci on the scanning plan. From this azimuth focus, the minimum f-number (FN) for a -3dB opening angle of the beam is 1.7 for 8MHz frequency of one element as example. Hence,we can have a maximum elements of 49 from this FN and focus.

Form the results shown in figures 32b and 34b, both radiation force and heating will increase with increase in aperture size, but maximum radiation force is achieved at lower frequencies for the bigger aperture size since the -3dB opening angle at lower frequency is large, we get contributions from most of the elements, where as for larger frequencies, the opening angle gets lower. However, for 48 elements, the maximum radiation force will become at 8MHz due to the after-mentioned reasons. In addition, at 8Mhz frequency there is a 25% increase in URF from half aperture size than from 48 elements aperture size as reference to figure 32, but the heating of the transducer will increase by 33% since the heating of the transducer is proportional with the power delivered to a single element.

From figure 30b we found that the magnitude of the ultrasound radiation force is $9.8KN/m^3$ (a pressure gradient of $9800Pa/m$). This force corresponds to $1g/cm^3$ which is the density of water. The total magnitude of the radiation force will increase with respect the duty cycle. Hence the impulse transfered will then depend on the effective exposure (time) of irradiated medium. However, due to the vectorial nature of the radiation force with respect the capillaries as shown in (B.8), for an even distribution of the capillary directions and radiating in a single direction, approximately, in average, to a minimum of 60 % of the force contributes efficiently for pushing the particles. Hence, this pressure gradient could compensated to the lack of pressure gradient of tumors [14] by reducing the intestinal fluid pressure (IFP) of patient tumor that ranges from a minimum of 2.6mm-Hg to a maximum of 40mm-Hg in contrast to the IFP of normal tissue which is typically between -3 and +3mm-Hg [15], and increase the convection of the therapeutic agents from the capillaries to the tumor tissue deep in to the interstitial of the tumor tissue until inside of the tumor cells [11]. In addition, this force could induce small displacements and strains on the tissue.

However, the attenuation constant of the health prostate tissue is found $0.78 \pm 0.24dB/MHz.cm$ [43] , and could a have a small impact on attenuating the pressure wave and decrease the magnitude of the radiation force.

6.4 Ultrasound thermal heating (UTH) and Temperature on the tissue

One of the ultrasound mechanisms that create biological effect due to exposure is through the generation of heat on tissues.The heat generation resultants from this absorption of energy where the volumetric rate of heat ,as show in equation (3.56), being produced is directly proportional to the specific absorption coefficient of the tissue being exposed and the intensity of the ultrasound wave. However, there is a more transversal coupling due to the blood flow which has a thermal conductivity of $0.572W/m.K$ (plasma, human) and thermal diffusivity of $1210cm^2/s$ (plasma, human) for normal and unperfused blood [52], which decreases the heat and temperature although the dissipation of the heat due to blood flow is lower in tumors than in normal tissue [21].

The net amount of heat generated in the tissue, and the temperature elevation resulting at focus are shown in figures 33 and 35 with a maximum values in the range of $\mu J/m$ and $\mu^o K$ respectively. Their magnitude shows that they are too small to make any cavitation for the tissues and also to have any thermal effect on the process of the delivery. And the result of the temperature was also proved during an animal experiment though temperature measurement before and after exposure to the URF.
The other two main parameter of monitoring safety of the diagnostic and therapeutic application of ultrasound are the mechanical index(MI), which provides a measure of the potential for inducing acoustic cavitation, and the thermal index (TI), which estimates the expected tissue heating. The estimated mechanical index(MI) is 0.2 (from the negative peak pressure of 0.6MPa at 8MHz transmitted frequency) which is below the threshold limit of 1.9. And the TI describes the temperature rise in the tissue and have got almost negligible both from the simulated, and measured before and after exposure.

Therefore,the pulse characteristic of the transducer and the tissue characteristics used for this study are shown in table 8. All the parameters were chosen based the performance of the transducer and the maximum acoustic radiation force that can be achieved with a minimum tissue heating.

Table 8: The pulse characteristic of the transducer used in the experiment.

center frequency fc(MHz)	8
Number of periods Np	10
Number of elements	48
Azimuth Aperture (Da (mm))	14.4
Focal length in azimuth (Fa(mm))	25
Focal length in elevation (Fe(mm))	25
F-number ($F_{\#} = F/Da$)	1.7
Acoustic pressure output on focus (Pf(MPa))	0.83 *
Pulse duration ($T_{on}(\mu s)$)	1.25
Pulse repetition frequency (PRF (KHz))	10
Duty cycle (%)	1.25
Azimuth beam width (mm) at -6dB	0.3
Elevation beam width (mm) at -6dB	1.5
Axial beam width (mm) at -6dB	3
Intensity on focus ($Watt/cm^2$)	20.9
Mechanical index (MI)	0.2 *

The pulse characteristic of the transducer used in the experiment which are selected based on the theoretical simulations and measured results. Note that the acoustic pressure output was directly convert from the 22V measured to 18V which were used on the experiment using linear dependency. Note that: * indicates result from hydrophone measurements

6.5 Effect of the URF exposure on the drugs

Previous studies shows that ultrasound has a capacity to increase local uptake of drugs in solid tumor through mechanical interactions with tissues. The mechanical interactions arises through cavitation or radiation force depending on the parameters of the ultrasound. In this study, the effect of ultrasound radiation force on the uptake of doxorubicin and PBCA nano particles in prostate tumors were investigated. Although it is very difficult to give a concrete conclusion without comparing the quantified values of the florescences for doxorubicin and PBCA nano particles from each of the two treatment methods, the fluorescence photomicrographs no legible significant difference was observed for the distribution of the two drugs when we compared without and with ultrasound exposures. However, the distribution of the two drugs are different which could be arisen due to the difference in transport properties of the two drugs. In addition, to understand the distribution of the drugs, the visualization of the blood vessels is essential. However, this is hardly seen on both of the drugs in the ultrasound exposure controls.

Ultrasound radiation force(URF) is generated by a propagating acoustic wave in which part of its momentum is transferred to its propagation medium through loss mechanisms. These forces can induce small displacements and strains on less fluid tissues, such as solid tissues, and also induce streaming on the fluid medium which is know as acoustic streaming. The small displacement on the tissues create gaps between endothelial cells [18], and widen the intracellular space to enhance the interstitial transport [19], hence increase the drug extravasation [53]. In addition, the URF (pressure gradient) could compensated to the lack of pressure gradient of tumors [14] by reducing the intestinal fluid pressure (IFP) of patient tumor and increase the convection of the therapeutic agents from the capillaries to the tumor tissue deep in to the interstitial of the tumor tissue until inside of the tumor cells [11]. However, magnitude of ultrasound radiation force dependents on tissue properties and ultrasonic beam characteristics .

The ultrasonic beam characteristics is determined by the performance of the transducer. The maximum radiation force that can be achieved in the focal region is proportional to the average intensity of the wave which increases with increase in acoustic power of the transducer, and the extinction cross section of the medium that increase due to non linear absorption of the medium resulted from the non linear propagation of wave form distortion which causes higher order harmonics which is also frequency and acoustic power dependent.

In the previous studies in pulsed focused ultrasound(pFUS), acoustic intensities used ranges from $\sim 1110 W/cm^2$ [54] to $\sim$ 2660 W/cm^2 (peak negative pressure of 8.95 MPa) [10] although it is not clear which acoustic intensity will give the maximal enhancement on the delivery. In the two studies, the transmitted frequency was 1MHz, and used liposomal doxorubicin, and nanoparticles with a diameter of 200 nm drugs respectivelly, and also shown that the enhancement was nonthermal but cavitation is present . In our system, the intensity used were 20.9 W/cm^2(peak negative pressure of 0.5MPa) which is much smaller than the other studies to avoid the cavitaton mechanisms, but we used higher transmit frequency 8MHz to increase the extinction cross section, hence the URF. The intensity or pressure at the focal region could increase by increasing the acoustic power, hence the URF, which may help to increased interstitial space and vessel wall opening, and/or increase the convection of the therapeutic agents from the capillaries to the tumor tissue deep in to the interstitial of the tumor tissue until inside of the tumor cells [11] and enhance drug uptake in tumors. However, in order to keep the transducer and the thermal heating of the tissue at safe level, the option to increase power is limited due to the power loss on the transducer and the temperature increase in the tissue.

The nonthermal effect of the ultrasound increases the blood flow and capillary permeability [55] which enhance the supply of fluids form the vasculature hence the drugs. However, a decrease in temperature was observed. This decrement is due to the cooling of the tumor and the surrounding tissue within the water bag and gel used as a medium during the exposure. And it is also consistent with UTH simulated which is in the range of μ^oK. Hence there is no theraml mechanism for the distribution of both doxorubicin and PBCA nano particles drugs.

However, the delivery of the drugs could be affected not only by the magnitude of the URF but also by effective exposure time, the concentration of the drugs, and the size of the irradiated tumor. The fist two parametrs are really defined by the performance of the transducer. In addition, ultrasound exposure can also shot down the blood vessels by creating microbbles on the vessels [56]. Goertz and his co-workers [56] studied the uptake of docetaxel in same type of tumor cells to our study, and found that relatively low ultrasound exposure levels (lower than employed in ablative high intensity focused ultrasound) achieve anti-vascular tumors which causes shut-down of the blood flow. In their study, a 1MHz transducer with a peak negative pressure at focus of 1.65MPa were used. Hence, the tumor blood vessels might be hence affected by the URF for both of the administered drugs.

To best of our knowledge, this is the first microscopic study of the effect of URF exposure at 8MHz on the therapeutic agents distribution and penetration on the cells.

7 Conclusion

Although it is very difficult to give a concrete conclusion without comparing the quantified values of the florescences for doxorubicin and PBCA nano particles from each of the two treatment methods, the fluorescence photomicrographs no legible significant difference was observed for the distribution of the two drugs when we compared without and with ultrasound exposures.

In this study we used 8MHz exposure to increase the ultrasound radiation force that are precisely localized and precisely controlled in amplitude in the focal zone. This is found by increasing extinction cross section of the wave with the possible maximum acoustic power waves that keeps the transducer and the tissue in safe level, and the thermal and acoustic cavitation mechanisms has to be also excluded . However, in this study, the option to increase power is mainly limited due to the power loss on the transducer. Therefore, the optimal drive voltage and duty cycle for probe was therefore found to be 18V and 1.25% respectively at 8MHz transmitted frequency and 1.25μ sec long pulse with reputation frequency of (PRF) 10KHz. According our simulation, we found an ultrasound radiation force of $9800N/m^3$ which corresponds to 75mmHg/m.

However, the structural nature of the tumor, particularly the extracellular matrix, and some electrostatic forces originated from the nano particles (drugs) and charges originated from the micro or macro molecular composition of the medium (tumor) could produce an anti drag force that can effect the transport of the drugs to the specified target. Moreover, the attenuation constant of the health prostate tissue is found $0.78 \pm 0.24dB/MHz.cm$ [43] , and could a have a small impact on attenuating the pressure wave and decrease the magnitude of the radiation force.

Hence, the impact of the ultrasound radiation force is not clear yet, but a further analysis should be done in quantifying the distribution and penetration of the drugs for more comparison.

8 Further work

To gain a greater understanding of the mechanisms of the ultrasound radiation force mediated drug delivery, we will need to continue the procedures with higher acoustic power, and also the magnitude of the URF and the other parameters has to be simulated in accordance with respect to the boundary conditions of the individual medium.

9 Reference

References

[1] Ultrasonix. 4DL14-5/38 datasheet.

[2] WHO WHO. WHO | cancer, 2013.

[3] Yueh-Hsun Chuang, Po-Wen Cheng, and Pai-Chi Li. Combining radiation force with cavitation for enhanced sonothrombolysis. *IEEE transactions on ultrasonics, ferroelectrics, and frequency control*, 60:97–104, 2013. PMID: 23287916.

[4] D Bommannan, G.K. Menon, H. Okuyama, P.M. Elias, and R.H. Guy. Sonophoresis. II. examination of the mechanism(s) of ultrasound-enhanced transdermal drug delivery. *Pharmaceutical Research*, 9:1043–1047, 1992.

[5] Victor Frenkel. Ultrasound mediated delivery of drugs and genes to solid tumors. *Advanced Drug Delivery Reviews*, 60:1193–1208, 2008.

[6] Paolo A. Netti, Leena M. Hamberg, John W. Babich, Diane Kierstead, Wendy Graham, George J. Hunter, Gerald L. Wolf, Alan Fischman, Yves Boucher, and Rakesh K. Jain. Enhancement of fluid filtration across tumor vessels: Implication for delivery of macromolecules. *Proceedings of the National Academy of Sciences*, 96:3137–3142, 1999.

[7] Jan Lankelma, Henk Dekker, Rafael Fernndez Luque, Sylvia Luykx, Klaas Hoekman, Paul van der Valk, Paul J. van Diest, and Herbert M. Pinedo. Doxorubicin gradients in human breast cancer. *Clinical Cancer Research*, 5:1703–1707, 1999.

[8] Carl-Henrik Heldin, Kristofer Rubin, Kristian Pietras, and Arne Ostman. High interstitial fluid pressure - an obstacle in cancer therapy. *Nature reviews. Cancer*, 4:806–813, 2004. PMID: 15510161.

[9] Aaron F.H. Lum, Mark A. Borden, Paul A. Dayton, Dustin E. Kruse, Scott I. Simon, and Katherine W. Ferrara. Ultrasound radiation force enables targeted deposition of model drug carriers loaded on microbubbles. *Journal of Controlled Release*, 111:128134, 2006.

[10] Brian E. O'Neill, Howard Vo, Mary Angstadt, King P.C. Li, Tim Quinn, and Victor Frenkel. Pulsed high intensity focused ultrasound mediated

nanoparticle delivery: Mechanisms and efficacy in murine muscle. *Ultrasound in Medicine & Biology*, 35:416–424, 2009.

[11] Katherine D Watson, Chun-Yen Lai, Shengping Qin, Dustin E Kruse, Yueh-Chen Lin, Jai Woong Seo, Robert D Cardiff, Lisa M Mahakian, Julie Beegle, Elizabeth S Ingham, Fitz-Roy Curry, Rolf K Reed, and Katherine W Ferrara. Ultrasound increases nanoparticle delivery by reducing intratumoral pressure and increasing transport in epithelial and epithelial-mesenchymal transition tumors. *Cancer research*, 72:1485–1493, 2012. PMID: 22282664.

[12] Katherine W. Ferrara. Driving delivery vehicles with ultrasound. *Advanced Drug Delivery Reviews*, 60:1097–1102, 2008.

[13] Abhay V Patil, Joshua J Rychak, John S Allen, Alexander L Klibanov, and John A Hossack. Dual frequency method for simultaneous translation and real-time imaging of ultrasound contrast agents within large blood vessels. *Ultrasound in medicine & biology*, 35:2021–2030, 2009. PMID: 19828229.

[14] Live Eikenes, yvind S Bruland, Christian Brekken, and Catharina de Lange Davies. Collagenase increases the transcapillary pressure gradient and improves the uptake and distribution of monoclonal antibodies in human osteosarcoma xenografts. *Cancer research*, 64:4768–4773, 2004. PMID: 15256445.

[15] Arindam Sen, Maegan L. Capitano, Joseph A. Spernyak, John T. Schueckler, Seneca Thomas, Anurag K. Singh, Sharon S. Evans, Bonnie L. Hylander, and Elizabeth A. Repasky. Mild elevation of body temperature reduces tumor interstitial fluid pressure and hypoxia, and enhances efficacy of radiotherapy in murine tumor models. *Cancer research*, 71:3872–3880, 2011. PMID: 21512134 PMCID: PMC3184616.

[16] Paul A Dayton, A Klibanov, G Brandenburger, and K Ferrara. Acoustic radiation force in vivo: a mechanism to assist targeting of microbubbles. *Ultrasound in medicine & biology*, 25:1195–1201, 1999. PMID: 10576262.

[17] Paul A Dayton, John S Allen, and Katherine W Ferrara. The magnitude of radiation force on ultrasound contrast agents. *The Journal of the Acoustical Society of America*, 112:2183–2192, 2002. PMID: 12430830.

[18] Ali H Mesiwala, Lindi Farrell, H.Jurgen Wenzel, Daniel L Silbergeld, Lawrence A Crum, H.Richard Winn, and Pierre D Mourad. High-

intensity focused ultrasound selectively disrupts the blood-brain barrier in vivo. *Ultrasound in Medicine & Biology*, 28:389–400, 2002.

[19] Victor Frenkel, E Kimmel, and Y Iger. Ultrasound-induced intercellular space widening in fish epidermis. *Ultrasound in medicine & biology*, 26:473–480, 2000. PMID: 10773379.

[20] Hiroya Hashizume, P Baluk, S Morikawa, J W McLean, G Thurston, S Roberge, R K Jain, and D M McDonald. Openings between defective endothelial cells explain tumor vessel leakiness. *The American journal of pathology*, 156:1363–1380, 2000. PMID: 10751361.

[21] Chang W. Song, Anna Lokshina, Juong G. Rhee, Marsha Patten, and Seymour H. Levitt. Implication of blood flow in hyperthermic treatment of tumors. *IEEE Transactions on Biomedical Engineering*, BME-31:9–16, 1984.

[22] Victor Frenkel and King CP Li. Potential role of pulsed-high intensity focused ultrasound in gene therapy. *Future Oncology*, 2:111–119, 2006.

[23] Stefan Pfaffenberger, Branka Devcic-Kuhar, Stefan P. Kastl, Kurt Huber, Gerald Maurer, Johann Wojta, and Michael Gottsauner-Wolf. Ultrasound thrombolysis. *Thrombosis and Haemostasis*, 2005.

[24] Kullervo Hynynen. Focused ultrasound for bloodbrain disruption and delivery of therapeutic molecules into the brain. *Expert Opinion on Drug Delivery*, 4:27–35, 2007.

[25] Vikash P Chauhan, Triantafyllos Stylianopoulos, Yves Boucher, and Rakesh K Jain. Delivery of molecular and nanoscale medicine to tumors: transport barriers and strategies. *Annual review of chemical and biomolecular engineering*, 2:281–298, 2011. PMID: 22432620.

[26] Paolo A. Netti, David A. Berk, Melody A. Swartz, Alan J. Grodzinsky, and Rakesh K. Jain. Role of extracellular matrix assembly in interstitial transport in solid tumors. *Cancer Research*, 60:2497–2503, 2000. PMID: 10811131.

[27] Yong Wang and Fan Yuan. Delivery of viral vectors to tumor cells: Extracellular transport, systemic distribution, and strategies for improvement. *Annals of Biomedical Engineering*, 34:114–127, 2006.

[28] Yves Boucher and Rakesh K. Jain. Microvascular pressure is the principal driving force for interstitial hypertension in solid tumors: Implications for vascular collapse. *Cancer Research*, 52:5110–5114, 1992.

[29] Rakesh K. Jain. Temperature distributions in normal and neoplastic tissues during normothermia and hyperthermia*. *Annals of the New York Academy of Sciences*, 335:4866, 1980.

[30] David C Miller, Khaled S Hafez, Andrew Stewart, James E Montie, and John T Wei. Prostate carcinoma presentation, diagnosis, and staging: an update form the national cancer data base. *Cancer*, 98:1169–1178, 2003. PMID: 12973840.

[31] B.A.J Angelsen. *Ultrasound Imaging: Waves, Signals, and Signal Processing*, volume I. Norway, emantec edition, 2000.

[32] B.A.J Angelsen. *Ultrasound Imaging: Waves, Signals, and Signal Processing*, volume II. Norway, emantec edition, 2000.

[33] Christian Fossen. Abersim - ultrasound simulation software.

[34] Marko Liebler, Siegfried Ginter, Thomas Dreyer, and Rainer E. Riedlinger. Full wave modeling of therapeutic ultrasound: Efficient time-domain implementation of the frequency power-law attenuation. *The Journal of the Acoustical Society of America*, 116:2742–2750, 2004.

[35] http://en.wikipedia.org/wiki/Acoustic_attenuation. Acoustic attenuation, April 2013. Page Version ID: 549519293.

[36] Lisa Clarke, Andrew Edwards, and Elizabeth Graham. Acoustic streaming: An in vitro study. *Ultrasound in Medicine & Biology*, 30:559–562, 2004.

[37] O. Saunders, S. Clift, and F. Duck. Ultrasound transducer self heating: development of 3-d finite-element models. *Journal of Physics: Conference Series*, 1:72, 2004.

[38] F. A. Duck, H. C. Starritt, G. R. ter Haar, and M. J. Lunt. Surface heating of diagnostic ultrasound transducers. *British Journal of Radiology*, 62:1005–1013, 1989.

[39] Vermon . http://www.vermon.com/.

[40] Trond Varslot and Svein-Erik Msy. Forward propagation of acoustic pressure pulses in 3D soft biological tissue. *Modeling, Identification and Control*, 27:181–200, 2006.

[41] Bjorn A. J. Angelsen. Nonlinear imaging with dual band pulse complexes, 2012.

[42] Mark.L. Palmeri and K.R. Nightingale. On the thermal effects associated with radiation force imaging of soft tissue. *IEEE Transactions on Ultrasonics, Ferroelectrics and Frequency Control*, 51:551–565, 2004.

[43] K.J. Parker, S.R. Huang, R.M. Lerner, Jr. Lee, F., D. Rubens, and D. Roach. Elastic and ultrasonic properties of the prostate. In *Ultrasonics Symposium, 1993. Proceedings., IEEE 1993*, pages 1035–1038 vol.2, 1993.

[44] Martin O. Culjat, David Goldenberg, Priyamvada Tewari, and Rahul S. Singh. A review of tissue substitutes for ultrasound imaging. *Ultrasound in Medicine & Biology*, 36:861–873, 2010.

[45] Siv Eggen, Mercy Afadzi, Esben A. Nilssen, Solveig Bjrum Haugstad, Bjrn Angelsen, and Catharina de L. Davies. Ultrasound improves the uptake and distribution of liposomal doxorubicin in prostate cancer xenografts. *Ultrasound in Medicine & Biology*, 2013.

[46] Kimberley M. Laginha, Sylvia Verwoert, Gregory J. R. Charrois, and Theresa M. Allen. Determination of doxorubicin levels in whole tumor and tumor nuclei in murine breast cancer tumors. *Clinical Cancer Research*, 11:6944–6949, 2005. PMID: 16203786.

[47] wikisonix. wikisonix documentation http://www.ultrasonix.com/wikisonix/index.php/Voltage_Levels, 2013.

[48] Gerard Fleury, David Melo de Lima, Kullervo Hynynen, Remi Berriet, Olivier Le Baron, and Bertrand Huguenin. New piezocomposite transducers for therapeutic ultrasound. pages 227–236, 2003.

[49] Prepared by the Safety Group of the British Medical Ultrasound Society. Guidelines for the safe use of diagnostic ultrasound equipment. *Ultrasound*, 18(2):52–59, May 2010.

[50] Kathryn R. Nightingale, P.J. Kornguth, and G.E. Trahey. The use of acoustic streaming in breast lesion diagnosis: A clinical study. *Ultrasound in Medicine and Biology*, 25:75–87, 1999.

[51] Oleg. V Rudenko, A. P. Sarvazyan, and S. Y. Emelianov. Acoustic radiation force and streaming induced by focused nonlinear ultrasound in a dissipative medium. *The Journal of the Acoustical Society of America*, 99:2791–2798, 1996.

[52] Francis A. Duck. *Physical properties of tissue. A comprehensive reference book.* 1990.

[53] Hilary A. Hancock, Lauren H. Smith, Julian Cuesta, Amir K. Durrani, Mary Angstadt, Mark L. Palmeri, Eitan Kimmel, and Victor Frenkel. Investigations into pulsed high-intensity focused UltrasoundEnhanced delivery: Preliminary evidence for a novel mechanism. *Ultrasound in Medicine & Biology*, 35:1722–1736, 2009.

[54] Esther L. Yuh, Suzanne G. Shulman, Shilpa A. Mehta, Jianwu Xie, Lili Chen, Victor Frenkel, Mark D. Bednarski, and King C. P. Li. Delivery of systemic chemotherapeutic agent to tumors by using focused ultrasound: Study in a murine model. *Radiology*, 234:431–437, 2005.

[55] M. W. Dewhirst G. Kong. Review hyperthermia and liposomes. *International Journal of Hyperthermia*, 15:345–370, 1999.

[56] David E. Goertz, Margarita Todorova, Omid Mortazavi, Vlad Agache, Branson Chen, Raffi Karshaflian, and Kullervo Hynynen. Antitumor effects of combining docetaxel (taxotere) with the antivascular action of ultrasound stimulated microbbles. *PLos ONE*, 2012.

Appendices

A Electrical Transfer function of the transducer element

The electrical transfer function is used to estimate the voltage on the electrode using the electrical impedance of the cable as a transmission model, and the transducer element impedance at the connector as shown in figure 4. We have only a possibility to measure the voltage and impedance at the connector. Therefore, in order to know the voltage on the electrodes , hence we evaluated the electrical transfer function as follows:

By definition transfer function is given by:

$$H = \frac{Vo}{Vi} = \frac{V_{tt}}{V_{cn}} = \frac{Z_{el}}{Z_{eq}} \tag{A.1}$$

Where Z_{eq} is the equivalent impedance of the circuit. Using circuit diagram analysis, Z_{eq} can be written as:

$$Z_{eq} = \frac{Z_{el}(Z_b + Z_a) + 2Z_aZ_b + Z_a^2}{Z_{el} + Z_a + Z_b} \tag{A.2}$$

Hence, H will become:

$$H = \frac{Z_{el}(Z_{el} + Z_a + Z_b)}{Z_{el}(Z_b + Z_a) + 2Z_aZ_b + Z_a^2} \tag{A.3}$$

Where Z_{el} is the estimated impedance on the element on the electrode, and Z_a and Z_b are as stated in figure 4.

B Radiation force efficiency with uniform capillary direction

Radiation force is a vector quantity that describes both by magnitude and direction. Hence, assume the radiation force is in the x_3 -direction and the capillaries has angle ϕ with the x_3 -direction. The component of the radiation force normal to the capillary is then given by:

$$\Delta F_n = \Delta F sin\phi \tag{B.1}$$

With uniform distribution of the direction of the capillaries, the average fraction of the radiation force normal to capillaries is

$$\Delta\bar{F} = \frac{\Delta F 2\pi \int_0^\pi d\phi sin\phi sin\phi}{2\pi \int_0^\pi d\phi sin\phi} = \frac{\pi/2}{2}\Delta F \approx 0.75\Delta F \tag{B.2}$$

When ϕ is small, the component of the radiation force normal to the capillary becomes:

$$\Delta F_n = \Delta F sin^m \phi \tag{B.3}$$

which gives an average radiation force of

$$\Delta\bar{F} = \frac{\Delta F 2\pi \int_0^\pi d\phi sin^m \phi sin\phi}{2\pi \int_0^\pi d\phi sin\phi} \tag{B.4}$$

Fro example when m=2 , equation (B.4) evaluates as

$$\Delta\bar{F} = \frac{\Delta F 2\pi \int_0^\pi d\phi sin^2 \phi sin\phi}{2\pi \int_0^\pi d\phi sin\phi} = \frac{4/3}{2}\Delta F \approx 0.67\Delta F \tag{B.5}$$

And for m=4 we calculate the numerator as

$$\begin{aligned}\int_0^\pi d\phi sin^4\phi sin\phi = \int_0^\pi d\phi (1 - cos^2\phi)^2 sin\phi = \int_0^\pi d\phi (1 - cos^2\phi + cos^4\phi) sin\phi \\ = -cos\phi + \frac{2}{3}cos^3\phi - \frac{1}{5}cos^5\phi]_0^\pi = 2 - 4/3 + 2/5 = 16/15\end{aligned} \tag{B.6}$$

Inserting into equation (B.4):

$$\Delta\bar{F} = \frac{16/15}{2}\Delta F \approx 0.53\Delta F \tag{B.7}$$

In general we can reduce to

$$\Delta\bar{F} \approx 0.6\Delta F \tag{B.8}$$

C Matlab code

C.1 Electric impedance , surface pressure, efficiency and power losses

```
% Electrical imedance elements
close all;clear all;clc
for i=1:128

    filename=strcat('Zc',int2str(i),'.mat');
    load(filename)
    f_vec(i,:)=f;
    mag_vec(i,:)= mag;
    phase_vec(i,:)= phase;
end

figure;
subplot(2,1,1)
for i=1:128
plot(f_vec(1,:)*1e-6,mag_vec(i,:))
ylim([0 200]); grid
xlabel('frequency [MHz]'); ylabel('abs(Z)[Ohm]');
title(' Measured 3D prpbe Electrical impedance of each
   element');
leghandle = legend('abs(Z) of 128 elements', 'location'
   , 'NE');
legend(leghandle, 'boxoff'); % no box around legend
hold on

end
for i=1:128
subplot(2,1,2)
plot(f_vec(1,:)*1e-6,phase_vec(i,:))
xlabel('frequency [MHz]'); ylabel(' phase [degree]');
title(' Measured 3D probe Phase of each element ');
hold on
%end
end
%% for finding impedance of the trasducer at electrod
   form ele. ckt model
```

```
%capacitor model
R=0; %  assume resitance of the generator in ohm
l=2.15; % length of the cable
Cc= l*60e-12;  %
ft=f_vec(64,:);
mag_tun= mag_vec(64,:);
phase_tun= phase_vec(64,:)*pi./180;
Zi=mag_tun.*exp(1i.*phase_tun);
Z_xd= Zi./(1+R-(1i*2*pi*Cc*ft.*Zi)-1i*2*pi*Cc*ft*R);

% For pi model
C1=Cc/2;
Zo= 80; % characterstic impedance of the cable
Lo= Zo^2*Cc; %characterstic inductance
Z_xdt= (1i*2*pi*ft*Lo+R+Zi.*((2*pi*ft).^2*C1*Lo-1-1i*pi*ft*C1*R))./((Zi.*(2i*2*pi*ft*C1)-1i*(2*pi*ft).^3*C1^2*Lo)+(2*pi*ft).^2*Lo*C1-1);

% for Transmision model
Lt=0;% series tuning inductor on the element
L=Lo;   % H/m  % i have to check (characterstic inductance of the cable
Zc=Zo; %sqrt(L/Cc); charactersitc impedance of the cable(80 ohm)
c_cable=l*sqrt(1/(L*Cc));
kl=2*pi*ft*l./c_cable;
Zg=R; % resitance of the generator
Z_xdtt=Zc*(Zi-1i*Zc.*tan(kl)-1i*2*pi.*ft*Lt+Zg)./(Zc-1i*Zi.*tan(kl)-2*pi.*ft*Lt.*tan(kl)-1i*Zg.*tan(kl));

figure
subplot(2,1,1)
plot(ft*1e-6,mag_vec(2,:),ft*1e-6,abs(Z_xd),ft*1e-6,abs(Z_xdt),ft*1e-6,abs(Z_xdtt))
title('3D probe Elecrical impadace of one element at connector and at elecrical port simulated')
xlabel('frequency [MHz]'); ylabel('abs(Z)[Ohm]');
leghandle = legend('at connector','capacitor model', 'pi model','Transmision model', 'location', 'NE');
legend(leghandle, 'boxoff'); % no box around legend
ylim([0 150])
```

```
hold on
line(8,mag_vec(2,:))
subplot(2,1,2)
plot(ft*1e-6,phase_vec(2,:),ft*1e-6,(angle(Z_xd)*180./pi),ft*1e-6,(angle(Z_xdt)*180./pi),ft*1e-6,(angle(Z_xdtt)*180./pi))
title('3D probe phase of one element at connector and at elecrical port')
xlabel('frequency [MHz]'); ylabel(' phase [degree]');
leghandle = legend('at connector measured','capacitor model cable', 'pi model cable','Transmision model cable', 'location', 'NE');
legend(leghandle, 'boxoff'); % no box around legend
axis([0 20 -100 0])
%% surface pressure (Po) estimation using hydrophone measurement
addpath C:\Users\peter\Desktop\ProbeLab\ProbeLab1.5
Z_L= 1.5e6;N=25000; m=1;n=94;
z_10elem=1.5:0.5:48; i=1;
  filename1=strcat('zaxis_press_3D_10cycle.mat'); % this is from my data1 (the same with ..kPa.mat)
    load(filename1)
   filename2=strcat('input_voltage_10elem.mat'); % this is from my data1
    load(filename2)

    rf_input(:,1)=rf;  rf_pres(:,:,1)=Data1.Pressure.rf;
     w=tukeywin(25000-8000,0.2);  win=[zeros(8000,1);w];
    rf_pres_wind(:,1,1)=win.*rf_pres(:,i,1);   % resam by P/Q*N
    rms_pres_10elem(1,:,1)=sqrt(mean(rf_pres(:,:,1).^2));  % resampling will not change any ting her
   to(1,:,1)=Data1.t0;Ts=Data1.Ts(1,1);  fs=1/Ts;
   f=(0:(N-1)).*fs/N;  t=(0:N-1).*Ts;     % at N=80 is 8 MH
   RF_pres(:,:,1)=fft(rf_pres(:,:,1),N);  RF_inputfft(:,1)= fft(rf_input(:,1),N);
   RF_pres_wind(:,1,1)=fft(rf_pres_wind(:,1,1),N);
   e=max(abs(RF_inputfft(:,1)))/1000; % to avoid division by zero
```

```
     Htt(:,1)= (squeeze(RF_pres_wind(:,i,1)).*conj(RF_inputfft(:,1)))./(((abs(RF_inputfft(:,1)))*Z_L)+e);
      h=ifft(Htt(:,1));
% for phase
    RF_presselc=fft(ifftshift((squeeze(rf_pres(10000:18000,i,1)))));
    RF_inputselc=fft(ifftshift((rf_input(1:length(RF_presselc),1))));
     M=8000;
    fsel=(0:(M)).*fs/M; tsel=(0:M).*Ts;
     e2=max(abs(RF_inputselc))/1000; % to avoid division by zero
figure
subplot(2,1,1)
plot(f*1e-6,abs(Po_10elem)*1e-6);
title('Estimated pressure on the surface from 10 elements')
 xlabel('f(MHz)'); ylabel('MPa');grid;
xlim([0 20]);%ylim([-100 100])

subplot(2,1,2)
plot(t*1e6,rf_pres(:,i,1)*1e-3)
title('Estimated pressure on the surface')
 xlabel('t(microsec)'); ylabel('KPa');grid;
figure
subplot(2,1,1)
plot(f*1e-6,abs(Po_10elem_10cycle)*1e-6); %% windowed
title('Measured pressure on the surface from 10 elements')
 xlabel('f(MHz)'); ylabel('MPa');grid;
xlim([0 20]);%ylim([-100 100]
subplot(2,1,2)
plot(t*1e6,rf_pres_wind(:,i,1)*1e-3)
title('Measured pressure on the surface')
 xlabel('t(microsec)'); ylabel('KPa');grid
%% in put voltage
figure
subplot(2,1,1)
plot(t*1e6,(rf_input));
```

```
title('Input voltage on the connector to the 10 elements')
 xlabel('t(microsec)'); ylabel('V');grid;
 xlim([0 2.0])

subplot(2,1,2)
plot(f*1e-6,abs(V_10cycle));
title('voltage as function frequency  on the connector')
 xlabel('f(MHz)'); ylabel('v');grid;
xlim([0 20]);%ylim([-100 100])
figure
 plot(z_10elem,rms_pres_10elem(1,:,1)*1e-3)
 title(' Axial beam profile from 10 elements')
 xlabel('Axial distance (mm)'); ylabel('Amplitude(KPa)');grid;
figure
plot(t*1e6,(h))%%% impulse responce
 title('3D probe impulse responce')
 xlabel('t(microsec)'); ylabel('Amplitude(m/v.s)');grid;
figure
subplot(2,1,1)
plot( f*1e-6,20*log10(abs(Htt(:,1))./max(abs(Htt(:,1)))))
title('3D probe Transfer function')
 xlabel('f(MHz)'); ylabel('Amplitude(dB)');grid;
xlim([0 20]); ylim([-60 0])
hold on
line( f*1e-6,-6)
subplot(2,1,2)
phase=angle(fftshift(Htt2));%*180./pi;
phas=(detrend(unwrap(((phase)))));%*180./pi;
plot( fsel*1e-6,phas);
title('phase')
 xlabel('f(MHz)'); ylabel('rad');grid;
xlim([0 20]);%ylim([-100 100])
figure
plot(f*1e-6,abs(Htt(:,1)));
title('Estimated transfer function on the surface')
 xlabel('f(MHz)'); ylabel('MPa');grid;
```

```
xlim([0 20]);%ylim([-100 100])

%% Efficiency, power loss,  esimations
close all;clear all;clc;
Z_L= 1.5e6; %
Z_el= Z_xdtt;  % impedance from the Transmion model assumtions
V_in=ifft(V_10cycle);
V_Lp=decimate(V_in,(2.5e9/125e6),'fir');
Po_in=ifft(Po_10elem_10cycle);
Po_Lp=decimate(Po_in,(2.5e9/125e6),'fir');
Htt_in=ifft(Htt_10cycle);
Htt_Lp=decimate(Htt_in,(2.5e9/125e6),'fir');
N=4096; fs=125e6; Ts=1/fs; M=(2.5e9/125e6); %sampling factor for amplitude
fv=(0:(N-1)).*fs/N; tv=(0:N-1).*Ts;
V_LPfft=fft(V_Lp,N);
Po_LPfft=fft(Po_Lp,N);
Htt_LPfft=fft(Htt_Lp,N);
Htt_log=20.*log10(abs(Htt_LPfft)./max(abs(Htt_LPfft)));
fv2=fv(1:floor(length(fv)/6)-26); % only interplation for our orginalsignal measured, so 0-20MHz  8
Z_el_interp=interp1(ft,Z_el,fv2,'spline');  % this becomes as fun fv2
Z_el_i2 = [Z_el_interp,zeros(1,(length(fv)/2)-length(Z_el_interp))];
Z_el_signal = [Z_el_i2,fliplr(conj(Z_el_i2))] ;
ang_el= angle(Z_el_signal)*180./pi;
G_hf=1./real(Z_el_signal);
A = (0.3*5)*1e-6; % area of one element
Zo= Z_L; % in water  (MRayl= M.kg/m^2s)
Zc=80;
l=2.15; % length of the cable
Cc= l*60e-12;
Lt=0;% series tuning inductor on the element
L=Zc^2*Cc;
f_hf=8e6;
c_cable=l*sqrt(1/(L*Cc));
kl=2*pi*fv(1:length(fv)/2)*l./c_cable;
Zg=0;
```

```
Num=Z_el_i2.*((Z_el_i2.*sin(kl) + 1i*Zc.*tan(kl/2)).*sin(kl)-1i*Zc);
Den=Z_el_i2.*(1i*Zc.*tan(kl/2).*sin(kl)-1i*Zc)+2*Zc^2*tan(kl/2)-Zc^2.*tan(kl/2).^2.*sin(kl);
Hit2=Num./(Den);
Hit2_signal = [Hit2, fliplr(conj(Hit2))];
 V_tt= V_LPfft.*Hit2_signal';
Htt_electrode= Htt_LPfft'./Hit2_signal;
 Po_hf= Po_LPfft';
f1= 8.00e+006; %fv(263)
Nc=263; % 8MHz
Win= abs(V_tt(Nc))^2*(cos(angle(Z_el_signal(Nc))))/(2*abs(Z_el_signal(Nc))*M^2); % elec(from imp)=0.0025
Wac= A*abs(Po_hf(Nc))^2/(2*Zo*M^2);
e_wo2= Wac/Win;     % out/in effic
Po_pk=(max(real(ifft(Po_10elem_10cycle))));
V_pk=(max(real(ifft((V_LPfft))))); % on the connector
V_tt_pk=(max(real(ifft(V_tt)))); % on the electrode
e_wo= ((abs(Po_hf(Nc)))^2*A*abs(Z_el_signal(Nc))/((abs(V_tt(Nc)))^2*(cos(angle(Z_el_signal(Nc))))*Zo*1));% or by substing the eq.
e_el_10by10=((abs(Z_el_signal)).*(abs(Po_hf)).^2*A)./((cos(angle(Z_el_signal))).*(abs(V_tt))'.^2*Zo+(max((cos(angle(Z_el_signal))).*(abs(V_tt))'.^2*Zo)/100));
Nel=48; %number of elements
Toff=0;%1*1e-6; % in micro seconds
T_on=(0:1:20)*1e-6; % in micro seconds
nT_on=length(T_on);
Tr =(0:1:60)*1e-6;  %
nTr=length(Tr);
W_trav=zeros(nT_on,nTr);  %length(T_on)=121

for nn=1:nTr
     for kk=1:nT_on %se
      H_trav=(1-e_wo)*(abs(V_tt(Nc))).^2.*cos(angle(Z_el_signal(Nc)))./(2.*abs(Z_el_signal(Nc))*M^2);% at w
      Q_tr= Nel*T_on.*(1-e_wo)*(abs(V_tt(Nc))).^2.*cos(angle(Z_el_signal(Nc)))./(2.*abs(Z_el_signal(Nc))*M^2);% at wo
```

```
      W_trav(kk,nn)=Nel*H_trav*T_on(kk)./Tr(nn);  % (J/s=Watt) at wo
     end
end

%% in terms of duty cycle (To/Tr in%)
duty=0:0.01:1;
V_expect=(V_pk:100);  % Note Vtt=Hit*Vcon
nV_expect=length(V_expect);
nduty=length(duty);
W_expect=zeros(nV_expect,nduty);
Po_tm=zeros(1,nV_expect);
temp_tm=zeros(nT_on,nV_expect);
for mm=1:nV_expect
  for rr=1:nduty
      W_expect(mm,rr)= Nel*duty(rr).*(1-e_wo)* V_expect(mm).^2.*(cos(angle(Z_el_signal(Nc)))./(2*abs(Z_el_signal(Nc)));
  end
    Po_tm(1,mm)=Po_pk*V_expect(mm)./V_pk;  % linear dependency
end
figure
subplot(2,1,1)
plot(tv*1e6,real(ifft(V_tt)));
title('Input voltage on the electrode from 10 cycle')
 xlabel('t(microsec)'); ylabel('V');grid;
 xlim([0 2])
 subplot(2,1,2)
 plot(fv*1e-6,abs(V_tt));
title('Power spectrum of voltage on the electrode')
 xlabel('f(MHz)'); ylabel('volt');grid;
xlim([0 20]);%ylim([-100 100])
fel=fv(1:length(fv)/2);tel=tv(1:length(tv)/2);
figure
plot(fel*1e-6,abs(Hit2));
title('Electrical transfer function form connector to electrode')
 xlabel('f(MHz)'); ylabel('abs(H)');grid;
 xlim([0 20])
%plot of heat, power, temperature
```

```
figure
mesh(Tr*1e6, T_on*1e6,abs(W_trav));colorbar;
title('Power dissipated on the transducer ')
ylabel('T_{on} [microsec]');xlabel('T_r (microsec)'); zlabel('Wtrav [Watt]')
figure
plot(T_on*1e6,abs(Q_tr)); grid;
title(' Heat on the transducer')
xlabel('T_{on} [microsec]');ylabel('dQ [J]');
figure
mesh(duty*100,V_expect,abs(W_expect)); colorbar;
title('Power dissipated on the transducer as function of voltage and duty cycle ')
xlabel('duty [%]'); ylabel('V [v]'); zlabel('W [watt]');
% pressure of voltage
figure
plot(V_expect,abs(Po_tm)*1e-6)
 title('Possible surface pressure vs volatge')
 xlabel('Vttm[volt]'); ylabel('Ptm [MPa]');grid;
figure
plot(fv*1e-6,abs(e_el_10by10)*100)
title('Efficiency of the transducer element')
xlabel('f[MHz]'); ylabel('etta [%]');grid;
xlim([0 20]);ylim([0 1])
```

C.2 Beam profiles

```
%% Azimuth and elevation beam profile 64 elem estimation from hydrophone meas
% Azimuth from 64 elements
filename=strcat('pres_xaxis_scan_64elem.mat');
    load(filename)
   i=1;
    rf_pres_azi(:,:,i)=Data1.Pressure.rf;to(1,:,i)=Data1.t0;Ts(1,:,i)=Data1.Ts;
  rms_pres_azi(1,:,i)=sqrt(mean(rf_pres_azi(:,:,i).^2));
  fs=1/Ts(1,1,1); f=(0:(N-1)).*fs/N; t=(0:N-1).*Ts(1,1,1);
  RF_pres(:,:,i)=fft(rf_pres(:,:,i),N);
```

```
%Azimuth beam profile at different depth this is x, dB.
figure
plot(x11,20*log10(rms_pres_azi(1,:,1)/max(rms_pres_azi(1,:,1))));
 title('Azimuth beam profile at focus from half aperture ')
 xlabel('Azimuth (mm)'); ylabel('Amplitude(dB)');grid;
leghandle = legend('at 25mm', 'location', 'NE');
legend(leghandle, 'boxoff'); % no box around legend
 hold on
 line(x11,-6)
figure
plot(t*1e6,rf_pres_azi(:,41,1)*1e-6);
 title('rf signal of the pressure at focus from half aperture ')
 xlabel('t(microsec)'); ylabel('Pressure(MPa)');grid;
leghandle = legend('at 25mm', 'location', 'NE');
legend(leghandle, 'boxoff'); % no box around legend
 hold on
xlim([0 2])
% elevation scan from 64 elements
filename=strcat('pres_yaxis_scan_64elem_same_with128.mat');
    load(filename)

    rf_pres_azi(:,:,i)=Data1.Pressure.rf;to(1,:,i)=Data1.t0; Ts(1,:,i)=Data1.Ts;
  rms_pres_azi(1,:,i)=sqrt(mean(rf_pres_azi(:,:,i).^2));
  fs=1/Ts(1,1,1); f=(0:(N-1)).*fs/N; t=(0:N-1).*Ts(1,1,1);
  RF_pres(:,:,i)=fft(rf_pres(:,:,i),N);
  %Elevaton beam profile at different depth this is x, dB.
figure
plot(x11,20*log10(rms_pres_azi(1,:,1)/max(rms_pres_azi(1,:,1))));
 title('Elevation beam profile at focus from half aperture ')
 xlabel('Elevation(mm)'); ylabel('Amplitude(dB)');grid;
leghandle = legend('at 25mm', 'location', 'NE');
```

```
legend(leghandle, 'boxoff'); % no box around legend
 hold on
 line(x11,-6)
figure
plot(t*1e6,rf_pres_azi(:,41,1)*1e-6);
 title('rf signal of the pressure at focus from half aperture ')
 xlabel('t(microsec)'); ylabel('Pressure(MPa)');grid;
leghandle = legend('at 25mm', 'location', 'NE');
legend(leghandle, 'boxoff'); % no box around legend
 hold on
%% Azimuth and elevaton beam profile hydrohphone meas from 48 elements
% Azimuth for 48 elements
filename1=strcat('press_xscan_data1_14w.mat');
    load(filename1)
    rf_pres(:,:,i)=Data1.Pressure.rf;rf_volt(:,:,i)=Data1.Voltage.rf;
   to(1,:,i)=Data1.t0;Ts(1,:,i)=Data1.Ts;
  rms_pres(1,:,i)=sqrt(mean(rf_pres(:,:,i).^2));
   fs=1/Ts(1,1,1);f=(0:(N-1)).*fs/N; t=(0:N-1).*Ts(1,1,1);
   RF_pres(:,:,i)=fft(rf_pres(:,:,i),N);
%Azimuth beam profile at different depth this is x, dB.
figure
plot(x11,20*log10(rms_pres(1,:,1)/max(rms_pres(1,:,1))));
 xlabel('Azimth distance (mm)'); ylabel('Amplitude(dB)');grid;
 hold on
 line(x11,-6)
xlim([-10 10]); ylim([-40 0])
figure;
plot(t*1e6,rf_pres(:,41,i)*1e-6);grid;
xlabel('time(microsec)'); ylabel('Pf (MPa)');grid;
xlim([0 20])
%elevaton from 48 elements
filename1=strcat('press_yscan_data4_8w.mat');
    load(filename1)
   rf_pres(:,:,i)=Data4.Pressure.rf; to(1,:,i)=Data4.t0;Ts(1,:,i)=Data4.Ts;
```

```
  rms_pres(1,:,i)=sqrt(mean(rf_pres(:,:,i).^2));
   fs=1/Ts(1,1,1);f=(0:(N-1)).*fs/N;  t=(0:N-1).*Ts(1,1,1);
   RF_pres(:,:,i)=fft(rf_pres(:,:,i),N);
%Elevation beam profile at different depth this is x, dB.
figure
plot(x11,20*log10(rms_pres(1,:,1)/max(rms_pres(1,:,1))));
 xlabel('Elevation distance (mm)'); ylabel('Amplitude(dB)');grid;
 hold on
 line(x11,-6)
xlim([-10 10])
figure;
plot(t*1e6,rf_pres(:,41,i)*1e-6);grid;
xlabel('time(microsec)'); ylabel('Pf (MPa)');grid;
xlim([0 20])
```

C.3 Simulation of URF, UTH, and Temperature

```
runfreqs = [5:11]*1e6; %8e6;%
nfreqs = length(runfreqs);

% Run simulations for all setups
for kk = 1:nfreqs
close all;

    prctrl = initPropcontrolMat;
    prctrl.nw = 1024;
    prctrl.nx = 64;
    prctrl.ny = 64;
    prctrl.fc = runfreqs(kk); %
    prctrl.Fs = 10*prctrl.fc;
    prctrl.Fs_lf = 10*prctrl.fc;
    prctrl.Rmax = 40e-3;
    prctrl.c0 = 1561;
    prctrl.beta_n = 3.9e6; %(e6 is scaling factor )
    prctrl.kappa = 4.12e-10;
    prctrl.dx = 3e-4;
    prctrl.dy = 3e-4;
```

```
    prctrl.esizex=prctrl.dx;
    prctrl.esizey=prctrl.dy;

    cp = 4.2e6; % Joule / Kelvin  Volumetric heat capacity

    nt = prctrl.nw;
    nw = nt;
    nx = prctrl.nx;
    ny = prctrl.ny;
    dx = prctrl.dx;
    dy = prctrl.dy;
    dz = prctrl.dz;

    c0 = prctrl.c0;

    xx = (-nx/2:nx/2-1).*dx;
    yy = (-ny/2:ny/2-1).*dy;

    mx = nx/2+1;
    my = ny/2+1;

    nz = ceil(prctrl.Rmax/prctrl.dz);
    %% Pulse generation
    % Center frequencies
    fc = prctrl.fc;                                   % HF and LF
    Fs = prctrl.Fs;
    F = [25e-3, 25e-3];
    Ap_hf =[14.4e-3, 5e-3];% [F(1)/Fnumber_azi, F(2)/Fnumber_elev];
    Ap = Ap_hf;
    % Surface pressure
    u0_hf = 0.15;
    % Pulse length
    Nmul = 5;  %  d
    Np = Nmul*2.0;% pulselength expressed as a number of periods(cycles)
    Tp = Np/fc;
    offset = 0;
```

```
    pulseform = 'TUKEY'; % Pulseform SYMMETRIC,
       ASYMMETRIC or TUKEY
    lensefoc = 1;          % Lense over LF
    apod = 0;              % Transmit apodization
    % Create HF and LF pulses
    [u_hf, prctrl] = excitationGen(prctrl, Ap, ...
        u0_hf, fc(1), Np(1), pulseform, F, apod);
    u0 = u_hf;
    f = ifftshift((-floor(nw/2):ceil(nw/2)-1)')*prctrl.
       Fs/nw;
    w = 2*pi*f;
    t = ((-floor(nw/2):ceil(nw/2)-1)')*1/prctrl.Fs;

    % Plot initial surface excitation
    figure;
    subplot(2,1,1);
    plot(t, squeeze(u0(:,mx,my)), 'r');
    title('Initial pulse');
    grid on;

    subplot(2,1,2);
    plot(f, abs(fft(u0(:,mx,my))), 'r');
    xlim([0 50]*1e6);
    grid on;

    %% Absorbtion parameters
    % Absorbtion and extinction cross-section params
    sigma_a0 = 0.5;% 0.78; % % dB / cmMHz
    sigma_r0 =0.15;% 0.2;   % increaseing the vale will
        decreas the urf
    b = 1.1;
    a =2.5;
    w0 = 2*pi*fc(1);
    nlflag = 2;
    %% Wavenumbers
    zz = (dz:dz:prctrl.Rmax)*1e3;

    % Absorbtion and extinction cross-section
    [loss,extinc] = getAbsorbtionMat(prctrl, sigma_a0,
       sigma_r0, b, a, w0);
    % Wavenumber operator
```

```
    Kz = getWavenumbersMat(prctrl, 2.5, 1.1, loss); % 0.52 to 2.5

    %% Run simulation
    [~,on_ax,bprf_azi,bprf_elev] = propagateMat(prctrl, ...
        Kz, u0, iodir,nlflag,0,0);

    %% Calculate radiation force and temperature increase due to one pulse
    % [N / m^3 ]
    F = radForceCalc(prctrl, extinc, fft(on_ax), 1060, Tp);

    temp_pressure = max(on_ax);  % temporay  pressure
    %pressure(kk)= temp_pressure(25);
    % [K]
    dT = heatGenCalc(prctrl, w0, sigma_a0, sigma_r0, b, fft(on_ax), 1060, cp);

    %% Calculate Energy delivered to tissue pr pulse and unit length
    % [J / m]
    dE = zeros(nz,1);
    for ii = 1:nz
        tmp = load([iodir, '_', num2str(ii), 'mm.mat']);
        dE(ii) = calcEnergyDelivered(prctrl, w0, sigma_a0, b, ...
            sigma_r0, fft(tmp.u_z), 1060);
    end
end
```